

Search for resonant and nonresonant new phenomena in high-mass dilepton final states at $\sqrt{s} = 13$ TeV



The CMS collaboration

E-mail: cms-publication-committee-chair@cern.ch

ABSTRACT: A search is presented for physics beyond the standard model (SM) using electron or muon pairs with high invariant mass. A data set of proton-proton collisions collected by the CMS experiment at the LHC at $\sqrt{s} = 13$ TeV from 2016 to 2018 corresponding to a total integrated luminosity of up to 140 fb^{-1} is analyzed. No significant deviation is observed with respect to the SM background expectations. Upper limits are presented on the ratio of the product of the production cross section and the branching fraction to dileptons of a new narrow resonance to that of the Z boson. These provide the most stringent lower limits to date on the masses for various spin-1 particles, spin-2 gravitons in the Randall-Sundrum model, as well as spin-1 mediators between the SM and dark matter particles. Lower limits on the ultraviolet cutoff parameter are set both for four-fermion contact interactions and for the Arkani-Hamed, Dimopoulos, and Dvali model with large extra dimensions. Lepton flavor universality is tested at the TeV scale for the first time by comparing the dimuon and dielectron mass spectra. No significant deviation from the SM expectation of unity is observed.

KEYWORDS: Beyond Standard Model, Hadron-Hadron scattering (experiments), Lepton production, Particle and resonance production

ARXIV EPRINT: [2103.02708](https://arxiv.org/abs/2103.02708)

Contents

1	Introduction	1
2	The CMS detector	4
3	Signal models	4
3.1	Models with resonant signatures	5
3.2	Models with nonresonant signatures	6
4	Simulated event samples	8
5	Lepton reconstruction and event selection	10
5.1	Electron reconstruction and selection	10
5.2	Muon reconstruction and selection	12
5.3	Event disambiguation	13
6	Background estimation	14
7	Systematic uncertainties	15
8	Results	17
9	Statistical interpretation	19
9.1	Search for resonant signals	20
9.2	Search for nonresonant signals	28
9.3	Search for lepton flavor universality violation	31
10	Summary	33
	The CMS collaboration	42

1 Introduction

The presence of new phenomena, both resonant and nonresonant, in the high-mass dilepton final state is predicted by various theoretical models aiming to extend the standard model (SM) of particle physics. In this paper, the production of new spin-1 or spin-2 resonances, as well as the nonresonant production of high-mass lepton pairs, is considered.

The existence of new neutral gauge bosons is a possible signature of grand unified theories, such as superstring and left-right-symmetric (LRS) models, that include a unification of the three forces at a high energy scale [1, 2].

One persistent puzzle in modern particle physics is the large difference in the energy scale of electroweak symmetry breaking and the energy scale of gravitation. This could be explained in theories including spatial extra dimensions, where the gravitational force can propagate into additional dimensions. In models by Arkani-Hamed, Dimopoulos, and Dvali (ADD) [3, 4], the SM particles are confined to the traditional four dimensions of space and time, while in models proposed by Randall and Sundrum (RS) [5] the SM particles could also propagate into the additional dimensions. Possible signatures of these theories at LHC energies are graviton excitations, either as distinct spin-2 high-mass resonances in the RS model, or as a series of nearly mass-degenerate excitations that result in an overall nonresonant excess of events at high mass in the ADD model.

Based on many astrophysical and cosmological observations, it is assumed that dark matter (DM) accounts for the majority of matter in the universe [6]. Models have been proposed in which the DM consists of particles that can interact with those of the SM via high-mass, weakly coupled mediator particles [7]. These mediators could then be observed via their decay into SM particles, including the dilepton final state.

It has long been speculated that the presence of three generations of quarks and leptons is a sign that these particles are not fundamental but rather composed of constituent particles commonly called “preons” [8]. At energies observable at collider experiments, the preons would be confined into bound states by a new interaction analogous to quantum chromodynamics (QCD). This new interaction is characterized by an energy scale Λ , at which its effects would be directly observable. At center-of-mass energies far below Λ , the presence of the preon bound states would manifest itself as a flavor-diagonal “contact interaction” (CI) [9], resulting in a nonresonant excess of events at high mass.

Hints for lepton flavor universality violation in several measurements recently reported by the LHCb Collaboration [10–12], together with other flavor anomalies in B-meson decays summarized in ref. [13], have sparked interest in models for physics beyond the SM that could explain these effects. These include models with heavy neutral gauge bosons [2] or leptoquarks [14]. Some of these models would result in a significant deviation from unity of the ratio of the dimuon to dielectron differential cross section as a function of dilepton mass $m_{\ell\ell}$,

$$R_{\mu^+\mu^-/e^+e^-} = \frac{d\sigma(q\bar{q} \rightarrow \mu^+\mu^-)/dm_{\ell\ell}}{d\sigma(q\bar{q} \rightarrow e^+e^-)/dm_{\ell\ell}}, \quad (1.1)$$

at high $m_{\ell\ell}$ [15].

Searches for high-mass Z' gauge bosons in dilepton final states have a long history at the LHC, with the CMS Collaboration having reported results using proton-proton (pp) collision data from the LHC Run 1 (2010–2012) at $\sqrt{s} = 7$ TeV [16, 17] and 8 TeV [18, 19], and more recently from the beginning of the LHC Run 2 (2015–2018) at 13 TeV [20, 21] using early data corresponding to an integrated luminosity of 36 fb^{-1} collected in 2016. Similar searches have also been performed by the ATLAS Collaboration with data collected at 7 TeV [22, 23], 8 TeV [24], and 13 TeV [25]. Most recently, the ATLAS Collaboration reported results obtained using data recorded at $\sqrt{s} = 13$ TeV, corresponding to an integrated luminosity of 139 fb^{-1} [26].

Results of searches for spin-2 dilepton resonances, as well as constraints on DM models, have been reported by the ATLAS and CMS Collaborations [18, 21, 24, 27].

For the case of nonresonant signatures, the CMS Collaboration has reported results at 8 [19] and 13 TeV [28]. Additional constraints on these models have been reported by the CMS Collaboration from diphoton and dijet final states [29, 30] and by the ATLAS Collaboration from dijet final states [31]. The ATLAS Collaboration has presented similar results for these models in the dilepton final state, the most recent using data at 8 TeV [32] for the ADD model and at 13 TeV [33] for the CI model.

This paper significantly extends the previous CMS results by using the full data set recorded at $\sqrt{s} = 13$ TeV during the years 2016–2018, corresponding to 137 (140) fb^{-1} in the dielectron (dimuon) channel [34–36]. The additional data in the dimuon channel are recorded with the detector in conditions unsuitable for electron reconstruction. Deviations from the SM predictions are searched for in the dilepton invariant mass spectrum for both dielectron and dimuon events. The contribution from dileptonic decays of tau lepton pairs to the signal is small and neglected. The shapes of contributions from SM processes are estimated from simulation, except for backgrounds containing leptons produced inside jets or jets misidentified as leptons, which are estimated from control regions in data. The simulated events describing the dominant Drell-Yan (DY) background are corrected to the highest order calculations available. The resulting background shape is normalized to the observed data yields in a mass window of 60–120 GeV around the Z boson peak, separately for the dielectron and dimuon channels.

Two analysis strategies are followed, targeting resonant and nonresonant signatures. For resonant signatures, the search is performed in a mass window around the assumed resonance mass, whose size depends on the assumed intrinsic decay width of the resonance and the mass-dependent detector resolution. A range of masses and widths is scanned to provide results covering a wide selection of signal models. Unbinned maximum likelihood fits are performed inside the mass windows, allowing the background normalization to be determined from data. The background parametrizations are obtained from fits to the $m_{\ell\ell}$ distribution of the background estimates.

Upper limits are set on the ratio of the product of the production cross section and the branching fraction of a new narrow dilepton resonance to that of the SM Z boson. Thus, many experimental and theoretical uncertainties common to both measurements cancel out or are reduced, leaving only uncertainties in the ratio that vary with the dilepton mass to be considered.

In the case of nonresonant signatures, the event sample is divided into several bins in invariant mass and, improving upon previous CMS analyses, the scattering angle $\cos\theta^*$ in the Collins-Soper frame [37]. The result is then obtained from a combination of the individual counting experiments within these bins. While most of the sensitivity to new physics stems from the highest mass bins where the signal-to-background ratio is most favorable, the bins at lower masses still contain valuable information, for example on possible interference between the signal and SM backgrounds. In this approach, the signal is not normalized to the Z boson cross section, and the background estimate cannot be obtained from the data. Therefore, this part of the analysis is more affected by uncertainties in the signal and background modeling.

In addition to these two search strategies, lepton flavor universality is tested for the first time in these final states by measuring the dimuon to dielectron ratio $R_{\mu^+\mu^-/e^+e^-}$ and comparing it to the SM expectation of unity, including corrections for detector effects, lepton acceptances, and lepton efficiencies.

This paper is structured as follows. The CMS detector is briefly described in section 2. A description of the signal models is given in section 3, followed by a description of simulated event samples used in the analysis in section 4. The event reconstruction and selection is given in section 5 and the estimation of SM backgrounds is described in section 6. Systematic uncertainties are described in section 7, followed by the results and their statistical interpretation in sections 8 and 9, respectively. The paper is summarized in section 10. Tabulated results are provided in HEPDATA [38].

2 The CMS detector

The central feature of the CMS detector is a superconducting solenoid providing an axial magnetic field of 3.8 T and enclosing an inner tracker, an electromagnetic calorimeter (ECAL), and a hadron calorimeter (HCAL). The inner tracker is composed of a silicon pixel detector and a silicon strip tracker, and measures charged particle trajectories in the pseudorapidity range $|\eta| < 2.5$. Before the data taking period in 2017, an upgraded pixel detector was installed, adding an additional barrel layer closer to the interaction point and additional disks in the two forward parts of the detector [39]. The ECAL and HCAL, each composed of a barrel and two endcap sections, extend over the range $|\eta| < 3.0$. The finely segmented ECAL consists of nearly 76 000 lead tungstate crystals, while the HCAL is constructed from alternating layers of brass and scintillator. Forward hadron calorimeters encompass $3.0 < |\eta| < 5.0$. The muon detection system covers $|\eta| < 2.4$ with up to four layers of gas-ionization detectors installed outside the solenoid and sandwiched between the layers of the steel flux-return yoke. A more detailed description of the CMS detector, together with a definition of the coordinate system used and the relevant kinematic variables, can be found in ref. [40].

Events of interest are selected using a two-tiered trigger system [41]. The first level (L1), composed of custom hardware processors, uses information from the calorimeters and muon detectors to select events at a rate of around 100 kHz within a fixed time interval of less than $4\,\mu\text{s}$. The second level, known as the high-level trigger (HLT), consists of a farm of processors running a version of the full event reconstruction software optimized for fast processing, and reduces the event rate to around 1 kHz before data storage.

3 Signal models

A large number of models predict new phenomena resulting in high-mass dilepton signatures. The available models may be classified depending on whether they predict resonant or non-resonant production.

3.1 Models with resonant signatures

We consider three types of models resulting in resonances at high dilepton masses: Z' particles in a class of $U'(1)$ gauge group models, spin-2 gravitons in the RS model of extra dimensions, and spin-1 dark matter mediators. The most prevalent are the theories that introduce new $U'(1)$ gauge groups. The symmetry properties of these groups, or a combination of them, are broken at some energy scale so that the SM group structure emerges as the low-energy limit of the new theory. If this breaking happens at the TeV scale, new gauge bosons Z' with masses accessible at the LHC could exist. The properties of the new Z' bosons depend on the mixing of the $U'(1)$ generators, which can be described by a continuously varying angle within a class of models. Commonly considered classes are the generalized sequential model (GSM) [42], containing the sequential SM boson Z'_{SM} that has SM-like couplings to SM fermions [43]; LRS extensions of the SM based on the $SU(2)_L \otimes SU(2)_R \otimes U(1)_{B-L}$ gauge group, where B–L refers to the difference between the baryon and lepton numbers [42], which predict high-mass neutral bosons; and grand unified theories based on the E_6 gauge group, containing the Z'_ψ boson [1, 44].

In the narrow width approximation [45], the Z' production cross section can be expressed as $c_u w_u + c_d w_d$, where c_u (c_d) are its couplings to up-type (down-type) quarks and w_u (w_d) are the parton distribution functions (PDFs) for these quarks [42, 46]. As the values of the model-dependent couplings depend on the aforementioned mixing of the $U'(1)$ generators, each class of models can be represented by a unique contour in the (c_d, c_u) plane as a function of the mixing angle. The properties of a variety of benchmark models in the three model classes mentioned above are shown in table 1. Ref. [42] shows that the finite width of the resonance, which can reach up to 12% for the Z'_Q , has negligible effects on the translation of experimental limits obtained in the narrow width approximation into the (c_d, c_u) plane. Similarly, the effect of interference between the signal and SM backgrounds can be neglected as long as the signal cross section is considered in a sufficiently narrow window around the Z' mass [45].

The RS model of extra dimensions [5, 47] introduces an additional warped spatial dimension where gravity can propagate through all of the five-dimensional bulk. This leads to the prediction of spin-2 Kaluza-Klein (KK) excitations of the graviton (G_{KK}) that could be resonantly produced at the LHC and observed in their decay into lepton pairs. These new resonances are characterized by their masses and the coupling $k/\overline{M}_{\text{Pl}}$, where k is the warp factor of the five-dimensional anti-de Sitter space and \overline{M}_{Pl} is the reduced Planck mass. The ratios of the intrinsic widths of the first excitation of the graviton to its mass for the coupling parameters $k/\overline{M}_{\text{Pl}}$ of 0.01, 0.05, and 0.10 are 0.01%, 0.36%, and 1.42%, respectively.

To ensure a consistent search strategy and comparability between the results of different searches, the LHC Dark Matter Working Group has defined a variety of simplified models to be used as benchmarks for DM searches at the LHC [48, 49]. In this paper, we consider a model that assumes the existence of a single DM particle that interacts with the SM particles through a spin-1 mediator, which can be either a vector or axial-vector boson. The model is fully described by the following parameters: the DM mass m_{DM} , the mediator mass m_{med} , the coupling g_{DM} between the mediator and the DM particle, and

$U'(1)$ model	Mixing angle	$\mathcal{B}(\ell^+\ell^-)$	c_u	c_d	c_u/c_d	$\Gamma_{Z'}/M_{Z'}$
GSM						
$U(1)_{\text{SM}}$	-0.072π	0.031	2.43×10^{-3}	3.13×10^{-3}	0.78	0.0297
$U(1)_{\text{T3L}}$	0	0.042	6.02×10^{-3}	6.02×10^{-3}	1.00	0.0450
$U(1)_{\text{Q}}$	0.5π	0.125	6.42×10^{-2}	1.60×10^{-2}	4.01	0.1225
LRS						
$U(1)_{\text{R}}$	0	0.048	4.21×10^{-3}	4.21×10^{-3}	1.00	0.0247
$U(1)_{\text{B-L}}$	0.5π	0.154	3.02×10^{-3}	3.02×10^{-3}	1.00	0.0150
$U(1)_{\text{LR}}$	-0.128π	0.025	1.39×10^{-3}	2.44×10^{-3}	0.57	0.0207
$U(1)_{\text{Y}}$	0.25π	0.125	1.04×10^{-2}	3.07×10^{-3}	3.39	0.0235
E_6						
$U(1)_{\chi}$	0	0.061	6.46×10^{-4}	3.23×10^{-3}	0.20	0.0117
$U(1)_{\psi}$	0.5π	0.044	7.90×10^{-4}	7.90×10^{-4}	1.00	0.0053
$U(1)_{\eta}$	-0.29π	0.037	1.05×10^{-3}	6.59×10^{-4}	1.59	0.0064
$U(1)_{\text{S}}$	0.129π	0.066	1.18×10^{-4}	3.79×10^{-3}	0.31	0.0117
$U(1)_{\text{N}}$	0.42π	0.056	5.94×10^{-4}	1.48×10^{-3}	0.40	0.0064

Table 1. Various benchmark models in the GSM [42], LRS [42], and E_6 [1, 44] model classes, with their corresponding mixing angles, their branching fraction (\mathcal{B}) to dileptons, the c_u , c_d parameters and their ratio, and the width-to-mass ratio of the associated Z' boson.

the universal couplings g_ℓ and g_q between the mediator and the SM charged leptons and quarks, respectively. Two signal scenarios have been defined that feature nonzero values of g_ℓ , so that the mediator could be directly observed in its decay into the dilepton final state. The first choice represents a relative strength of the couplings to quarks and charged leptons typical of some models with a pure vector mediator, while the second choice is a representative case found in the simplest complete models with axial-vector Z' bosons [48]:

- Vector mediator with small couplings to leptons: $g_{\text{DM}} = 1.0$, $g_q = 0.1$, $g_\ell = 0.01$;
- Axial-vector mediator with equal couplings to quark and leptons: $g_{\text{DM}} = 1.0$, $g_q = g_\ell = 0.1$.

Interference between the mediator exchange and the SM processes resulting in the dilepton final state has been studied and found to be negligible for experimental searches [48].

3.2 Models with nonresonant signatures

We consider two types of nonresonant excess at high $m_{\ell\ell}$: a series of virtual spin-2 graviton excitations in the ADD model of large extra dimensions [3], and a four-fermion CI caused

by fermion substructure [8]. In these models, the differential cross section for dilepton pair production can be expressed as:

$$\frac{d\sigma_{X \rightarrow \ell\ell}}{dm_{\ell\ell}} = \frac{d\sigma_{DY}}{dm_{\ell\ell}} + \eta_X \mathcal{I}(m_{\ell\ell}) + \eta_X^2 \mathcal{S}(m_{\ell\ell}), \quad (3.1)$$

where $d\sigma_{DY}/dm_{\ell\ell}$ is the SM DY differential cross section, η_X is a model-specific parameter, and the signal contribution terms are separated into an interference term (\mathcal{I}) and a pure signal term (\mathcal{S}). Interference between the signal process and the SM DY background is possible when the new process acts on the same initial state and yields the same final state, and can be either constructive or destructive, depending on the sign of η_X .

In the ADD model, which is an attempt to describe quantum gravity with an effective field theory, spacetime is extended by n additional compactified spatial dimensions of size L . SM particles are confined to the four-dimensional subspace (the brane), while gravity can propagate to all $D = n + 4$ dimensions (the bulk). If L is sufficiently large, the D -dimensional fundamental Planck mass M_D , which is related to the effective Planck mass M_{Pl} in three dimensions by

$$M_D^{2+n} \sim M_{Pl}^2 / L^n, \quad (3.2)$$

can then be probed at the TeV scale. In contrast to the RS model, the ADD model predicts the presence of a quasi-continuous spectrum of KK graviton modes as a result of the compactification of the extra dimensions with a large compactification radius. The number of excited modes increases with the interaction scale, resulting in a nonresonant excess at high dilepton masses from the decay of the virtual gravitons, which cannot be individually resolved with the LHC detectors.

These processes can be characterized by the single energy cutoff scale Λ_T in the Giudice-Rattazzi-Wells (GRW) convention [50], the string scale M_S in the Hewett convention [51], or the number of additional dimensions n in conjunction with M_S in the Han-Lykken-Zhang (HLZ) convention [52]. The generic form factor η_X in eq. (3.1) is replaced by η_G , which depends on the chosen convention:

$$\text{GRW:} \quad \eta_G = \frac{1}{\Lambda_T^4}; \quad (3.3)$$

$$\text{Hewett:} \quad \eta_G = \frac{2}{\pi} \frac{\lambda}{M_S^4} \quad \text{with } \lambda = \pm 1; \quad (3.4)$$

$$\text{HLZ:} \quad \eta_G = \begin{cases} \ln(M_S^2/\hat{s}) \frac{1}{M_S^4} & \text{for } n = 2, \\ \frac{2}{n-2} \frac{1}{M_S^4} & \text{for } n > 2. \end{cases} \quad (3.5)$$

Here \hat{s} is the square of the parton center-of-mass energy. In the ADD model, interference with DY is limited, as the production of virtual gravitons is dominated by gluon-induced processes. Positive interference is assumed in this analysis, but the choice has negligible effects on the results. The effective field theory will only yield reliable results up to a certain energy scale, above which a more exact theory of quantum gravity is necessary. Both Λ_T and M_S act as this ultraviolet cutoff parameter in their respective conventions.

In case of the CI model, assuming that quarks and leptons share common constituents, the Lagrangian for the CI process $q\bar{q} \rightarrow \ell\ell$, where ℓ is a charged lepton, can be expressed as

$$\mathcal{L}_{q\ell} = \frac{g_{\text{contact}}^2}{\Lambda^2} \left[\eta_{LL} (\bar{q}_L \gamma^\mu q_L) (\bar{\ell}_L \gamma_\mu \ell_L) + \eta_{RR} (\bar{q}_R \gamma^\mu q_R) (\bar{\ell}_R \gamma_\mu \ell_R) \right. \\ \left. + \eta_{LR} (\bar{q}_L \gamma^\mu q_L) (\bar{\ell}_R \gamma_\mu \ell_R) + \eta_{RL} (\bar{q}_R \gamma^\mu q_R) (\bar{\ell}_L \gamma_\mu \ell_L) \right], \quad (3.6)$$

where $q_L = (q_u, q_d)_L$ is a left-handed quark doublet; q_R represents a sum over the right-handed quark singlets (q_u - and q_d -type); the η_{ij} are real numbers between -1 and 1 ; and ℓ_L and ℓ_R are the left- and right-handed lepton fields, respectively. By convention, $g_{\text{contact}}^2/4\pi = 1$ and the helicity parameters η_{ij} are taken to have unit magnitude. The compositeness scale, represented by Λ , is potentially different for each of the individual terms in the Lagrangian. Therefore, the individual helicity currents for “left-left” (LL), “right-right” (RR), and the combination of “left-right” (LR) and “right-left” (RL) in eq. (3.6), together with their scales (Λ_{LL} , Λ_{RR} , Λ_{LR} , and Λ_{RL}), are considered separately in this search, and in each case all other currents are assumed to be zero. While the LL and RR models favor positive values of $\cos\theta^*$, as does the DY background, the distribution is inverted for the LR and RL models, which favor negative values.

A given η_{ij} can be related to the form factor in the differential cross section in eq. (3.1) by

$$\eta_X = -\frac{\eta_{ij}}{\Lambda_{ij}^2}. \quad (3.7)$$

4 Simulated event samples

Numerous simulated event samples are used to describe both background and signal processes. Dedicated samples are generated for each of the three years of data taking considered in this analysis, reflecting the changing beam and detector conditions from year to year. Different generators are used to generate the individual processes.

The dominant DY background is generated with POWHEG v2 [53–58] using next-to-leading order (NLO) matrix elements. In the sample generation, PDFs are evaluated using the LHAPDF library [59–61]. For the 2016 samples, the NNPDF3.0 [62] PDF set at NLO is used, while for the samples describing the 2017 and 2018 data, the NNPDF3.1 PDF set computed at the next-to-next-to-leading order (NNLO) [63] is used. The PYTHIA 8.212 (8.230) [64] generator is used to simulate parton showering and hadronization in the 2016 (2017 and 2018) samples. For all 2016 samples, the PYTHIA tune CUETP8M1 [65] is used. It is replaced for 2017 and 2018 with the CP5 [66] tune, which is optimized for the NNPDF3.1 PDF set.

The NLO cross sections obtained from POWHEG are corrected for NNLO effects in perturbative QCD, as well as for missing electroweak effects at NLO, using a correction factor that depends on the dilepton invariant mass, obtained using the FEWZ 3.1.b2 program [67]. In these calculations, the LUXqed_plus_PDF4LHC15_nnlo_100 [68] PDF set is used. It combines the QCD PDFs, based on the PDF4LHC recommendations [69], with the photon PDFs to account for pure quantum electrodynamics effects. This allows the inclusion of

the background arising from a $\gamma\gamma$ initial state via t - and u -channel processes [70, 71] in the correction.

The $t\bar{t}$, $q_t W$, and WW backgrounds are simulated using POWHEG v2, with parton showering and hadronization described by PYTHIA, using the same PDF sets as for the DY samples. The $t\bar{t}$ background is normalized to the NNLO cross section calculated with TOP++ [72] assuming a top quark mass of 172.5 GeV, while the $q_t W$ simulation is normalized to the cross section computed up to next-to-next-to-leading logarithmic accuracy [73].

In addition to the WW samples, WZ and ZZ events are considered. As the analysis in the dimuon channel for 2016 is unchanged from ref. [21], samples simulated at leading order (LO) using the PYTHIA program along with the NNPDF2.3 PDFs at LO are used. For the analysis of the 2016 data in the electron channel, as well as the 2017 and 2018 data in both channels, samples are generated at NLO with POWHEG and MADGRAPH5_aMC@NLO version 2.2.2 [74], using the NNPDF3.1 PDF set. The process involving $\gamma^*/Z \rightarrow \tau^+\tau^-$ decays, which is not included in the POWHEG DY samples described above, as well as the W +jets process, are simulated at LO with the MADGRAPH5_aMC@NLO generator. Cross sections for these processes have been calculated up to NNLO with MCFM 6.6 [75–78].

The NNPDF3.1 NNLO PDF set was found to predict unphysical cross sections at very high dilepton invariant masses (>4 TeV). The DY and $t\bar{t}$ events generated with POWHEG are therefore reweighted so that the generated $m_{\ell\ell}$ distribution matches the prediction of the NNPDF3.0 NLO set that was used in ref. [21], which does not exhibit this undesired behavior. For the DY samples, these weights are applied before they are further corrected to the higher order cross section calculated with FEWZ described above. Thus, the DY background estimate is consistent among the three years of data taking. Other processes also generated with the NNPDF3.1 PDF set are less affected and have only small contributions to the overall background predictions. No reweighting is applied to them.

As the properties of high-mass events containing a spin-1 resonance can be studied by using the DY background samples, only one sample containing a Z'_{SSM} boson with a mass of 5000 GeV is generated for illustrative purposes. The RS G_{KK} samples with the graviton generated at different mass values from 250 to 4000 GeV have been generated for all three years. In all samples, the high-mass resonances decay to electron and muon pairs. These signal samples are generated using the PYTHIA 8.205 program with the NNPDF2.3 LO PDF set for 2016, and PYTHIA 8.230 with the NNPDF3.0 LO PDF set for 2017 and 2018 samples.

For the nonresonant signal models, samples for both CI and ADD are simulated at LO using PYTHIA 8.205 for 2016, and PYTHIA 8.230 for 2017 and 2018 samples. The NNPDF2.3 LO PDF set is used for 2016 samples while for 2017 and 2018, NNPDF3.1 NNLO is used. For consistency, the generated mass distribution of the 2017 and 2018 samples is reweighted to match that of the 2016 samples. The departures of these weights from unity are assigned as systematic uncertainties. In both cases, signal and DY background are simulated simultaneously to model interference effects.

The CI samples, as well as ADD samples for 2017 and 2018, are generated with a lower threshold of 300 GeV on the dilepton invariant mass, while for the ADD samples for 2016, a threshold of 1700 GeV is applied. In case of the CI samples, separate samples for the LL, LR+RL, and RR helicity states are generated, where the PYTHIA implementation of

this signal model summed the LR and RL currents into a single process. The generated events in these samples are therefore reweighted to recover the individual LR and RL models. Dedicated PYTHIA DY samples are produced with the same generator settings and subtracted from the signal samples to obtain the respective pure signal yields. In the case of ADD samples, NNLO calculations in QCD show that the correction factor to the LO cross section can be as high as 1.6 [79], and that it always exceeds 1.3 in the considered dilepton mass range. Furthermore, NLO electroweak corrections are not taken into account. This motivates applying the minimal correction factor of 1.3 in the analysis, which also allows a direct comparison to previous results [19].

During the 2016 and 2017 data taking, the CMS L1 trigger was affected by a slowly increasing shift of the reconstructed cluster time in the ECAL, predominantly at high η . This led to a loss of a fraction of events in the trigger, as these clusters could be assigned to the wrong LHC bunch crossing (“trigger prefiring”) [80]. As this effect is not present in simulation, simulated events in the dielectron channel are reweighted to account for this inefficiency.

The detector response is simulated using the GEANT4 [81] package. The presence of additional pp interactions in the same or adjacent bunch crossing observed in data (pileup) is incorporated into simulated events by including extra pp interactions that have been generated with PYTHIA. In the dielectron channel, simulated samples are reweighted to reproduce the same pileup distribution as measured in data (pileup reweighting). In the dimuon channel, the trigger, reconstruction, and identification efficiencies exhibit no significant pileup dependence, and no such reweighting is performed.

5 Lepton reconstruction and event selection

The electron and muon reconstruction algorithms remain close to those used in ref. [21], with a few updates implemented. In the electron channel, the 2016 data are reprocessed using an updated electron calibration that corrected for a drift in the energy response at very high energy. For the 2017 and 2018 data sets, there are some modifications to the criteria for both electron and muon identification and electron isolation, as well as for the overall event selection. These improve the treatment of the higher pileup and the selection efficiency for leptons with very high (several TeV) transverse momentum p_T .

5.1 Electron reconstruction and selection

To select dielectron events in the L1 trigger, events are required to contain at least two electron candidates. The p_T thresholds evolved with time, but never exceeded 25 GeV for the electron with the higher p_T and 17 GeV for the electron with the lower p_T . As a safeguard against cases where one of the electrons fails the L1 trigger, events containing at least one electron, jet, or tau lepton candidate passing the higher p_T thresholds at L1 are also considered at HLT level. In the HLT, dielectron events were collected with a trigger requiring two electrons with $p_T > 33$ GeV and $|\eta| < 2.5$ in 2016 and 2017. These electrons were also required to pass loose identification criteria using the shower shape in the calorimeter and the matching of a pixel detector track with the energy deposit. The p_T threshold was

lowered to 25 GeV in 2018, since the electron trigger was improved by making use of the upgraded pixel detector. Secondary trigger paths with progressively higher p_T thresholds and fewer selection requirements are employed to monitor the performance of the main trigger.

Electron candidates are reconstructed from energy clusters in the ECAL and tracks from the inner tracker. Typically, electrons lose some of their energy due to bremsstrahlung emission in the tracking detector, which is recovered by adding compatible energy deposits to the ECAL cluster. The final clusters are then associated geometrically with tracks to form electron candidates. As the measurement of the track parameters can be unreliable for high-energy electrons because of bremsstrahlung, the energy of the candidate is taken directly from the ECAL cluster without combination with track information. However, the direction of the electron used in the analysis is still obtained from the combined track and ECAL cluster information. This minor mis-reconstruction has a negligible effect on the dielectron mass measurement.

We select electron candidates with $p_T > 35$ GeV that satisfy $|\eta_C| < 1.44$ (ECAL barrel region) or $1.57 < |\eta_C| < 2.50$ (ECAL endcap region), where η_C is the pseudorapidity of the cluster of ECAL deposits making up the electron with respect to the nominal center of the CMS detector. The transition region $1.44 < |\eta_C| < 1.57$ is excluded since it leads to lower quality reconstructed clusters, owing mainly to inactive material consisting of services and cables exiting between the barrel and endcap calorimeters.

Electrons are required to pass a set of selection criteria optimized for the identification of high-energy electrons [82]. The lateral spread of energy deposits in the ECAL associated with the electron's cluster is required to be consistent with that of a single electron. The electron's track is required to be matched geometrically to the ECAL cluster and to be compatible with originating from the nominal interaction point. Energy deposits in the HCAL in the direction of the electron, corrected for noise and pileup, are required to be less than 5% of the electron's energy. Misreconstructed electrons, and electrons in jets, are suppressed by requiring that the electron be isolated in a cone of radius $\Delta R = \sqrt{(\Delta\eta)^2 + (\Delta\phi)^2} = 0.3$ in both the calorimeter and tracker [20]. Only well-measured tracks that are consistent with originating from the same vertex as the electron are included in the isolation sum. The efficiency of the trigger to select events with two electrons passing the analysis selection requirements, measured in data as discussed below, is at least 95% for barrel (endcap) electrons satisfying $p_T > 36(37)$ GeV in 2016, $p_T > 38(40)$ GeV in 2017, and $p_T > 27(29)$ GeV in 2018.

In the endcap region of the detector, there is a large background of events with hadronic jets misreconstructed as electrons, which comes from W+jets events and from events composed uniquely of jets produced through the strong interaction, referred to as QCD multijet events. To reduce this background, we require that at least one of the electrons be located in the barrel region. The subset of events with both electrons in the endcap region is expected to be overwhelmingly dominated by this background, and is used as a control region for the jet background estimate.

No requirement is made on the sign of electrons because of the increasing probability of charge misidentification for high-energy electrons, which would result in a significant efficiency loss from an opposite-sign selection. The fraction of same-sign events in DY

simulation was found to increase from about 1% at the Z boson peak to $\approx 10\%$ for masses of several TeV. In data, it was found to be consistent with this expectation.

The efficiency to trigger, reconstruct, and select an electron pair with invariant mass $m_{ee} = 1$ TeV within the detector acceptance is 72 (68)% for 2016 (2017 and 2018) for barrel-barrel events and 67, 60, and 67% for the three years, for barrel-endcap events. It remains stable within a few percent for larger masses. The lower efficiency for barrel-barrel events in 2017 and 2018 is caused by changes to the trigger making use of the upgraded pixel detector to control the trigger rate. The reduction for barrel-endcap events in 2017 is mostly due to trigger prefire. The total efficiency is estimated using simulated DY events, and the efficiencies of the various selection steps are compared in data and simulation using a method similar to that described in ref. [83]. Using high- p_T Z bosons, it is possible to probe the efficiencies up to $p_T = 1$ (0.7) TeV for electrons in the barrel (endcap) region, with a precision of less than 10%. Based on those measurements, a correction factor is applied to the trigger efficiency in simulation to model the lower p_T turn-on observed in data. No correction is found to be necessary for the offline selection.

5.2 Muon reconstruction and selection

For the selection of dimuon events, in the L1 trigger, events with at least one single muon with $p_T > 22$ GeV are accepted. At HLT, single-muon triggers requiring $p_T > 50$ GeV and $|\eta| < 2.4$ and without an isolation requirement were available during the whole data taking period. During 2017 and 2018, an upgraded version of the muon reconstruction in the HLT was deployed, and as a backup the algorithm used in 2016 was used in an HLT path requiring $p_T > 100$ GeV [84]. The backup trigger increased the overall trigger efficiency for dimuon events with invariant masses above 1 TeV by $\approx 1\%$. To collect an event sample unbiased by the trigger turn-on for a data normalization region around the Z boson mass ($60 < m_{\ell\ell} < 120$ GeV), a prescaled HLT path with a reduced pT threshold of 27 GeV was used. The average prescale value ranged from about 140 in 2016 to about 460 in 2018.

Muon candidates are reconstructed by combining hits in the inner tracking detector with those in the muon system. For muons with $p_T > 200$ GeV, dedicated reconstruction algorithms take into account radiative energy losses in the detector material [85, 86]. As no calorimeter information is used in the muon reconstruction, data corresponding to an integrated luminosity of about 3 fb^{-1} recorded with ECAL or HCAL in a degraded condition are included in the analysis of the dimuon final state. Muons are required to have $p_T > 53$ GeV, $|\eta| < 2.4$, and to pass a set of selection criteria optimized for high- p_T muons [19]. To reject muons produced inside jets, we require that the scalar p_T sum of all tracks identified to come from the same pp collision and within a cone of $\Delta R = 0.3$ around the muon candidate, excluding the muon candidate itself, does not exceed 10% of the p_T of the muon.

Dimuon candidates are formed from two muons with invariant mass $m_{\mu\mu} > 150$ GeV. While the searched-for neutral dilepton final states would decay to truly opposite-sign dileptons, in principle leptons with misreconstructed charge are usable (and are in fact used in the case of electrons, as described above). For muons, misreconstruction of the charge indicates poor resolution of the track fit and thus an unreliable p_T measurement. Therefore, the two muons are required to have opposite charge. As the charge misidenti-

cation probability is of the order of 10^{-4} for muon momenta of 2 TeV [86], this requirement has a negligible effect on the signal efficiency. The muon tracks are fit to a common vertex, which improves mass resolution at high mass. A loose requirement on the quality of the vertex fit rejects some residual background and potentially badly measured signal events (less than 1% in simulation). Backgrounds from cosmic ray muons are reduced to a negligible level by requiring that the three-dimensional angle between the two muons be less than $\pi - 0.02$. The remaining contribution of this background after the full selection for events containing muons with $p_T > 300$ GeV is less than 0.2%.

The trigger efficiency for dimuon events that pass these offline muon selection criteria has been measured in data using Z boson events. For all three years of data taking, it is above 99.3% for events where both muons are in the barrel region ($|\eta| < 1.2$) of the detector and above 99.0% if one or more muons are located in the endcaps ($|\eta| > 1.2$). Measured in data using Z events, the overall efficiency to trigger on, reconstruct, and identify muon pairs within the detector acceptance is 93%, with little dependence on the dimuon invariant mass.

Detailed studies of the muon reconstruction performance revealed a slight inefficiency for muons with $|\eta| > 1.6$, which increases with muon momentum, caused by electromagnetic showers in the detector material [86]. This effect is more pronounced in data than in simulation. This difference is included in a mass-dependent systematic uncertainty.

The dimuon mass resolution for events with high- p_T muons has been studied using highly Lorentz-boosted Z boson events. It was found that for events where at least one muon is in the endcap, the simulation predicted better mass resolution than observed in the data. To correct for this effect, the reconstructed dimuon mass for simulated events in this category is smeared by 15%, bringing data and simulation into good agreement.

The combined product of the acceptance and the efficiency as a function of mass is obtained from simulation for both dielectron and dimuon pairs. This product is shown in figure 1, separately for spin-1 and spin-2 particles. The values for the different years of data taking are averaged, weighted by the integrated luminosity of the data sets for each year. Mixtures of polynomials and exponential functions are used to parameterize the mass dependence of the product of the acceptance and the efficiency. The observed turn-on in the low-mass region is a consequence of the lepton p_T threshold and the p_T -dependent selection efficiency. For $m_{\ell\ell} > 200$ GeV, the reconstruction and selection efficiencies do not significantly depend on mass, and changes in the product of acceptance and efficiency are due to the changing acceptance as the angular distribution of the leptons changes. For the spin-2 RS graviton, the slight drop at high mass is related to the different production modes (gg and $q\bar{q}$) that lead to different angular distribution for the leptons. The fraction of the latter increases with mass and results in a slightly larger fraction of leptons emitted outside the detector acceptance.

5.3 Event disambiguation

In a small fraction of the events ($<1\%$), originating mostly from WZ and ZZ production, more than two leptons are present. If several dilepton pairs can be formed in the same event, and if at least one pair has a mass within 20 GeV of the Z boson mass, then the pair closest in mass to the Z boson mass is chosen. Otherwise, the pair with the two

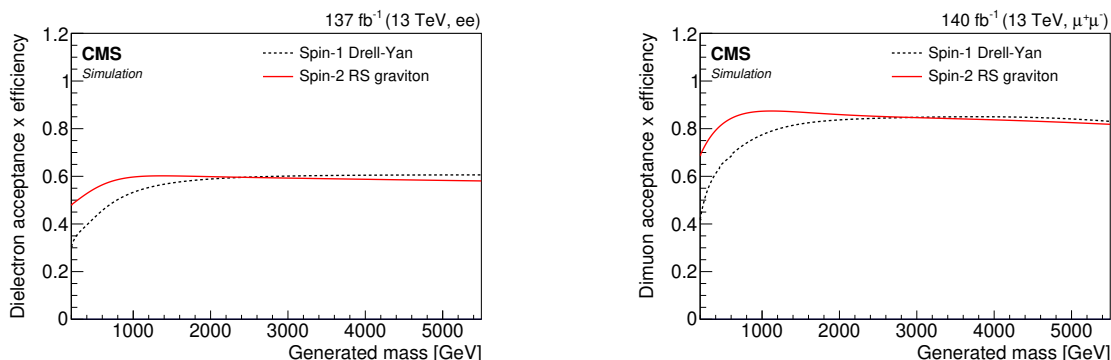


Figure 1. Product of the acceptance and the efficiency for (left) dielectron and (right) dimuon pairs as a function of generated mass in simulated events. The DY samples are used to represent spin-1 particles, and RS graviton samples are used for spin-2 particles.

highest- p_T leptons is selected. For dimuon events, the analysis has not been changed from the published result based on the 2016 data, and the pair with the two highest p_T muons is always selected [21]. Events with both a dimuon and dielectron pair that pass the event selection are very rare and both pairs are considered in the analysis.

For both the CI and ADD models, the sensitivity of the analysis can be improved by studying the angle of the outgoing negatively charged lepton with respect to the z axis in the Collins-Soper frame, given by

$$\cos \theta^* = \frac{p_z(\ell^+ \ell^-)}{|p_z(\ell^+ \ell^-)|} \frac{2(p_1^+ p_2^- - p_1^- p_2^+)}{m(\ell^+ \ell^-) \sqrt{m(\ell^+ \ell^-)^2 + p_T(\ell^+ \ell^-)^2}}. \quad (5.1)$$

Here p^\pm represents $\frac{1}{\sqrt{2}}(E \pm p_z)$, and the indices 1 and 2 correspond to the negatively and positively charged leptons, respectively. Events with same-sign electrons are included in the selected event sample, which introduces an ambiguity in the calculation of $\cos \theta^*$. To resolve the ambiguity, same-sign events in the dielectron channel are assumed to originate from charge misidentification. The measured charge of the electron with the lower value of η_C is assumed to be correct and the charge of the other electron is taken to be mismeasured and assigned to be the opposite. This results in the correct lepton being chosen in 76% of same-sign events, according to the simulation.

6 Background estimation

The dominant (and irreducible) source of background in the signal selection is the DY process. Further sources of high-mass dilepton events are $t\bar{t}$ and $q_t W$ production and diboson production (especially WW events). In addition, both QCD multijet events and W +jets events can be reconstructed as dilepton events if jets or nonisolated leptons are identified as isolated leptons; this category is called “jet misidentification” below.

The DY background shape is estimated directly from the POWHEG samples described above, including the mass-dependent higher-order corrections to the cross section. For the

$DY \rightarrow \tau\tau$ process, the MADGRAPH5_aMC@NLO sample is used. Given the small size of this background, no mass-dependent corrections are applied. The other backgrounds, with the exception of the jet misidentification backgrounds, are also estimated from simulation. The second-largest background contribution originates from $t\bar{t}$ events and is estimated from the POWHEG samples. The simulation of this process is validated in a data control region containing an $e\mu$ pair passing the same lepton requirements as discussed above and is found to describe both the shape of the mass distribution and the event yield observed in data, within uncertainties.

Backgrounds arising from jets misidentified as electrons are estimated from data control regions enriched in QCD multijet events with the methods described in ref. [19]. Similar methods are used to evaluate the background contributions from jets or nonisolated muons to the sample of selected muons. Even though the uncertainty in these estimates is as high as 50% for the entire mass range, this background has a negligible effect on the results of the analysis, as its contribution to the overall event yield is about 1–3%. The jet background estimate is found to be independent of $\cos\theta^*$ and is therefore scaled by 0.5 when the event sample is split into $\cos\theta^* < 0$ and ≥ 0 in the nonresonant interpretation.

Finally, the combined background shape is normalized to the data in the control region around the Z boson mass ($60 < m_{\ell\ell} < 120$ GeV). For the 2017 and 2018 data, the DY simulation generated with the NNPDF3.1 NNLO PDF set does not accurately describe the Z boson p_T spectrum at low p_T . The simulated events are therefore reweighted to match the prediction obtained with the NNPDF3.0 NLO PDF, as used for the 2016 samples. For the dimuon channel, a prescaled trigger with a muon p_T threshold of 27 GeV was used to collect events in this region. The corresponding offline threshold on the muon p_T is 30 GeV. To calculate the normalization factors, the numbers of events in that region are multiplied by the corresponding trigger prescale factor. In the electron channel the normalization factor is 0.95, independent of the year of data taking. In the dimuon channel, these factors are 0.97 for 2016, 1.03 for 2017, and 1.00 for 2018 data.

7 Systematic uncertainties

Various effects can impact the shape or the normalization of the dilepton invariant mass distribution and lead to systematic uncertainties in the signal and background estimates.

One source of uncertainty describes possible residual systematic effects leading to mis-modeling in the simulation of the lepton selection efficiency and momentum measurements at high mass, which are not absorbed in the normalization at the Z boson peak. These uncertainties are estimated from measurements performed with on-shell Z bosons with large transverse boost and measured up to 1 TeV in electron p_T and above 2 TeV in muon momentum. High-energy cosmic ray muons are also used to study the muon energy scale [86].

Based on these studies, the overall event selection efficiency including trigger, reconstruction, and identification is assigned a relative uncertainty of 6% for barrel-barrel and 8% for barrel-endcap events in the dielectron channel, while an uncertainty of 1–2% is assigned everywhere for the dimuon channel. As discussed in section 5, a loss of efficiency for very energetic muons caused by electromagnetic showers in the detector material was

observed. As this effect is significantly stronger in data compared to simulations, an additional mass-dependent, one-sided uncertainty is assigned. Its magnitude is the largest in 2016 data where it reaches -1.0 (-6.5)% at $m_{\mu\mu} = 4$ TeV for barrel-barrel (barrel-endcap plus endcap-endcap) events. It is -2% or smaller in other years [86]. The difference in the uncertainty between the years is due to the limited size of the data control samples.

The uncertainty in the mass scale is 2 (1)% for dielectron pairs in the barrel-barrel (barrel-endcap) category. For dimuon events, potential biases in the mass scale are studied using the generalized endpoint method [86]. The associated uncertainty is 1 (3)% in the barrel-barrel (barrel-endcap plus endcap-endcap) category for 2016, independent of mass. In 2017 and 2018, a mass-dependent uncertainty is assigned that reaches 1–2% at $m_{\mu\mu} = 5$ TeV.

For dimuon events, an uncertainty in the mass resolution of 15% is assigned for 2016 and 8.5% for 2017 and 2018, based on the studies discussed in section 5. The difference in the uncertainty between the years is the result of different parameterizations of the mass resolution being chosen. The uncertainty in the dielectron mass resolution is negligible.

The uncertainty in the pileup reweighting procedure in the dielectron channel is evaluated by recalculating the weights, shifting the assumed total inelastic cross section by 4.6% around the nominal value [87]. The resulting changes in the event yield estimates are below 0.6%.

The uncertainty in the trigger prefiring rate in the forward region of the ECAL endcap in 2016 and 2017 is 20%, resulting in a 2–3% uncertainty in the acceptance for dielectron events in which one electron is in the endcap for 2017. Averaged over the full data set, the uncertainty is well below 1%.

Theoretical uncertainties in the DY cross section at high mass related to higher-order corrections and PDF uncertainties grow with mass and reach 20% at $m_{\ell\ell} = 6$ TeV. Here, the PDF uncertainty is determined with the PDF4LHC procedure [69] using replicas of the NNPDF3.0 PDF set. The contribution from other backgrounds estimated from simulations is mostly relevant for masses below 1–2 TeV, and a 7% uncertainty is applied based on the uncertainties in the cross section calculations of the individual processes.

The estimate for the background from jet misidentification (W+jets, QCD), obtained from data, is assigned a 50% uncertainty in both dimuon and dielectron channels for all years. These estimates are based on the validation of the method in a control region enriched in events with one genuine electron and one misidentified electron in the dielectron channel, and on uncertainties in the measurement of the misidentification rate at high mass in the dimuon channel. The stability of the analysis results against potential further uncertainties in the extrapolation of this background estimate to the highest mass values has been tested and the effect on the results was found to be negligible.

Source	Uncertainty
Electron selection efficiency	6–8%
Muon selection efficiency	1–2% (two-sided), 0–6.5% (one-sided)
Mass scale uncertainty	0–3%
Dimuon mass resolution uncertainty	8.5–15%

Table 2. Sources of systematic uncertainties considered in the search for resonant signals and their relative magnitude.

The uncertainty in the Z peak normalization factor in the dielectron channel is 1% in 2016 and 2 (4)% for barrel-barrel (barrel-endcap) events for 2017 and 2018, driven by the typical electron p_T in this region being close to the trigger threshold. It is 5% in the dimuon channel for all three years of data taking, arising from the use of a trigger, whose prescale changed with instantaneous luminosity, to collect the Z boson sample.

The uncertainties arising from the limited sizes of the simulated background and signal samples affect the results differently for the resonant and nonresonant signals. In the resonant case they are accounted for in the uncertainty in the parameters in the background parametrization discussed below. For nonresonant signals they are included as a systematic uncertainty in the background and signal yield estimates.

For nonresonant signals, an additional uncertainty is assigned to the reweighting of the 2017 and 2018 samples to match the 2016 PDF set. The size of this uncertainty is mass dependent and reaches 30% at a mass of 5 TeV. The impact of this uncertainty on the limits on the model parameters Λ and Λ_T in these signal models is as large as 5%. As no signal simulation is used in the resonant case, it is unaffected by this uncertainty.

In the statistical interpretation for resonant signals, the signal is normalized to the data at the Z boson peak and the backgrounds are normalized to the data in the mass windows around the resonance mass. Uncertainties in the background normalization are taken into account with an overall statistical uncertainty and any remaining uncertainties in the background shape are covered by it. Therefore, only uncertainties in the signal modeling whose impact on the analysis depend on the dilepton mass have to be considered in this case. PDF uncertainties in the signal cross section are considered to be theoretical uncertainties and are not included here. These uncertainties are summarized in table 2.

For the limits on nonresonant signals and the measurement of $R_{\mu^+\mu^-/e^+e^-}$, the full set of uncertainties is taken into account. The full set of uncertainties is also taken into account in the uncertainty bands for data to simulation comparisons. The impact of these uncertainties on the background estimate for different mass thresholds is shown in table 3.

8 Results

The invariant mass distributions of electron and muon pairs are shown in figure 2, combining the 2016–2018 data sets. For illustration, simulated G_{KK} and Z'_{SSM} signals with masses close to the exclusion sensitivity of the analysis are shown.

Uncertainty source	Impact on background [%]			
	$m_{\ell\ell} > 1 \text{ TeV}$		$m_{\ell\ell} > 3 \text{ TeV}$	
	ee	$\mu\mu$	ee	$\mu\mu$
Lepton selection efficiency	6.8	0.8	6.4	1.3
Muon trigger efficiency	—	0.9	—	0.9
Mass scale	7.0	2.7	15.4	2.4
Dimuon mass resolution	—	0.1	—	0.6
Pileup reweighting	0.3	—	0.5	—
Trigger prefiring	0.5	—	0.2	—
PDF	3.7	3.0	9.4	10.2
Cross section for other simulated backgrounds	0.6	0.8	0.2	0.4
Z peak normalization	2.3	5.0	2.0	5.0
Simulated sample size	0.4	0.4	1.3	1.6

Table 3. Systematic uncertainties considered in the search for nonresonant signals. The relative impact of the uncertainties on the background yield estimates is shown for two dilepton invariant mass thresholds, 1 and 3 TeV. The uncertainty in the jet misidentification background has a negligible effect on the overall background estimate and is not listed.

Agreement is observed between the data yields and the expected background, which is quantified in section 9, although a slight excess of events is seen in the dielectron channel for masses above 1.8 TeV. Careful inspection of those events did not reveal any pathologies. Four events are observed with mass above 3 TeV, two each in the dielectron and dimuon channels. The measured masses are 3.35 and 3.47 TeV in the dielectron channel and 3.07 and 3.34 TeV in the dimuon channel.

Table 4 presents the observed and expected number of events for various mass ranges for the dielectron and dimuon pairs. The uncertainty in the total background is calculated taking into account correlations in the uncertainties among the different background sources. No jet background estimate is available in the dimuon channel for $60 < m_{\ell\ell} < 120 \text{ GeV}$, since the data in this control region are collected with the prescaled trigger. However, this background is negligible in this mass range given the large cross section for the Z boson resonance.

The mass distributions are shown again in figure 3, split into the two bins in $\cos\theta^*$ used in the search for nonresonant signals, and using the same mass bins as those used in the statistical interpretation for the CI signal, as described in section 9.2. A CI signal from the LR model is shown to illustrate the improved signal-to-background ratio in the $\cos\theta^* < 0$ bin for these types of signals.

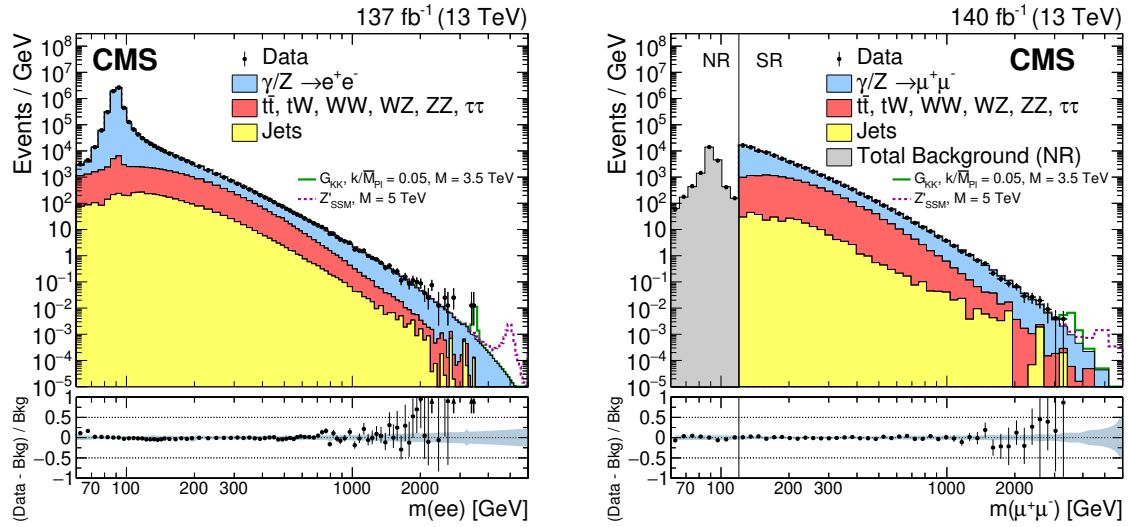


Figure 2. The invariant mass distribution of pairs of (left) electrons and (right) muons observed in data (black dots with statistical uncertainties) and expected from the SM processes (stacked histograms). For the dimuon channel, a prescaled trigger with a p_T threshold of 27 GeV was used to collect events in the normalization region (NR) with $m_{\mu\mu} < 120$ GeV. The corresponding offline threshold is 30 GeV. Events in the signal region (SR) corresponding to masses above 120 GeV are collected using an unprescaled single-muon trigger. The bin width gradually increases with mass. The ratios of the data yields after background subtraction to the expected background yields are shown in the lower plots. The blue shaded band represents the combined statistical and systematic uncertainties in the background. Signal contributions expected from simulated G_{KK} and Z'_{SSM} resonances with masses of 3.5 and 5 TeV, respectively, are shown.

9 Statistical interpretation

Limits are calculated at 95% confidence level (CL) with Bayesian techniques known to have good frequentist coverage properties [88], using the framework developed for statistically combining Higgs boson searches [89], which is based on the ROOSTATS package [90]. For the signal cross section, we use a positive uniform prior, while the nuisance parameters for the uncertainties in dilepton efficiencies, resolution, and scale are modeled with log-normal priors. Two different approaches are followed for the statistical interpretation of the results. To search for resonances in the dilepton invariant mass spectrum, an unbinned maximum likelihood fit is performed to the $m_{\ell\ell}$ spectrum in data, while for nonresonant signals a binned likelihood in $m_{\ell\ell}$ is constructed. In both cases the likelihood fit is done simultaneously for dielectron and dimuon events, years of data taking, and the $|\eta|$ categories, within the two channels. To further increase the sensitivity to some of the models, the event sample in each of these categories is split into two bins, $\cos\theta^* < 0$ and $\cos\theta^* \geq 0$, in the nonresonant case. The likelihoods for all subcategories are then combined to obtain the results. When the electron and muon channels are combined, we assume that branching fractions of these two signals are the same.

m_{ee} range [GeV]	Observed yield	Total background	DY	Other prompt lepton backgrounds	Jet mis- identification
60–120	28194452	28200000 ± 710000	28000000 ± 710000	153000 ± 8000	11300 ± 5700
120–400	912504	942000 ± 37000	744000 ± 31000	179000 ± 11000	18900 ± 9500
400–600	16192	16400 ± 770	10900 ± 477	4910 ± 340	534 ± 267
600–900	3756	3660 ± 190	2800 ± 150	757 ± 52	103 ± 51.4
900–1300	704	696 ± 47	590 ± 42	89.8 ± 6.8	16.0 ± 8.0
1300–1800	135	131 ± 12	118 ± 11	11.0 ± 1.0	2.82 ± 1.41
>1800	44	29.2 ± 3.6	26.8 ± 3.5	1.60 ± 0.22	0.82 ± 0.41
$m_{\mu\mu}$ range [GeV]	Observed yield	Total background	DY	Other prompt lepton backgrounds	Jet mis- identification
60–120	164075	166000 ± 9360	165000 ± 9300	994 ± 89	—
120–400	977714	1050000 ± 60400	836000 ± 47000	210000 ± 19000	3070 ± 1540
400–600	24041	26100 ± 1580	16700 ± 970	9120 ± 820	212 ± 106
600–900	5501	5610 ± 337	4170 ± 250	1370 ± 120	74.0 ± 37.0
900–1300	996	1050 ± 65	863 ± 52	169 ± 15	19.9 ± 10.0
1300–1800	183	195 ± 13	169 ± 10	19.9 ± 1.8	6.7 ± 3.4
>1800	42	44.3 ± 3.4	38.7 ± 2.5	3.3 ± 0.3	2.2 ± 1.1

Table 4. Observed and expected background yields for different mass ranges in the (upper) dielectron channel and (lower) dimuon channel. The sum of all background contributions is shown as well as a breakdown into the three main categories. The quoted uncertainties include both the statistical and the systematic components.

9.1 Search for resonant signals

The signal is modeled with the convolution of a Breit-Wigner function to model the intrinsic decay width of the resonance and a double-sided Crystal Ball function [91] to model the mass-dependent mass resolution, except for 2016 data in the muon channel, where a Gaussian function with exponential tails to either side is used [92]. Selection efficiency, mass resolution, and mass scale are taken into account as nuisance parameters in the signal description. The parameters are treated as uncorrelated between the different channels. The relative mass scale between them is the only uncertainty with a noticeable impact. The background is modeled with two different functions for the two dilepton channels. In the dielectron channel it is given by:

$$\begin{aligned}
& m^\kappa \exp\left(\sum_{i=0}^3 \alpha_i m^i\right), & \text{if } m \leq m_{\text{threshold}}, \\
& m^\lambda \exp\left(\sum_{i=0}^3 \beta_i m^i\right), & \text{if } m > m_{\text{threshold}},
\end{aligned} \tag{9.1}$$

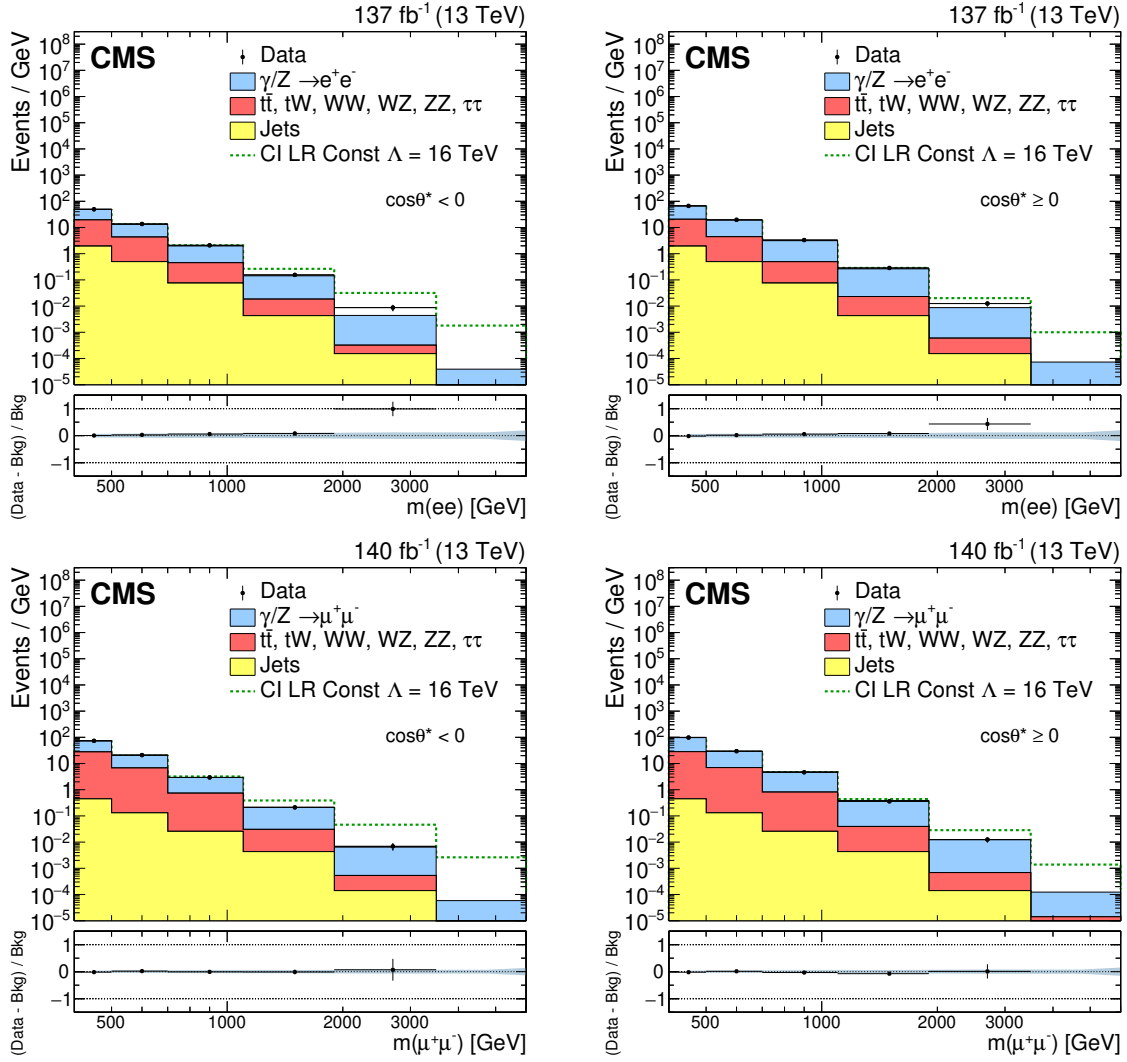


Figure 3. The invariant mass distribution of pairs of (upper) electrons and (lower) muons observed in data (black dots with statistical uncertainties) and expected from simulated SM processes (stacked histograms) for (left) $\cos\theta^* < 0$ and (right) $\cos\theta^* \geq 0$. The bin width gradually increases with mass. The ratios of the data yields after background subtraction to the expected background yields are shown in the lower plots. The blue band represents the combined statistical and systematic uncertainties in the background. The signal contributions expected from the constructive LL CI model with $\Lambda = 16$ TeV are shown as dashed green lines.

while for the dimuon channel the following functional form is used:

$$\begin{aligned}
 & m^\mu \exp\left(\sum_{i=0}^2 \gamma_i m^i\right), & \text{if } m \leq m_{\text{threshold}}, \\
 & m^\nu \exp\left(\sum_{i=0}^3 \delta_i m^i\right), & \text{if } m > m_{\text{threshold}}.
 \end{aligned} \tag{9.2}$$

Here m is the dilepton invariant mass; the other parameters do not represent physical quantities. In the dimuon channel, these functions are required to be continuously differentiable at the transition point $m_{\text{threshold}}$ between the low- and high-mass parameterizations, which is left free in the fits and ranges from 350 to 750 GeV. In the electron channel, $m_{\text{threshold}}$ is set to 600 GeV. They are first fit to the sum of the background estimates, the vast majority of which comes from simulation, as described in section 6, for masses above 150 GeV. In the limit calculation, the resulting background shapes are then normalized to data within mass windows. The function parameters are treated as nuisance parameters and left floating in the limit calculation. Their initial values are set to those obtained from the fit to the background estimates and they are constrained by log-normal priors whose widths are set to the uncertainties obtained from the same fits. Correlations between the parameters are not considered by these constraints.

The limits are calculated in a mass window of ± 4 times the signal width, defined as the sum of intrinsic width and mass resolution, with this window being symmetrically enlarged until there is a minimum of 100 data events in it. This sets an upper limit of 10% on the statistical uncertainty in the local background estimate in the mass window. It is chosen to be large enough to dominate the expected systematic uncertainties in the background shape at high mass, which do not have to be considered explicitly for this reason. To allow the background yield to be constrained by its statistical uncertainties, a log-normal prior with a width of three times these uncertainties is used.

The results have been found to be largely robust against the impact of any remaining uncertainty in the background shape, as well as the choice of background shape parameterization for the full range of considered resonance masses, in the case of a narrow resonance. However, for the largest signal width hypothesis considered, 10%, a significant bias in the limit values for low resonance masses from the choice of the parameterization can occur. Therefore, no results below a resonance mass of 700 GeV are shown for this width.

The parameter of interest is chosen to be the ratio of the cross section for dilepton production via a Z' boson to the observed cross section for $Z \rightarrow \ell\ell$ in the data control region of $60 < m_{\ell\ell} < 120$ GeV, R_σ :

$$R_\sigma = \frac{\sigma(\text{pp} \rightarrow Z' + X \rightarrow \ell\ell + X)}{\sigma(\text{pp} \rightarrow Z + X \rightarrow \ell\ell + X)}. \quad (9.3)$$

This variable has reduced dependence on the theoretical predictions for the Z' cross section and on systematic uncertainties that are correlated between high and low $m_{\ell\ell}$, such as trigger and selection efficiencies, for which only uncertainties in their stability at high mass remain. To ease comparison with the predicted cross section for various signal models, the limits on R_σ are presented multiplied by the theoretical prediction for $\sigma(\text{pp} \rightarrow Z + X \rightarrow \ell\ell + X)$ of 1928 pb, calculated at NNLO in QCD and NLO in EWK theory with the FEWZ 3.1 program [67].

The resulting limits for a narrow resonance with an intrinsic width of 0.6% are shown in figure 4. At high mass, where the background estimate approaches zero, the limits are independent of the resonance width. The limits are therefore applicable for both Z'_{SSM} and Z'_ψ . The observed limits are consistent with the expectation from SM backgrounds. The

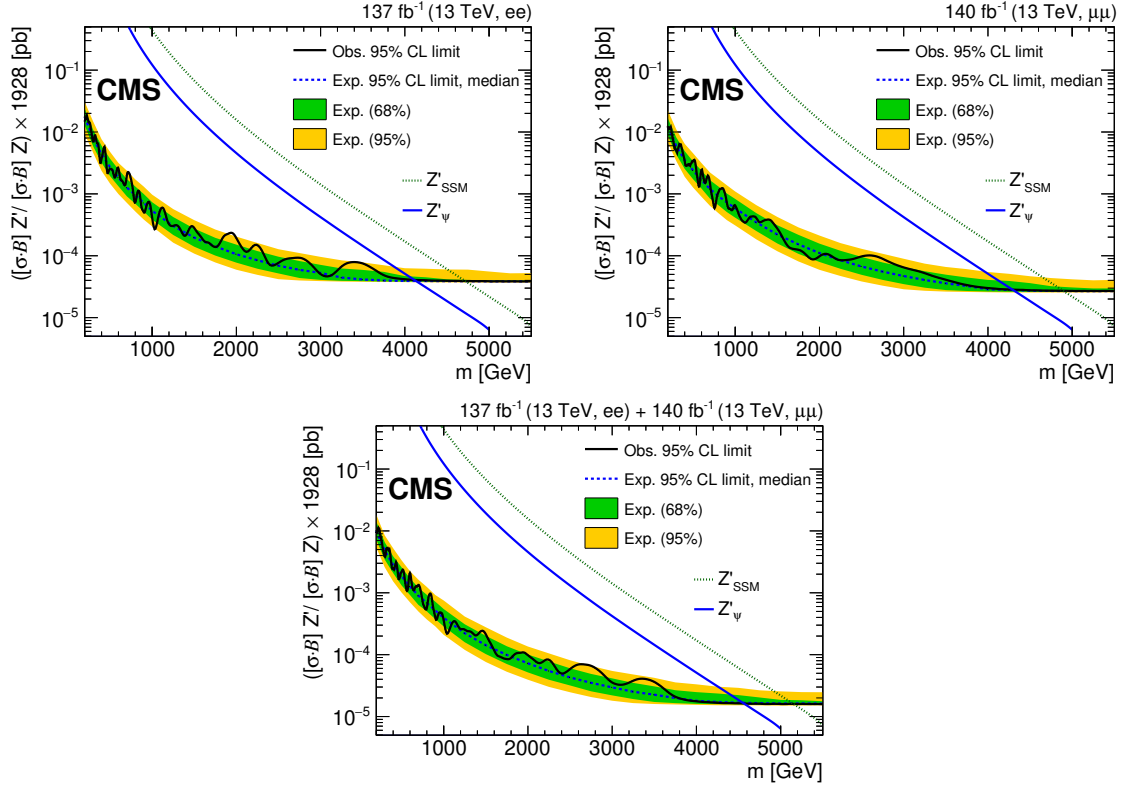


Figure 4. The upper limits at 95% CL on the product of the production cross section and the branching fraction for a spin-1 resonance with a width equal to 0.6% of the resonance mass, relative to the product of the production cross section and the branching fraction of a Z boson, multiplied by the theoretical value of $\sigma(pp \rightarrow Z + X \rightarrow \ell\ell + X)$ of 1928 pb, for (top left) the dielectron channel, (top right) the dimuon channel, and (bottom) their combination. The shaded bands correspond to the 68 and 95% quantiles for the expected limits. Simulated predictions for the spin-1 Z'_{SSM} and Z'_ψ resonances are shown for comparison.

Channel	Z'_{SSM}		Z'_ψ	
	Obs. [TeV]	Exp. [TeV]	Obs. [TeV]	Exp. [TeV]
ee	4.72	4.72	4.11	4.13
$\mu\mu$	4.89	4.90	4.29	4.30
ee + $\mu\mu$	5.15	5.14	4.56	4.55

Table 5. The observed (Obs.) and expected (Exp.) 95% CL lower limits on the masses of spin-1 Z'_{SSM} and Z'_ψ bosons, assuming a signal width of 0.6 (3.0)% of the resonance mass for Z'_ψ (Z'_{SSM}).

expected and observed mass limits in the Z'_{SSM} and Z'_ψ models are shown in table 5. For the combination of the dielectron and dimuon channels, the observed limits are 5.15 TeV for the Z'_{SSM} and 4.56 TeV for the Z'_ψ , well above the highest mass event observed in the data. For these models, the ATLAS Collaboration has recently set similar limits [26].

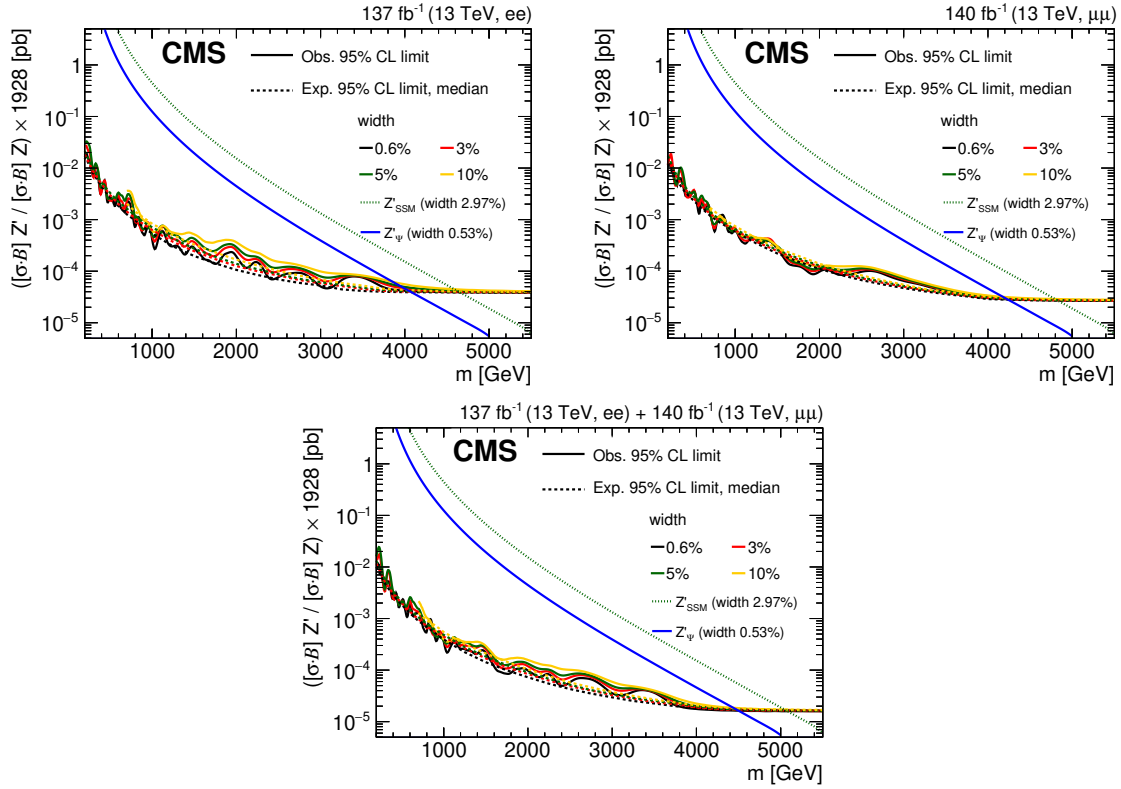


Figure 5. The upper limits at 95% CL on the product of the production cross section and the branching fraction for a spin-1 resonance, for widths equal to 0.6, 3, 5, and 10% of the resonance mass, relative to the product of the production cross section and the branching fraction for a Z boson, multiplied by the theoretical value of $\sigma(pp \rightarrow Z + X \rightarrow \ell\ell + X)$ of 1928 pb, for (upper left) the dielectron channel, (upper right) the dimuon channel, and (lower) their combination. Theoretical predictions for the spin-1 Z'_{SSM} and Z'_{ψ} resonances are also shown.

Limits are computed for several hypotheses for the resonance width. In figure 5, expected and observed limits are shown for 0.6% (identical to curves in figure 4), 3, 5, and 10%. As discussed above, lower thresholds on the resonance mass are chosen to avoid biasing the limits due to the choice of background shape for the wider resonances. The thresholds are 200 GeV for 0.6, 3, and 5%, and, as mentioned earlier, 700 GeV for 10% width. The limit curves for the different widths converge for high resonance masses, where the background expectation approaches zero. For lower masses, the limits become weaker with increasing width as wider resonances are not as easily distinguished from the background. The features in the observed limit curves corresponding to statistical fluctuations in the observed data are smoothed out for wider resonances.

The limits in the narrow width approximation are interpreted as limits on the generalized couplings in the (c_d, c_u) plane as shown in figure 6 for the combination of the dielectron and dimuon channels. The closed colored curves show the observed lower limits in the three classes of models (GSM, LRS, and E_6), as functions of the mixing angle within each class. For a given point in the plane, a lower mass limit can be obtained with the

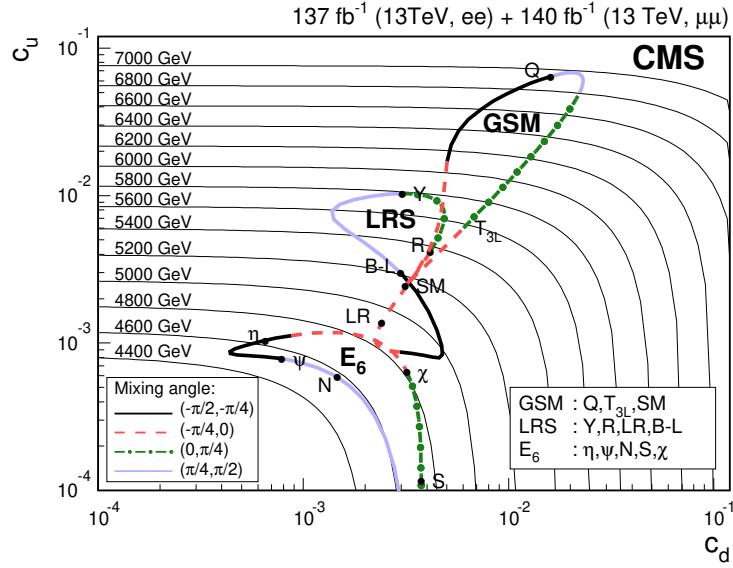


Figure 6. Lower limits in the (c_d, c_u) plane obtained by recasting the combined limit at 95% CL on the Z' boson cross section for narrow resonances from dielectron and dimuon channels. For a given Z' boson mass, the cross section limit results in a solid thin black line. These lines are labeled with the relevant Z' boson masses. The closed contours representing the GSM, LRS, and E_6 model classes are composed of thick curve segments. Each point on a segment corresponds to a particular model, and the location of the point gives the mass limit on the relevant Z' boson. As indicated in the lower left legend, the curve segment styles correspond to ranges of the particular mixing angle, for each considered model. The lower right legend indicates constituents of each model class.

help of the thin black lines, which are obtained from the observed limit and the ratio of parton luminosities [42]. The observed limit exceeds 4.5 TeV for all models considered and reaches close to 7 TeV in the GSM class of models.

To quantify any discrepancies between the observed data and the background estimates, the p -value for the background-only hypothesis is calculated, as a function of resonance mass hypothesis, following the methodology described in ref. [93]. The same mass windows as for the limit calculation are used and the resulting p -values therefore depend on the assumed resonance width. Similar to the exclusion limits computed for different width hypotheses, lower mass thresholds are determined based on the potential bias in the fitted number of signal events introduced by the choice of the background parameterization. As this extraction of signal yields is found to be more susceptible to these biases, the resulting thresholds are higher than for the limit setting. The threshold is 200 GeV for a width of 0.6%, 600 GeV for a width of 3%, and 1 TeV for widths of 5 and 10%.

The results are shown in figure 7. In the narrow width case, the most significant deviations in the dimuon channel are observed at 520 GeV with a local p -value of 0.0074, corresponding to a local significance of 2.4 standard deviations. The local p -value corresponds to the hypothesis in which a peak at the observed location (520 GeV in this case) is predicted. In both the dielectron channel and the combination, the largest deviation is located at 710 GeV, with local p -values of 0.0010 and 0.0014, respectively, corresponding to local sig-

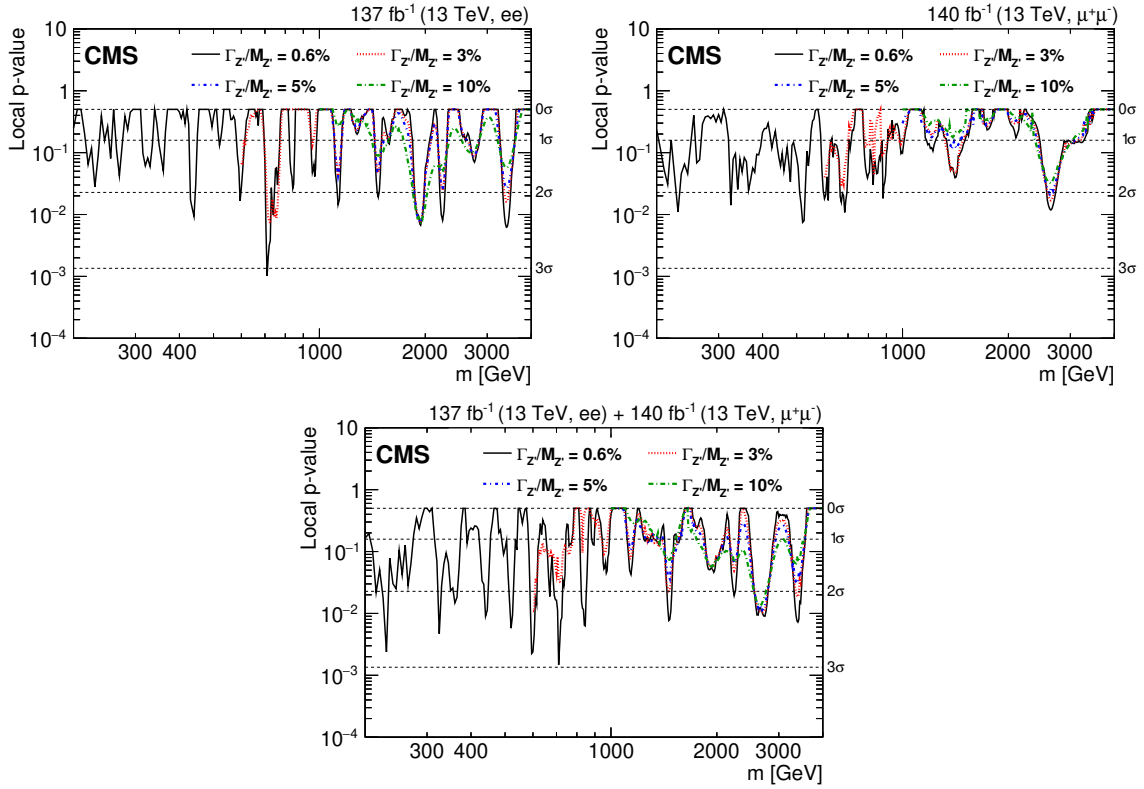


Figure 7. The observed local p -value for a given resonance mass hypothesis for (upper left) the dielectron channel, (upper right) the dimuon channel, and (lower) their combination, as a function of the dilepton invariant mass. The four different lines correspond to different signal width hypotheses.

nificances of 3.1 and 3.0 standard deviations. By repeating the p -value scan on an ensemble of toy data sets generated from the background parameterizations, a global p -value can also be computed, giving the probability of finding a local p -value as great or greater than that observed, anywhere in a specified mass range. The global p -value for the combination of the two channels is 0.76 in the mass range 500 to 5500 GeV. For such one-tailed tests (for which a p -value of 0.5 corresponds to 0 standard deviations) this formally corresponds to -1.4 standard deviations. Focusing on the vicinity of the observed fluctuation, the global p -value in the mass range 700 to 800 GeV is 0.19, corresponding to 0.9 standard deviations.

In addition to the spin-1 resonances considered thus far, limits are also calculated for spin-2 resonances and the results are shown in figure 8. The calculation is performed assuming a narrow width and differs from that for spin-1 resonances only in the detector acceptance for the different spin configurations. The limits in the spin-2 case are more stringent at low mass as the leptons are produced more centrally in the detector, which increases the acceptance, especially in the electron channel where events with two electrons in the endcaps are rejected. Lower mass limits for three example values of the coupling parameter $k/\overline{M}_{\text{Pl}}$ of 0.01, 0.05, and 0.10, corresponding to intrinsic widths of 0.01, 0.36, and 1.42%, are shown in table 6 and range from slightly over 2 to almost 5 TeV. This improves the previous CMS limits by about 370 to 530 GeV.

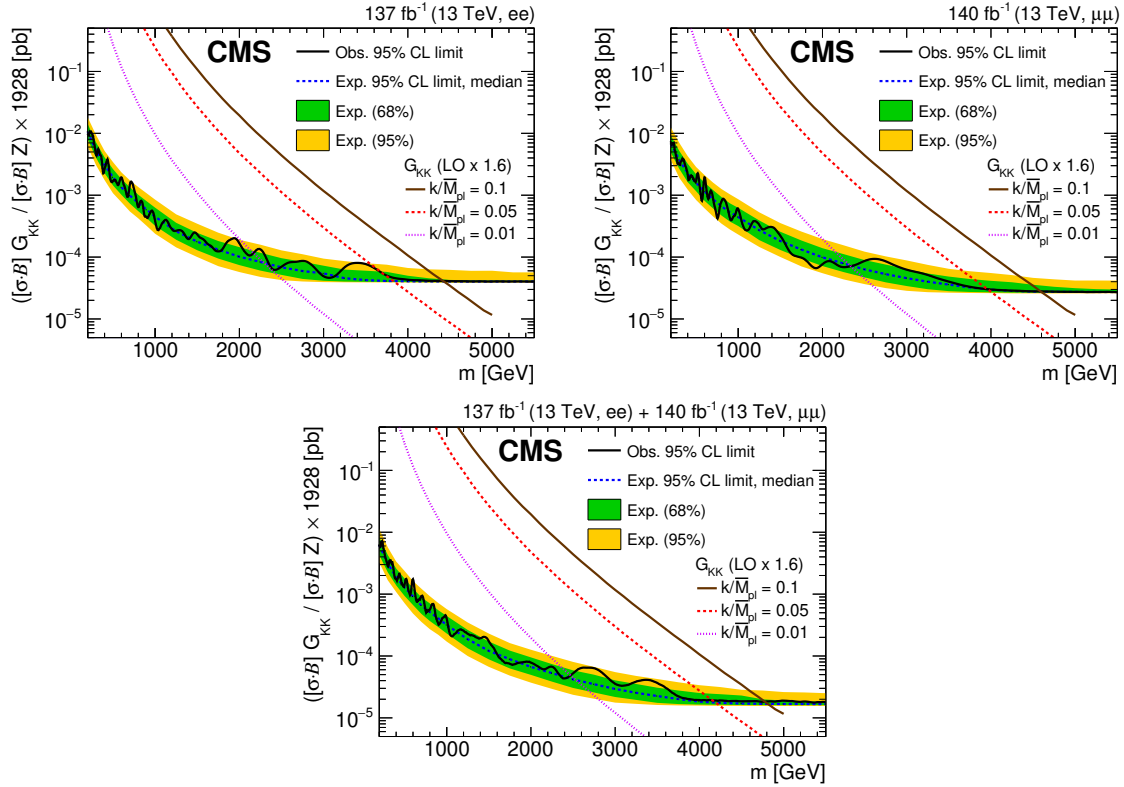


Figure 8. The upper limits at 95% CL on the product of the production cross section and the branching fraction for a spin-2 resonance, relative to the product of the production cross section and the branching fraction of a Z boson, multiplied by the theoretical value of $\sigma(pp \rightarrow Z + X \rightarrow \ell\ell + X)$ of 1928 pb, for (upper left) the dielectron channel, (upper right) the dimuon channel, and (lower) their combination. The shaded bands correspond to the 68 and 95% quantiles for the expected limits. Theoretical predictions for the spin-2 resonances for widths equal to 0.01, 0.36, and 1.42% corresponding to coupling parameters k/\overline{M}_{Pl} of 0.01, 0.05, and 0.10, respectively, are shown for comparison.

Channel	$k/\overline{M}_{Pl} = 0.01$		$k/\overline{M}_{Pl} = 0.05$		$k/\overline{M}_{Pl} = 0.1$	
	Obs. [TeV]	Exp. [TeV]	Obs. [TeV]	Exp. [TeV]	Obs. [TeV]	Exp. [TeV]
ee	2.16	2.29	3.70	3.83	4.42	4.43
$\mu\mu$	2.34	2.32	3.96	3.96	4.59	4.59
ee + $\mu\mu$	2.47	2.53	4.16	4.19	4.78	4.81

Table 6. The observed and expected 95% CL lower limits on the masses of spin-2 resonances for widths equal to 0.01, 0.36, and 1.42%, corresponding to coupling parameters k/\overline{M}_{Pl} of 0.01, 0.05, and 0.10.

The results are also interpreted in the context of the simplified DM models described in section 3. For this purpose, dilepton production cross sections in these models are calculated at NLO in QCD using the DMSIMP implementation [49] of the simplified model in MADGRAPH5_aMC@NLO version 2.6.5 [74]. The partial and total mediator decay widths are included using the MADWIDTH package [94] and are calculated at LO. In case of the axial-vector scenario with coupling $g_{\text{DM}} = 1.0$ and $g_q = g_\ell = 0.1$, and assuming $m_{\text{DM}} > m_{\text{med}}/2$, the production cross section for electron or muon pairs within detector acceptance ranges from approximately 100 pb for m_{med} around 200 GeV to 0.1 fb for m_{med} around 4 TeV.

In addition to the size of the mediator's coupling to leptons, the sensitivity of this search also depends on m_{DM} relative to m_{med} . For small m_{DM} , the mediator will dominantly decay to DM particles. This decay becomes suppressed for $m_{\text{DM}} > m_{\text{med}}/2$, enhancing the decays into leptons and increasing the sensitivity of the dilepton channel. Additionally, the decay width of the mediator is larger if the decay into DM particles is available. Therefore, the width of the mediator changes over the $m_{\text{med}}-m_{\text{DM}}$ plane. Expected and observed limits are therefore calculated for widths between 0.5 and 3.5% in steps of 0.25%. To determine if a point in the mass plane is excluded, the limit obtained with the width closest to the theoretical value for that point is used. The resulting exclusion contours are shown in figure 9 for both the vector and axial-vector coupling models. The limits are strongest for large values of m_{DM} where the decay width of the mediator is small. Here, mediators with masses below 1.92 (4.64) TeV are excluded in the vector (axial-vector) model. For $m_{\text{DM}} = 0$, the limit is 3.41 TeV in the axial-vector model. In the vector model, the largest excluded mediator mass for $m_{\text{DM}} = 0$ is 1.04 TeV. However, due to fluctuations in the observed limit, not all masses below that value are excluded. The ATLAS Collaboration has recently set similar limits [95].

9.2 Search for nonresonant signals

To set limits on nonresonant signal models, the parameter of interest in the statistical analysis is the ratio μ of observed to predicted signal cross section. The dilepton mass spectra are divided into multiple exclusive bins. The bin width is optimized separately for the CI and ADD models based on the expected limits. For CI, bins with lower edges of 400, 500, 700, 1100, 1900, and 3500 GeV are used. For the ADD model, the most sensitive part of the invariant mass spectrum, $m_{\ell\ell} > 1.8$ TeV, is subdivided into 400 GeV-wide search regions, with the final region covering all events above 3 TeV. For the 2016 data, the lowest bin ranges from 1900 to 2200 GeV to ensure that the reconstructed mass distribution is not affected by the lower cutoff on the generated mass of 1700 GeV in the signal samples for that year.

In each bin the background estimate as described in section 6 and the signal prediction obtained from the samples described in section 4 are compared. For both signal and backgrounds, all systematic uncertainties described in section 7 are considered as nuisance parameters modeled with log-normal distributions, taking into account correlations between the different categories where applicable.

The limits for ADD models are obtained using the signal samples produced in the GRW convention. The theoretical description of the model is only valid up to the ultraviolet

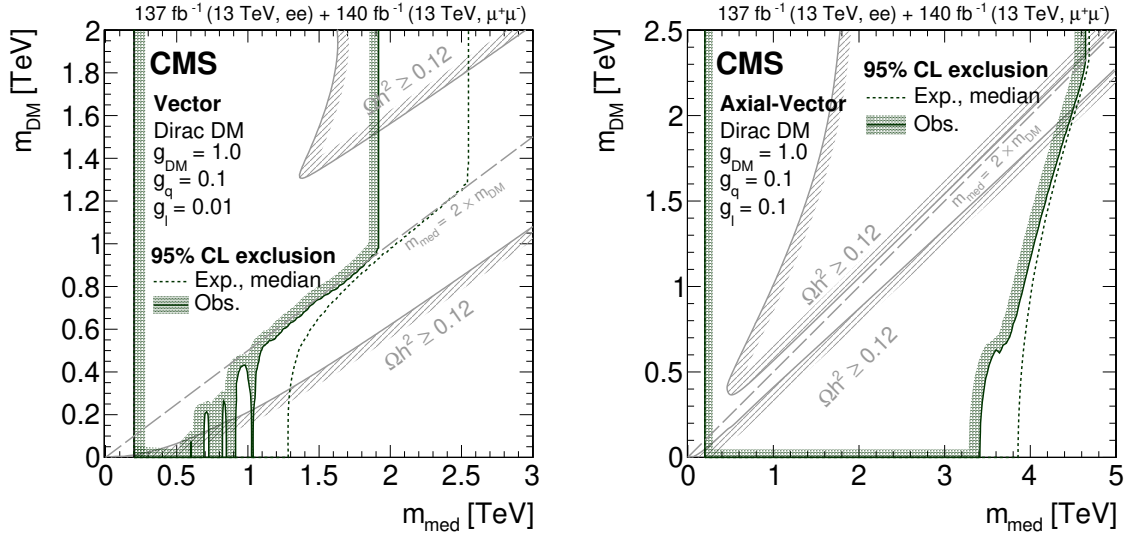


Figure 9. Summary of upper limits at 95% CL on the masses of the DM particle, which is assumed to be a Dirac fermion, and its associated mediator, in a simplified model of DM production via a (left) vector or (right) axial-vector mediator. The parameter exclusion regions are obtained by comparing the limits on the product of the production cross section and the branching fraction for decay to a Z boson with the values obtained from calculations in the simplified model. For each combination of the DM particle and mediator mass values, the width of the mediator is taken into account in the limit calculation. The curves with the hatching represent the excluded regions. The solid gray curves, marked as “ $\Omega h^2 \geq 0.12$ ”, correspond to parameter regions that reproduce the observed DM relic density in the universe [6, 48, 96, 97], with the hatched area indicating the region where the DM relic abundance exceeds the observed value.

cutoff parameter Λ_T . This is not taken into account in the signal simulation with PYTHIA. However, the signal cross section above the cutoff is small in the Λ_T range where limits are set, and has negligible impact on the results of this analysis.

In figure 10, the limits on the model parameters in the different ADD conventions are shown in the dielectron, dimuon, and combined channels. In the GRW convention, taking into account the NNLO correction factor of 1.3, the observed (expected) limits are 6.9 (7.2) TeV in the dielectron channel, 7.2 (7.4) TeV in the dimuon channel, and 7.5 (7.8) TeV for the combination. The limits are also translated into the Hewett convention and the HLZ convention for different numbers of extra dimensions using eqs. (3.4) and (3.5). All of the limits are shown in table 7. The case of $n = 2$ in the HLZ convention is not considered as there are very strong bounds on M_S from gravitational and astrophysical experiments far in excess of the reach of this analysis [98, 99]. For the considered models, the limits range from 5.9 to 8.9 TeV, depending on the model. These results are the best to date and improve on the previous most stringent limits by 0.5–1.0 TeV [28].

For the CI model, there can be significant negative interference between the signal and the SM DY process. This can lead to a negative effective signal prediction in some of the mass bins or even an overall negative signal contribution for high values of Λ . The interference term is therefore taken into account explicitly in the limit calculation. For the combination of the electron and muon channels, a universal CI is assumed.

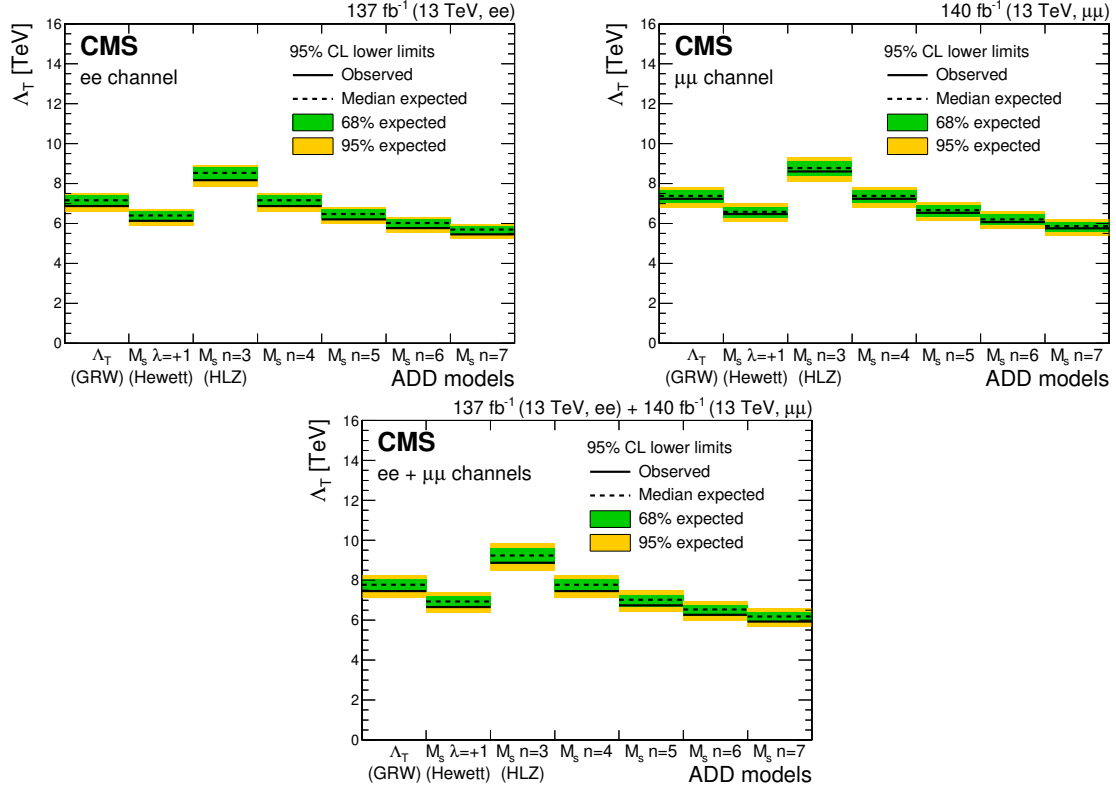


Figure 10. Exclusion limits at 95% CL on the ultraviolet cutoff for (upper left) the dielectron channel, (upper right) the dimuon channel, and (lower) their combination, with $m_{\ell\ell} > 1.8$ TeV ($m_{\ell\ell} > 1.9$ TeV for 2016) in the GRW (first bin), Hewett (second bin), and HLZ conventions (third to seventh bin) for the ADD model. Signal model cross sections are calculated up to LO, and an NNLO correction factor of 1.3 is applied.

The resulting limits for the dielectron, dimuon, and combined channels are shown in figure 11. The limits are given separately for the eight distinct CI models. In the electron channel, the observed limit is weaker than the expected limit by up to two σ . This is caused by the excess of electron events discussed in section 8. The effect is more pronounced here than in the limits in the ADD model as the shape of the mass distribution for the CI model makes it more sensitive to the mass range in which the excess is present. The lower limit on Λ ranges from 23.9 to 36.4 TeV, depending on the model, an improvement over previous CMS results by 3.5–4.5 TeV [28]. Using the same framework of contact interactions, ATLAS has set limits of up to 35.8 TeV [33]. Signal yields in the LR and RL models are reduced (enhanced) compared to LL and RR in the constructive (destructive) case. However, due to the improved signal-to-background ratio in the negative $\cos\theta^*$ bin for these models, the reduced sensitivity is mostly recovered in the constructive case, while in the destructive case the increased sensitivity compared to LL and RR is increased even further. The splitting of the event sample into two $\cos\theta^*$ ranges improves the limits by ≈ 1 TeV in the case of destructive interference and ≈ 3 TeV in the case of constructive interference.

Order	GRW	Hewett	HLZ				
	Λ_{T} [TeV]	M_{S} [TeV]	M_{S} [TeV]				
		$\lambda = +1$	$n = 3$	$n = 4$	$n = 5$	$n = 6$	$n = 7$
ee							
LO	6.7 (6.9)	5.9 (6.2)	7.9 (8.2)	6.7 (6.9)	6.0 (6.3)	5.6 (5.8)	5.3 (5.5)
LO $\times 1.3$	6.9 (7.2)	6.1 (6.4)	8.2 (8.5)	6.9 (7.2)	6.2 (6.5)	5.8 (6.0)	5.5 (5.7)
$\mu\mu$							
LO	7.0 (7.1)	6.2 (6.4)	8.3 (8.5)	7.0 (7.1)	6.3 (6.4)	5.9 (6.0)	5.6 (5.7)
LO $\times 1.3$	7.2 (7.4)	6.5 (6.6)	8.6 (8.8)	7.2 (7.4)	6.5 (6.7)	6.1 (6.2)	5.8 (5.9)
Combined ee and $\mu\mu$							
LO	7.3 (7.5)	6.5 (6.7)	8.6 (8.9)	7.3 (7.5)	6.6 (6.8)	6.1 (6.3)	5.8 (6.0)
LO $\times 1.3$	7.5 (7.8)	6.7 (6.9)	8.9 (9.2)	7.5 (7.8)	6.7 (7.0)	6.3 (6.5)	5.9 (6.2)

Table 7. Exclusion limits at 95% CL for the electron and muon channels, and their combination, for various parameter conventions of the ADD model. Signal model cross sections are calculated up to LO and the NNLO correction factor of 1.3 is applied. For each of the model parameters, the observed limit is shown first, followed by the expected limit in parentheses.

9.3 Search for lepton flavor universality violation

To search for signs of lepton flavor universality violation at high dilepton mass, we consider the ratio $R_{\mu^+\mu^-/e^+e^-}$ of the differential dilepton production cross sections in the muon and electron channels. The reconstructed distributions are distorted compared to particle level by bin-to-bin migration caused by mass scale and resolution effects, and by the detector acceptance and lepton efficiencies.

The mass distributions in data are unfolded after subtracting all backgrounds except for DY. For this purpose, the bin-to-bin migration is quantified as response matrices, i.e. 2D-histograms of the generated versus reconstructed dilepton mass in an event. They are obtained from the DY simulation for events passing the full analysis selection. The response matrices are then inverted and applied to the reconstructed mass spectra to unfold them to particle level using the ROOUNFOLD [100] utility. Since detailed studies found the off-diagonal elements of the response matrices to be small, no regularization is necessary. No significant dependence of the unfolded result on the characteristics of the DY simulation was observed. In the dimuon channel, the size of the unfolding correction rises from around 2% at low mass to around 10% at 3 TeV, caused by the worsening $m_{\ell\ell}$ resolution. The size of the unfolding corrections is 3-5% in the dielectron channel, where the resolution is largely independent of $m_{\ell\ell}$.

As the interest is in departures from the SM at high mass, we assume, as in the model of ref. [15], that departures are negligible in the mass region 200–400 GeV. Thus, to correct for the differences in acceptance and efficiency between the dielectron and dimuon channels

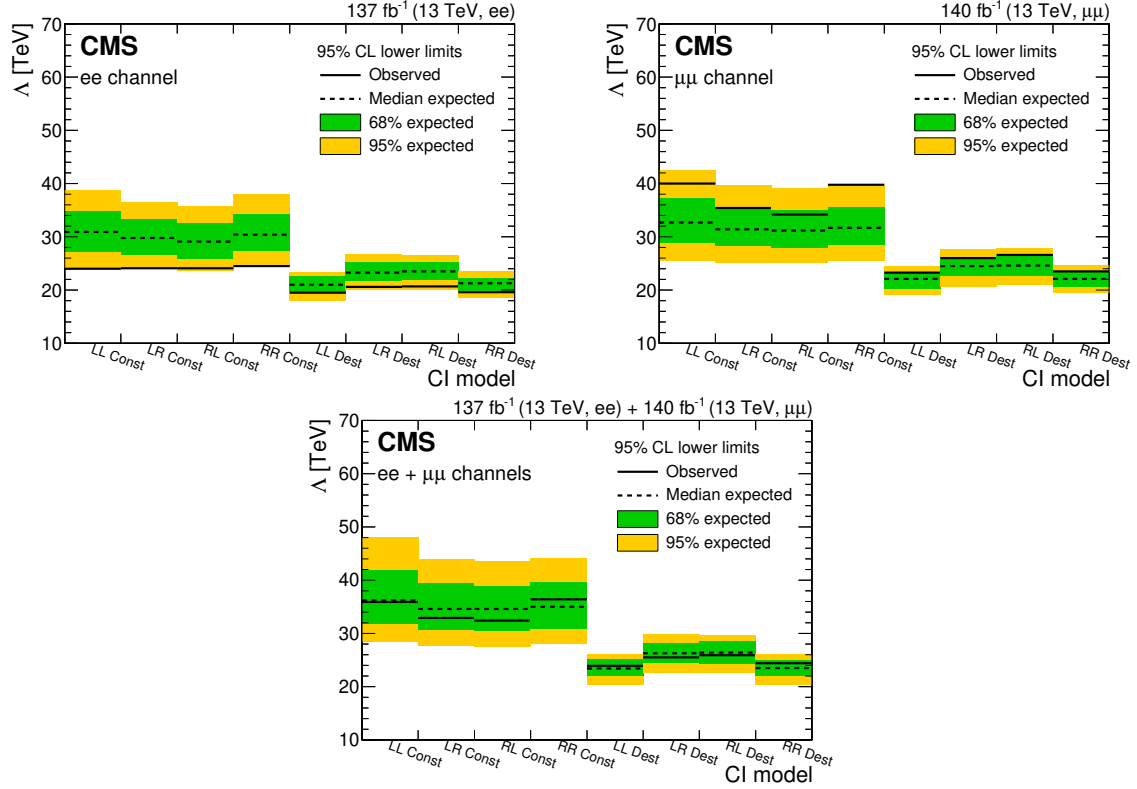


Figure 11. Dilepton lower exclusion limits at 95% CL on the CI scale (Λ) for the eight CI models considered, for (upper left) the dielectron channel, (upper right) the dimuon channel, and (lower) their combination. The limits are obtained for $m_{\ell\ell} > 400 \text{ GeV}$.

in this mass region, $R_{\mu^+\mu^-/e^+e^-}$ is normalized to unity here. To account for the remaining mass dependence of the difference between the channels, $R_{\mu^+\mu^-/e^+e^-}$ is measured in simulated DY events after application of the full event selection, the unfolding procedure, and the normalization of the ratio at low mass. The inverse of this ratio is then used to correct $R_{\mu^+\mu^-/e^+e^-}$ in data, which is obtained from the unfolded mass distributions. The size of this correction is up to 5% for events with central leptons and as large as 20% for events with forward leptons.

Several uncertainties, with the most significant originating from the PDFs, cancel in the flavor ratio. Uncertainties in the modeling of the mass resolution and scale are propagated through the unfolding procedure by obtaining response matrices for which the reconstructed mass values are smeared or shifted by the uncertainty. The uncertainties in the unfolded mass spectrum are then calculated as the differences between the mass spectra obtained with the different response matrices. The uncertainties in the detector acceptance and lepton efficiencies are propagated to the final flavor ratio via the acceptance and efficiency corrections.

The resulting ratio $R_{\mu^+\mu^-/e^+e^-}$ as a function of dilepton mass is shown in figure 12, for events with both leptons in the barrel region, events with at least one lepton in the

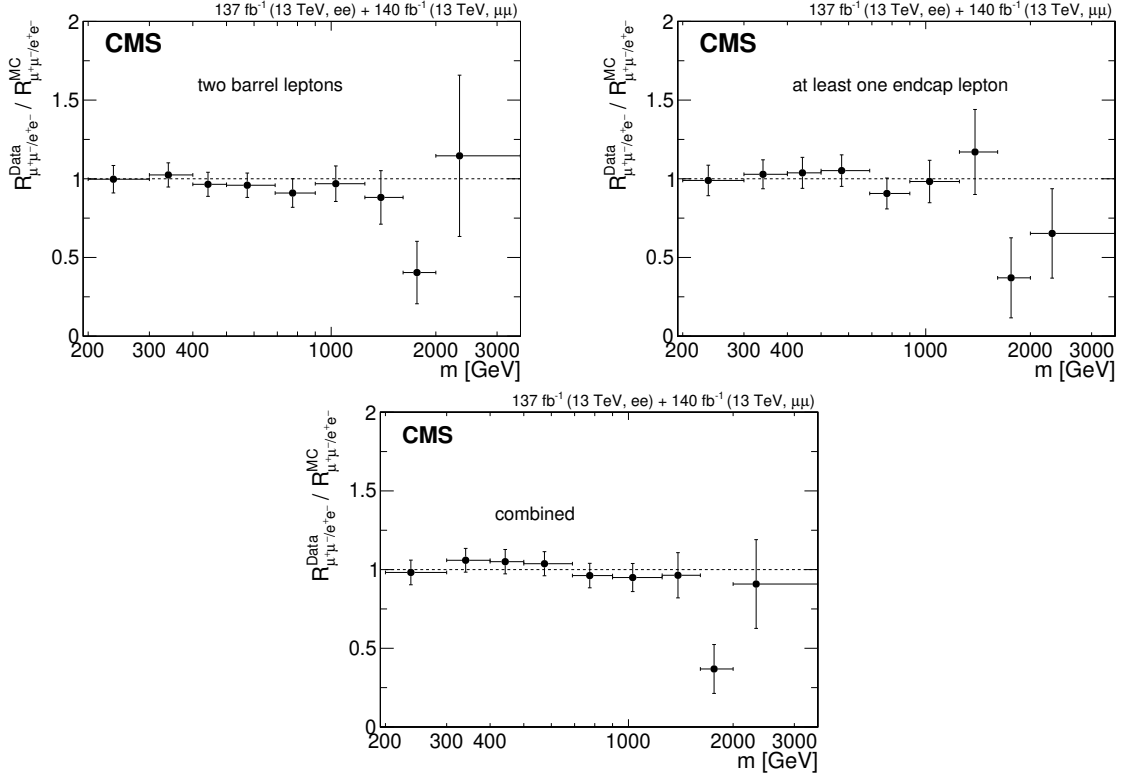


Figure 12. Ratio of the differential dilepton production cross section in the dimuon and dielectron channels $R_{\mu\mu/e e}^{\text{Data}} / R_{\mu\mu/e e}^{\text{MC}}$, as a function of $m_{\ell\ell}$ for (upper left) events with two barrel leptons, (upper right) at least one lepton in the endcaps, and (lower) their combination. The ratio is obtained after correcting the reconstructed mass spectra to particle level. The error bars include both statistical and systematic uncertainties.

endcaps, and their combination. Lepton flavor universality implies that this ratio is unity. Good agreement with this expectation is observed up to 1.5 TeV. At very high masses, the statistical uncertainties are large. Here, some deviations from unity are observed, caused by the slight excess in the dielectron channel discussed above. A χ^2 test for the mass range above 400 GeV is performed. The resulting χ^2/dof values are 11.2/7 for the events with two barrel leptons, 9.4/7 for those with at least one lepton in the endcaps, and 17.9/7 for the combined distribution. These correspond to one-sided p -values of 0.130 and 0.225, and 0.012, respectively.

As the flavor ratio unfolded to the particle level has been measured, these results can serve as a basis to test models that predict deviations from lepton flavor universality.

10 Summary

A search for resonant and nonresonant new phenomena in the dilepton invariant mass spectrum in proton-proton collisions at $\sqrt{s} = 13$ TeV corresponding to an integrated luminosity of up to 140 fb^{-1} has been presented. High-mass dielectron and dimuon events were reconstructed and selected with algorithms optimized for electrons and muons with high

transverse momenta. Standard model (SM) backgrounds were primarily estimated from simulation, with the dominant Drell-Yan background corrected to the highest order calculations available, including the contribution from photon-induced processes. When searching for resonant signals, the background normalizations were obtained from sidebands in the data, while for non-resonant signals, the background was normalized to the data in a control region around the Z boson peak. No significant deviation from SM expectation is observed.

Upper limits are set on the ratio of the product of the production cross section and the branching fraction in a dilepton channel of a new resonance with an intrinsic width of up to 10% to that of the SM Z boson at 95% confidence level. The limits are interpreted in the context of a sequential SM (SSM) and a superstring-inspired model that predict spin-1 resonances. Lower mass limits of 5.15 (4.56) TeV are set in the Z'_{SSM} (Z'_{ψ}) models. The observed limit on narrow spin-1 resonances is translated into limits on generalized couplings of the Z' to up and down quarks in several classes of new physics models. For spin-2 graviton resonances in the Randall-Sundrum model of extra dimensions, lower limits on the graviton mass of 2.47–4.78 TeV are set for values of the coupling parameter k/\bar{M}_{Pl} between 0.01 and 0.1. The lower mass limits for spin-1 and spin-2 resonances are the most stringent to date.

For spin-1 resonances that act as a mediator between SM particles and dark matter (DM), exclusion limits are set in the mass plane of the mediator and DM particles. For large values of m_{DM} , mediator masses below 1.92 (4.64) TeV are excluded in a model where the mediator is a vector (axial vector) with small (large) coupling to leptons. For $m_{\text{DM}} = 0$, these limits are reduced to 1.04 and 3.41 TeV, respectively.

Two models of nonresonant signatures have been considered. In case of a four-fermion contact interaction, lower limits on the ultraviolet cutoff parameter Λ range from 23.8 to 36.4 TeV depending on the helicity structure of the interaction and the sign of its interference with the SM Drell-Yan background. In the Arkani-Hamed, Dimopoulos, and Dvali model of large extra dimensions, lower limits on the ultraviolet cutoff ranging from 5.9 to 8.9 TeV are set, depending on the parameter convention.

The dimuon and dielectron invariant mass spectra are corrected for the detector effects and, for the first time in this kind of analysis, compared at the TeV scale. No significant deviation from lepton flavor universality is observed.

Acknowledgments

We congratulate our colleagues in the CERN accelerator departments for the excellent performance of the LHC and thank the technical and administrative staffs at CERN and at other CMS institutes for their contributions to the success of the CMS effort. In addition, we gratefully acknowledge the computing centers and personnel of the Worldwide LHC Computing Grid and other centers for delivering so effectively the computing infrastructure essential to our analyses. Finally, we acknowledge the enduring support for the construction and operation of the LHC, the CMS detector, and the supporting computing infrastructure provided by the following funding agencies: BMBWF and FWF (Austria); FNRS and FWO (Belgium); CNPq, CAPES, FAPERJ, FAPERGS, and FAPESP (Brazil); MES (Bulgaria); CERN; CAS, MoST, and NSFC (China); COLCIENCIAS (Colombia);

MSES and CSF (Croatia); RIF (Cyprus); SENESCYT (Ecuador); MoER, ERC PUT and ERDF (Estonia); Academy of Finland, MEC, and HIP (Finland); CEA and CNRS/IN2P3 (France); BMBF, DFG, and HGF (Germany); GSRT (Greece); NKFIA (Hungary); DAE and DST (India); IPM (Iran); SFI (Ireland); INFN (Italy); MSIP and NRF (Republic of Korea); MES (Latvia); LAS (Lithuania); MOE and UM (Malaysia); BUAP, CINVESTAV, CONACYT, LNS, SEP, and UASLP-FAI (Mexico); MOS (Montenegro); MBIE (New Zealand); PAEC (Pakistan); MSHE and NSC (Poland); FCT (Portugal); JINR (Dubna); MON, RosAtom, RAS, RFBR, and NRC KI (Russia); MESTD (Serbia); SEIDI, CPAN, PCTI, and FEDER (Spain); MOSTR (Sri Lanka); Swiss Funding Agencies (Switzerland); MST (Taipei); ThEPCenter, IPST, STAR, and NSTDA (Thailand); TUBITAK and TAEK (Turkey); NASU (Ukraine); STFC (United Kingdom); DOE and NSF (U.S.A.).

Individuals have received support from the Marie-Curie program and the European Research Council and Horizon 2020 Grant, contract Nos. 675440, 724704, 752730, and 765710 (European Union); the Leventis Foundation; the Alfred P. Sloan Foundation; the Alexander von Humboldt Foundation; the Belgian Federal Science Policy Office; the Fonds pour la Formation à la Recherche dans l’Industrie et dans l’Agriculture (FRIA-Belgium); the Agentschap voor Innovatie door Wetenschap en Technologie (IWT-Belgium); the F.R.S.-FNRS and FWO (Belgium) under the “Excellence of Science — EOS” — be.h project n. 30820817; the Beijing Municipal Science & Technology Commission, No. Z191100007219010; the Ministry of Education, Youth and Sports (MEYS) of the Czech Republic; the Deutsche Forschungsgemeinschaft (DFG), under Germany’s Excellence Strategy — EXC 2121 “Quantum Universe” — 390833306, and under project number 400140256 - GRK2497; the Lendület (“Momentum”) Program and the János Bolyai Research Scholarship of the Hungarian Academy of Sciences, the New National Excellence Program ÚNKP, the NKFIA research grants 123842, 123959, 124845, 124850, 125105, 128713, 128786, and 129058 (Hungary); the Council of Science and Industrial Research, India; the Ministry of Science and Higher Education and the National Science Center, contracts Opus 2014/15/B/ST2/03998 and 2015/19/B/ST2/02861 (Poland); the National Priorities Research Program by Qatar National Research Fund; the Ministry of Science and Higher Education, project no. 0723-2020-0041 (Russia); the Programa Estatal de Fomento de la Investigación Científica y Técnica de Excelencia María de Maeztu, grant MDM-2015-0509 and the Programa Severo Ochoa del Principado de Asturias; the Thalís and Aristeia programs cofinanced by EU-ESF and the Greek NSRF; the Rachadapisek Sompot Fund for Postdoctoral Fellowship, Chulalongkorn University and the Chulalongkorn Academic into Its 2nd Century Project Advancement Project (Thailand); the Kavli Foundation; the Nvidia Corporation; the SuperMicro Corporation; the Welch Foundation, contract C-1845; and the Weston Havens Foundation (U.S.A.).

Open Access. This article is distributed under the terms of the Creative Commons Attribution License ([CC-BY 4.0](https://creativecommons.org/licenses/by/4.0/)), which permits any use, distribution and reproduction in any medium, provided the original author(s) and source are credited.

References

- [1] A. Leike, *The phenomenology of extra neutral gauge bosons*, *Phys. Rept.* **317** (1999) 143 [[hep-ph/9805494](#)] [[INSPIRE](#)].
- [2] P. Langacker, *The physics of heavy Z' gauge bosons*, *Rev. Mod. Phys.* **81** (2009) 1199 [[arXiv:0801.1345](#)] [[INSPIRE](#)].
- [3] N. Arkani-Hamed, S. Dimopoulos and G.R. Dvali, *The hierarchy problem and new dimensions at a millimeter*, *Phys. Lett. B* **429** (1998) 263 [[hep-ph/9803315](#)] [[INSPIRE](#)].
- [4] N. Arkani-Hamed, S. Dimopoulos and G.R. Dvali, *Phenomenology, astrophysics and cosmology of theories with submillimeter dimensions and TeV scale quantum gravity*, *Phys. Rev. D* **59** (1999) 086004 [[hep-ph/9807344](#)] [[INSPIRE](#)].
- [5] L. Randall and R. Sundrum, *A large mass hierarchy from a small extra dimension*, *Phys. Rev. Lett.* **83** (1999) 3370 [[hep-ph/9905221](#)] [[INSPIRE](#)].
- [6] PLANCK collaboration, *Planck 2015 results. XIII. Cosmological parameters*, *Astron. Astrophys.* **594** (2016) A13 [[arXiv:1502.01589](#)] [[INSPIRE](#)].
- [7] LHC NEW PHYSICS WORKING GROUP collaboration, *Simplified models for LHC new physics searches*, *J. Phys. G* **39** (2012) 105005 [[arXiv:1105.2838](#)] [[INSPIRE](#)].
- [8] E. Eichten, I. Hinchliffe, K.D. Lane and C. Quigg, *Super collider physics*, *Rev. Mod. Phys.* **56** (1984) 579 [*Addendum ibid.* **58** (1986) 1065] [[INSPIRE](#)].
- [9] E. Eichten, K.D. Lane and M.E. Peskin, *New tests for quark and lepton substructure*, *Phys. Rev. Lett.* **50** (1983) 811 [[INSPIRE](#)].
- [10] LHCb collaboration, *Test of lepton universality with $B^0 \rightarrow K^{*0} \ell^+ \ell^-$ decays*, *JHEP* **08** (2017) 055 [[arXiv:1705.05802](#)] [[INSPIRE](#)].
- [11] LHCb collaboration, *Search for lepton-universality violation in $B^+ \rightarrow K^+ \ell^+ \ell^-$ decays*, *Phys. Rev. Lett.* **122** (2019) 191801 [[arXiv:1903.09252](#)] [[INSPIRE](#)].
- [12] LHCb collaboration, *Test of lepton universality in beauty-quark decays*, [arXiv:2103.11769](#) [[INSPIRE](#)].
- [13] S. Bifani, S. Descotes-Genon, A. Romero Vidal and M.-H. Schune, *Review of lepton universality tests in B decays*, *J. Phys. G* **46** (2019) 023001 [[arXiv:1809.06229](#)] [[INSPIRE](#)].
- [14] D. Bečirević, N. Košnik, O. Sumensari and R. Zukanovich Funchal, *Palatable leptoquark scenarios for lepton flavor violation in exclusive $b \rightarrow s \ell_1 \ell_2$ modes*, *JHEP* **11** (2016) 035 [[arXiv:1608.07583](#)] [[INSPIRE](#)].
- [15] A. Greljo and D. Marzocca, *High- p_T dilepton tails and flavor physics*, *Eur. Phys. J. C* **77** (2017) 548 [[arXiv:1704.09015](#)] [[INSPIRE](#)].
- [16] CMS collaboration, *Search for resonances in the dilepton mass distribution in pp collisions at $\sqrt{s} = 7$ TeV*, *JHEP* **05** (2011) 093 [[arXiv:1103.0981](#)] [[INSPIRE](#)].
- [17] CMS collaboration, *Search for narrow resonances in dilepton mass spectra in pp collisions at $\sqrt{s} = 7$ TeV*, *Phys. Lett. B* **714** (2012) 158 [[arXiv:1206.1849](#)] [[INSPIRE](#)].
- [18] CMS collaboration, *Search for heavy narrow dilepton resonances in pp collisions at $\sqrt{s} = 7$ TeV and $\sqrt{s} = 8$ TeV*, *Phys. Lett. B* **720** (2013) 63 [[arXiv:1212.6175](#)] [[INSPIRE](#)].

- [19] CMS collaboration, *Search for physics beyond the standard model in dilepton mass spectra in proton-proton collisions at $\sqrt{s} = 8$ TeV*, *JHEP* **04** (2015) 025 [[arXiv:1412.6302](#)] [[INSPIRE](#)].
- [20] CMS collaboration, *Search for narrow resonances in dilepton mass spectra in proton-proton collisions at $\sqrt{s} = 13$ TeV and combination with 8 TeV data*, *Phys. Lett. B* **768** (2017) 57 [[arXiv:1609.05391](#)] [[INSPIRE](#)].
- [21] CMS collaboration, *Search for high-mass resonances in dilepton final states in proton-proton collisions at $\sqrt{s} = 13$ TeV*, *JHEP* **06** (2018) 120 [[arXiv:1803.06292](#)] [[INSPIRE](#)].
- [22] ATLAS collaboration, *Search for high mass dilepton resonances in pp collisions at $\sqrt{s} = 7$ TeV with the ATLAS experiment*, *Phys. Lett. B* **700** (2011) 163 [[arXiv:1103.6218](#)] [[INSPIRE](#)].
- [23] ATLAS collaboration, *Search for high-mass resonances decaying to dilepton final states in pp collisions at $\sqrt{s} = 7$ TeV with the ATLAS detector*, *JHEP* **11** (2012) 138 [[arXiv:1209.2535](#)] [[INSPIRE](#)].
- [24] ATLAS collaboration, *Search for high-mass dilepton resonances in pp collisions at $\sqrt{s} = 8$ TeV with the ATLAS detector*, *Phys. Rev. D* **90** (2014) 052005 [[arXiv:1405.4123](#)] [[INSPIRE](#)].
- [25] ATLAS collaboration, *Search for new high-mass phenomena in the dilepton final state using 36 fb^{-1} of proton-proton collision data at $\sqrt{s} = 13$ TeV with the ATLAS detector*, *JHEP* **10** (2017) 182 [[arXiv:1707.02424](#)] [[INSPIRE](#)].
- [26] ATLAS collaboration, *Search for high-mass dilepton resonances using 139 fb^{-1} of pp collision data collected at $\sqrt{s} = 13$ TeV with the ATLAS detector*, *Phys. Lett. B* **796** (2019) 68 [[arXiv:1903.06248](#)] [[INSPIRE](#)].
- [27] ATLAS collaboration, *Constraints on mediator-based dark matter and scalar dark energy models using $\sqrt{s} = 13$ TeV pp collision data collected by the ATLAS detector*, *JHEP* **05** (2019) 142 [[arXiv:1903.01400](#)] [[INSPIRE](#)].
- [28] CMS collaboration, *Search for contact interactions and large extra dimensions in the dilepton mass spectra from proton-proton collisions at $\sqrt{s} = 13$ TeV*, *JHEP* **04** (2019) 114 [[arXiv:1812.10443](#)] [[INSPIRE](#)].
- [29] CMS collaboration, *Search for physics beyond the standard model in high-mass diphoton events from proton-proton collisions at $\sqrt{s} = 13$ TeV*, *Phys. Rev. D* **98** (2018) 092001 [[arXiv:1809.00327](#)] [[INSPIRE](#)].
- [30] CMS collaboration, *Search for new physics in dijet angular distributions using proton-proton collisions at $\sqrt{s} = 13$ TeV and constraints on dark matter and other models*, *Eur. Phys. J. C* **78** (2018) 789 [[arXiv:1803.08030](#)] [[INSPIRE](#)].
- [31] ATLAS collaboration, *Search for new phenomena in dijet events using 37 fb^{-1} of pp collision data collected at $\sqrt{s} = 13$ TeV with the ATLAS detector*, *Phys. Rev. D* **96** (2017) 052004 [[arXiv:1703.09127](#)] [[INSPIRE](#)].
- [32] ATLAS collaboration, *Search for contact interactions and large extra dimensions in the dilepton channel using proton-proton collisions at $\sqrt{s} = 8$ TeV with the ATLAS detector*, *Eur. Phys. J. C* **74** (2014) 3134 [[arXiv:1407.2410](#)] [[INSPIRE](#)].

- [33] ATLAS collaboration, *Search for new non-resonant phenomena in high-mass dilepton final states with the ATLAS detector*, *JHEP* **11** (2020) 005 [Erratum *ibid.* **04** (2021) 142] [[arXiv:2006.12946](#)] [[INSPIRE](#)].
- [34] CMS collaboration, *CMS luminosity measurements for the 2016 data taking period*, Tech. Rep. [CMS-PAS-LUM-17-001](#), CERN, Geneva, Switzerland (2017).
- [35] CMS collaboration, *CMS luminosity measurement for the 2017 data-taking period at $\sqrt{s} = 13$ TeV*, Tech. Rep. [CMS-PAS-LUM-17-004](#), CERN, Geneva, Switzerland (2018).
- [36] CMS collaboration, *CMS luminosity measurement for the 2018 data-taking period at $\sqrt{s} = 13$ TeV*, Tech. Rep. [CMS-PAS-LUM-18-002](#), CERN, Geneva, Switzerland (2019).
- [37] J.C. Collins and D.E. Soper, *Angular distribution of dileptons in high-energy hadron collisions*, *Phys. Rev. D* **16** (1977) 2219 [[INSPIRE](#)].
- [38] A.M. Sirunyan et al., *Search for resonant and nonresonant new phenomena in high-mass dilepton final states at $\sqrt{s} = 13$ TeV*, [HEPDATA record for this analysis](#), (2021).
- [39] A. Dominguez et al., *CMS technical design report for the pixel detector upgrade*, Tech. Rep. [CERN-LHCC-2012-016](#), CERN, Geneva, Switzerland (2012) [CMS-TDR-11].
- [40] CMS collaboration, *The CMS experiment at the CERN LHC*, [2008 JINST](#) **3** S08004 [[INSPIRE](#)].
- [41] CMS collaboration, *The CMS trigger system*, [2017 JINST](#) **12** P01020 [[arXiv:1609.02366](#)] [[INSPIRE](#)].
- [42] E. Accomando, A. Belyaev, L. Fedeli, S.F. King and C. Shepherd-Themistocleous, *Z' physics with early LHC data*, *Phys. Rev. D* **83** (2011) 075012 [[arXiv:1010.6058](#)] [[INSPIRE](#)].
- [43] G. Altarelli, B. Mele and M. Ruiz-Altaba, *Searching for new heavy vector bosons in $p\bar{p}$ colliders*, *Z. Phys. C* **45** (1989) 109 [Erratum *ibid.* **47** (1990) 676] [[INSPIRE](#)].
- [44] J.L. Hewett and T.G. Rizzo, *Low-energy phenomenology of superstring inspired E_6 models*, *Phys. Rept.* **183** (1989) 193 [[INSPIRE](#)].
- [45] E. Accomando, D. Becciolini, A. Belyaev, S. Moretti and C. Shepherd-Themistocleous, *Z' at the LHC: interference and finite width effects in Drell-Yan*, *JHEP* **10** (2013) 153 [[arXiv:1304.6700](#)] [[INSPIRE](#)].
- [46] M. Carena, A. Daleo, B.A. Dobrescu and T.M.P. Tait, *Z' gauge bosons at the Tevatron*, *Phys. Rev. D* **70** (2004) 093009 [[hep-ph/0408098](#)] [[INSPIRE](#)].
- [47] L. Randall and R. Sundrum, *An alternative to compactification*, *Phys. Rev. Lett.* **83** (1999) 4690 [[hep-th/9906064](#)] [[INSPIRE](#)].
- [48] A. Albert et al., *Recommendations of the LHC dark matter working group: comparing LHC searches for dark matter mediators in visible and invisible decay channels and calculations of the thermal relic density*, *Phys. Dark Univ.* **26** (2019) 100377 [[arXiv:1703.05703](#)] [[INSPIRE](#)].
- [49] M. Backović, M. Krämer, F. Maltoni, A. Martini, K. Mawatari and M. Pellen, *Higher-order QCD predictions for dark matter production at the LHC in simplified models with s -channel mediators*, *Eur. Phys. J. C* **75** (2015) 482 [[arXiv:1508.05327](#)] [[INSPIRE](#)].
- [50] G.F. Giudice, R. Rattazzi and J.D. Wells, *Quantum gravity and extra dimensions at high-energy colliders*, *Nucl. Phys. B* **544** (1999) 3 [[hep-ph/9811291](#)] [[INSPIRE](#)].

- [51] J.L. Hewett, *Indirect collider signals for extra dimensions*, *Phys. Rev. Lett.* **82** (1999) 4765 [[hep-ph/9811356](#)] [[INSPIRE](#)].
- [52] T. Han, J.D. Lykken and R.-J. Zhang, *On Kaluza-Klein states from large extra dimensions*, *Phys. Rev. D* **59** (1999) 105006 [[hep-ph/9811350](#)] [[INSPIRE](#)].
- [53] P. Nason, *A new method for combining NLO QCD with shower Monte Carlo algorithms*, *JHEP* **11** (2004) 040 [[hep-ph/0409146](#)] [[INSPIRE](#)].
- [54] S. Frixione, P. Nason and C. Oleari, *Matching NLO QCD computations with parton shower simulations: the POWHEG method*, *JHEP* **11** (2007) 070 [[arXiv:0709.2092](#)] [[INSPIRE](#)].
- [55] S. Alioli, P. Nason, C. Oleari and E. Re, *A general framework for implementing NLO calculations in shower Monte Carlo programs: the POWHEG BOX*, *JHEP* **06** (2010) 043 [[arXiv:1002.2581](#)] [[INSPIRE](#)].
- [56] S. Alioli, P. Nason, C. Oleari and E. Re, *NLO vector-boson production matched with shower in POWHEG*, *JHEP* **07** (2008) 060 [[arXiv:0805.4802](#)] [[INSPIRE](#)].
- [57] S. Frixione, P. Nason and G. Ridolfi, *A positive-weight next-to-leading-order Monte Carlo for heavy flavour hadroproduction*, *JHEP* **09** (2007) 126 [[arXiv:0707.3088](#)] [[INSPIRE](#)].
- [58] E. Re, *Single-top Wt -channel production matched with parton showers using the POWHEG method*, *Eur. Phys. J. C* **71** (2011) 1547 [[arXiv:1009.2450](#)] [[INSPIRE](#)].
- [59] M.R. Whalley, D. Bourilkov and R.C. Group, *The Les Houches accord PDFs (LHAPDF) and LHAGLUE*, in *HERA and the LHC: a workshop on the implications of HERA and LHC physics*, (2005) [[hep-ph/0508110](#)] [[INSPIRE](#)].
- [60] D. Bourilkov, R.C. Group and M.R. Whalley, *LHAPDF: PDF use from the Tevatron to the LHC*, in *TeV4LHC workshop — 4th meeting*, (2006) [[hep-ph/0605240](#)] [[INSPIRE](#)].
- [61] A. Buckley et al., *LHAPDF6: parton density access in the LHC precision era*, *Eur. Phys. J. C* **75** (2015) 132 [[arXiv:1412.7420](#)] [[INSPIRE](#)].
- [62] NNPDF collaboration, *Parton distributions for the LHC run II*, *JHEP* **04** (2015) 040 [[arXiv:1410.8849](#)] [[INSPIRE](#)].
- [63] NNPDF collaboration, *Parton distributions from high-precision collider data*, *Eur. Phys. J. C* **77** (2017) 663 [[arXiv:1706.00428](#)] [[INSPIRE](#)].
- [64] T. Sjöstrand et al., *An introduction to PYTHIA 8.2*, *Comput. Phys. Commun.* **191** (2015) 159 [[arXiv:1410.3012](#)] [[INSPIRE](#)].
- [65] CMS collaboration, *Event generator tunes obtained from underlying event and multiparton scattering measurements*, *Eur. Phys. J. C* **76** (2016) 155 [[arXiv:1512.00815](#)] [[INSPIRE](#)].
- [66] CMS collaboration, *Extraction and validation of a new set of CMS PYTHIA8 tunes from underlying-event measurements*, *Eur. Phys. J. C* **80** (2020) 4 [[arXiv:1903.12179](#)] [[INSPIRE](#)].
- [67] Y. Li and F. Petriello, *Combining QCD and electroweak corrections to dilepton production in FEWZ*, *Phys. Rev. D* **86** (2012) 094034 [[arXiv:1208.5967](#)] [[INSPIRE](#)].
- [68] A. Manohar, P. Nason, G.P. Salam and G. Zanderighi, *How bright is the proton? A precise determination of the photon parton distribution function*, *Phys. Rev. Lett.* **117** (2016) 242002 [[arXiv:1607.04266](#)] [[INSPIRE](#)].
- [69] J. Butterworth et al., *PDF4LHC recommendations for LHC run II*, *J. Phys. G* **43** (2016) 023001 [[arXiv:1510.03865](#)] [[INSPIRE](#)].

- [70] D. Bourilkov, *Photon-induced background for dilepton searches and measurements in pp collisions at 13 TeV*, [arXiv:1606.00523](#) [[INSPIRE](#)].
- [71] D. Bourilkov, *Exploring the LHC landscape with dileptons*, [arXiv:1609.08994](#) [[INSPIRE](#)].
- [72] M. Czakon and A. Mitov, *Top++: a program for the calculation of the top-pair cross-section at hadron colliders*, *Comput. Phys. Commun.* **185** (2014) 2930 [[arXiv:1112.5675](#)] [[INSPIRE](#)].
- [73] N. Kidonakis, *Two-loop soft anomalous dimensions for single top quark associated production with a W^- or H^-* , *Phys. Rev. D* **82** (2010) 054018 [[arXiv:1005.4451](#)] [[INSPIRE](#)].
- [74] J. Alwall et al., *The automated computation of tree-level and next-to-leading order differential cross sections, and their matching to parton shower simulations*, *JHEP* **07** (2014) 079 [[arXiv:1405.0301](#)] [[INSPIRE](#)].
- [75] R. Boughezal et al., *Color singlet production at NNLO in MCFM*, *Eur. Phys. J. C* **77** (2017) 7 [[arXiv:1605.08011](#)] [[INSPIRE](#)].
- [76] J.M. Campbell, R.K. Ellis and W.T. Giele, *A multi-threaded version of MCFM*, *Eur. Phys. J. C* **75** (2015) 246 [[arXiv:1503.06182](#)] [[INSPIRE](#)].
- [77] J.M. Campbell, R.K. Ellis and C. Williams, *Vector boson pair production at the LHC*, *JHEP* **07** (2011) 018 [[arXiv:1105.0020](#)] [[INSPIRE](#)].
- [78] J.M. Campbell and R.K. Ellis, *An update on vector boson pair production at hadron colliders*, *Phys. Rev. D* **60** (1999) 113006 [[hep-ph/9905386](#)] [[INSPIRE](#)].
- [79] T. Ahmed et al., *NNLO QCD corrections to the Drell-Yan cross section in models of TeV-scale gravity*, *Eur. Phys. J. C* **77** (2017) 22 [[arXiv:1606.08454](#)] [[INSPIRE](#)].
- [80] CMS collaboration, *Performance of the CMS level-1 trigger in proton-proton collisions at $\sqrt{s} = 13$ TeV*, 2020 *JINST* **15** P10017 [[arXiv:2006.10165](#)] [[INSPIRE](#)].
- [81] GEANT4 collaboration, *GEANT4 — a simulation toolkit*, *Nucl. Instrum. Meth. A* **506** (2003) 250 [[INSPIRE](#)].
- [82] CMS collaboration, *Performance of electron reconstruction and selection with the CMS detector in proton-proton collisions at $\sqrt{s} = 8$ TeV*, 2015 *JINST* **10** P06005 [[arXiv:1502.02701](#)] [[INSPIRE](#)].
- [83] CMS collaboration, *Electron and photon reconstruction and identification with the CMS experiment at the CERN LHC*, 2021 *JINST* **16** P05014 [[arXiv:2012.06888](#)] [[INSPIRE](#)].
- [84] CMS collaboration, *Performance of the CMS muon trigger system in proton-proton collisions at $\sqrt{s} = 13$ TeV*, 2021 *JINST* **16** P07001 [[arXiv:2102.04790](#)] [[INSPIRE](#)].
- [85] CMS collaboration, *Performance of CMS muon reconstruction in pp collision events at $\sqrt{s} = 7$ TeV*, 2012 *JINST* **7** P10002 [[arXiv:1206.4071](#)] [[INSPIRE](#)].
- [86] CMS collaboration, *Performance of the reconstruction and identification of high-momentum muons in proton-proton collisions at $\sqrt{s} = 13$ TeV*, 2020 *JINST* **15** P02027 [[arXiv:1912.03516](#)] [[INSPIRE](#)].
- [87] CMS collaboration, *Measurement of the inelastic proton-proton cross section at $\sqrt{s} = 13$ TeV*, *JHEP* **07** (2018) 161 [[arXiv:1802.02613](#)] [[INSPIRE](#)].
- [88] PARTICLE DATA GROUP collaboration, *Review of particle physics*, *PTEP* **2020** (2020) 083C01 [[INSPIRE](#)].

- [89] ATLAS, CMS and LHC HIGGS COMBINATION GROUP collaborations, *Procedure for the LHC Higgs boson search combination in Summer 2011*, Tech. Rep. [CMS-NOTE-2011-005](#), CERN, Geneva, Switzerland (2011) [[ATL-PHYS-PUB-2011-11](#)].
- [90] L. Moneta et al., *The RooStats project*, *PoS ACAT2010* (2010) 057 [[arXiv:1009.1003](#)] [[INSPIRE](#)].
- [91] M.J. Oreglia, *A study of the reactions $\psi' \rightarrow \gamma\gamma\psi$* , Ph.D. thesis, [SLAC report SLAC-R-236](#), Stanford University, Stanford, CA, U.S.A. (1980).
- [92] BABAR collaboration, *Study of $B \rightarrow X\gamma$ decays and determination of $|V_{td}/V_{ts}|$* , *Phys. Rev. D* **82** (2010) 051101 [[arXiv:1005.4087](#)] [[INSPIRE](#)].
- [93] CMS collaboration, *Observation of a new boson at a mass of 125 GeV with the CMS experiment at the LHC*, *Phys. Lett. B* **716** (2012) 30 [[arXiv:1207.7235](#)] [[INSPIRE](#)].
- [94] J. Alwall, C. Duhr, B. Fuks, O. Mattelaer, D.G. Öztürk and C.-H. Shen, *Computing decay rates for new physics theories with FeynRules and MadGraph 5_aMC@NLO*, *Comput. Phys. Commun.* **197** (2015) 312 [[arXiv:1402.1178](#)] [[INSPIRE](#)].
- [95] ATLAS collaboration, *Dark matter summary plots for s-channel mediators*, Tech. Rep. [ATL-PHYS-PUB-2020-021](#), CERN, Geneva, Switzerland (2020).
- [96] M. Backović, A. Martini, K. Kong, O. Mattelaer and G. Mohlabeng, *MadDM: new dark matter tool in the LHC era*, *AIP Conf. Proc.* **1743** (2016) 060001 [[arXiv:1509.03683](#)] [[INSPIRE](#)].
- [97] M. Backović, K. Kong and M. McCaskey, *MadDM v.1.0: computation of dark matter relic abundance using MadGraph5*, *Physics of the Dark Universe* **5-6** (2014) 18 [[arXiv:1308.4955](#)] [[INSPIRE](#)].
- [98] E.G. Adelberger, J.H. Gundlach, B.R. Heckel, S. Hoedl and S. Schlamminger, *Torsion balance experiments: a low-energy frontier of particle physics*, *Prog. Part. Nucl. Phys.* **62** (2009) 102 [[INSPIRE](#)].
- [99] S. Hannestad and G.G. Raffelt, *Supernova and neutron star limits on large extra dimensions reexamined*, *Phys. Rev. D* **67** (2003) 125008 [*Erratum ibid.* **69** (2004) 029901] [[hep-ph/0304029](#)] [[INSPIRE](#)].
- [100] T. Adye, *Unfolding algorithms and tests using RooUnfold*, in *PHYSTAT 2011*, [CERN-2011-006.313](#), CERN, Geneva, Switzerland (2011) [[arXiv:1105.1160](#)] [[INSPIRE](#)].

The CMS collaboration

Yerevan Physics Institute, Yerevan, Armenia

A.M. Sirunyan[†], A. Tumasyan

Institut für Hochenergiephysik, Wien, Austria

W. Adam, J.W. Andrejkovic, T. Bergauer, S. Chatterjee, M. Dragicevic, A. Escalante Del Valle, R. Frühwirth¹, M. Jeitler¹, N. Krammer, L. Lechner, D. Liko, I. Mikulec, F.M. Pitters, J. Schieck¹, R. Schöffbeck, M. Spanring, S. Templ, W. Waltenberger, C.-E. Wulz¹

Institute for Nuclear Problems, Minsk, Belarus

V. Chekhovsky, A. Litomin, V. Makarenko

Universiteit Antwerpen, Antwerpen, Belgium

M.R. Darwish², E.A. De Wolf, X. Janssen, T. Kello³, A. Lelek, H. Rejeb Sfar, P. Van Mechelen, S. Van Putte, N. Van Remortel

Vrije Universiteit Brussel, Brussel, Belgium

F. Blekman, E.S. Bols, J. D'Hondt, J. De Clercq, M. Delcourt, S. Lowette, S. Moortgat, A. Morton, D. Müller, A.R. Sahasransu, S. Tavernier, W. Van Doninck, P. Van Mulders

Université Libre de Bruxelles, Bruxelles, Belgium

D. Beghin, B. Bilin, B. Clerbaux, G. De Lentdecker, L. Favart, A. Grebenyuk, A.K. Kalsi, K. Lee, M. Mahdavihorrani, I. Makarenko, L. Moureaux, L. Pétré, A. Popov, N. Postiau, E. Starling, L. Thomas, M. Vanden Bemden, C. Vander Velde, P. Vanlaer, D. Vannerom, L. Wezenbeek

Ghent University, Ghent, Belgium

T. Cornelis, D. Dobur, M. Gruchala, G. Mestdach, M. Niedziela, C. Roskas, K. Skovpen, M. Tytgat, W. Verbeke, B. Vermassen, M. Vit

Université Catholique de Louvain, Louvain-la-Neuve, Belgium

A. Bethani, G. Bruno, F. Bury, C. Caputo, P. David, C. Delaere, I.S. Donertas, A. Giammanco, V. Lemaitre, K. Mondal, J. Prisciandaro, A. Taliercio, M. Teklishyn, P. Vischia, S. Wertz, S. Wuyckens

Centro Brasileiro de Pesquisas Fisicas, Rio de Janeiro, Brazil

G.A. Alves, C. Hensel, A. Moraes

Universidade do Estado do Rio de Janeiro, Rio de Janeiro, Brazil

W.L. Aldá Júnior, M. Barroso Ferreira Filho, H. Brandao Malbouisson, W. Carvalho, J. Chinellato⁴, E.M. Da Costa, G.G. Da Silveira⁵, D. De Jesus Damiao, S. Fonseca De Souza, D. Matos Figueiredo, C. Mora Herrera, K. Mota Amarilo, L. Mundim, H. Nogima, P. Rebello Teles, L.J. Sanchez Rosas, A. Santoro, S.M. Silva Do Amaral, A. Sznajder, M. Thiel, F. Torres Da Silva De Araujo, A. Vilela Pereira

Universidade Estadual Paulista ^a, Universidade Federal do ABC ^b, São Paulo, Brazil

C.A. Bernardes^{a,a}, L. Calligaris^a, T.R. Fernandez Perez Tomei^a, E.M. Gregores^{a,b}, D.S. Lemos^a, P.G. Mercadante^{a,b}, S.F. Novaes^a, Sandra S. Padula^a

Institute for Nuclear Research and Nuclear Energy, Bulgarian Academy of Sciences, Sofia, Bulgaria

A. Aleksandrov, G. Antchev, I. Atanasov, R. Hadjiiska, P. Iaydjiev, M. Misheva, M. Rodozov, M. Shopova, G. Sultanov

University of Sofia, Sofia, Bulgaria

A. Dimitrov, T. Ivanov, L. Litov, B. Pavlov, P. Petkov, A. Petrov

Beihang University, Beijing, China

T. Cheng, W. Fang³, Q. Guo, T. Javai⁶, M. Mittal, H. Wang, L. Yuan

Department of Physics, Tsinghua University, Beijing, China

M. Ahmad, G. Bauer, C. Dozen⁷, Z. Hu, J. Martins⁸, Y. Wang, K. Yi^{9,10}

Institute of High Energy Physics, Beijing, China

E. Chapon, G.M. Chen⁶, H.S. Chen⁶, M. Chen, A. Kapoor, D. Leggat, H. Liao, Z.-A. Liu⁶, R. Sharma, A. Spiezia, J. Tao, J. Thomas-Wilsker, J. Wang, H. Zhang, S. Zhang⁶, J. Zhao

State Key Laboratory of Nuclear Physics and Technology, Peking University, Beijing, China

A. Agapitos, Y. Ban, C. Chen, Q. Huang, A. Levin, Q. Li, M. Lu, X. Lyu, Y. Mao, S.J. Qian, D. Wang, Q. Wang, J. Xiao

Sun Yat-Sen University, Guangzhou, China

Z. You

Institute of Modern Physics and Key Laboratory of Nuclear Physics and Ion-beam Application (MOE) - Fudan University, Shanghai, China

X. Gao³, H. Okawa

Zhejiang University, Hangzhou, China

M. Xiao

Universidad de Los Andes, Bogota, Colombia

C. Avila, A. Cabrera, C. Florez, J. Fraga, A. Sarkar, M.A. Segura Delgado

Universidad de Antioquia, Medellin, Colombia

J. Jaramillo, J. Mejia Guisao, F. Ramirez, J.D. Ruiz Alvarez, C.A. Salazar González, N. Vanegas Arbelaez

University of Split, Faculty of Electrical Engineering, Mechanical Engineering and Naval Architecture, Split, Croatia

D. Giljanovic, N. Godinovic, D. Lelas, I. Puljak

University of Split, Faculty of Science, Split, Croatia

Z. Antunovic, M. Kovac, T. Sculac

Institute Rudjer Boskovic, Zagreb, Croatia

V. Brigljevic, D. Ferencek, D. Majumder, M. Roguljic, A. Starodumov¹¹, T. Susa

University of Cyprus, Nicosia, Cyprus

A. Attikis, E. Erodotou, A. Ioannou, G. Kole, M. Kolosova, S. Konstantinou, J. Mousa, C. Nicolaou, F. Ptochos, P.A. Razis, H. Rykaczewski, H. Saka

Charles University, Prague, Czech Republic

M. Finger¹², M. Finger Jr.¹², A. Kveton

Escuela Politecnica Nacional, Quito, Ecuador

E. Ayala

Universidad San Francisco de Quito, Quito, Ecuador

E. Carrera Jarrin

Academy of Scientific Research and Technology of the Arab Republic of Egypt, Egyptian Network of High Energy Physics, Cairo, Egypt

S. Abu Zeid¹³, S. Elgammal¹⁴, S. Khalil¹⁵

Center for High Energy Physics (CHEP-FU), Fayoum University, El-Fayoum, Egypt

A. Lotfy, M.A. Mahmoud

National Institute of Chemical Physics and Biophysics, Tallinn, Estonia

S. Bhowmik, A. Carvalho Antunes De Oliveira, R.K. Dewanjee, K. Ehataht, M. Kadastik, J. Pata, M. Raidal, C. Veelken

Department of Physics, University of Helsinki, Helsinki, Finland

P. Eerola, L. Forthomme, H. Kirschenmann, K. Osterberg, M. Voutilainen

Helsinki Institute of Physics, Helsinki, Finland

E. Brücken, F. Garcia, J. Havukainen, V. Karimäki, M.S. Kim, R. Kinnunen, T. Lampén, K. Lassila-Perini, S. Lehti, T. Lindén, M. Lotti, H. Siikonen, E. Tuominen, J. Tuominiemi

Lappeenranta University of Technology, Lappeenranta, Finland

P. Luukka, H. Petrow, T. Tuuva

IRFU, CEA, Université Paris-Saclay, Gif-sur-Yvette, France

C. Amendola, M. Besancon, F. Couderc, M. Dejardin, D. Denegri, J.L. Faure, F. Ferri, S. Ganjour, A. Givernaud, P. Gras, G. Hamel de Monchenault, P. Jarry, B. Lenzi, E. Locci, J. Malcles, J. Rander, A. Rosowsky, M.Ö. Sahin, A. Savoy-Navarro¹⁶, M. Titov, G.B. Yu

Laboratoire Leprince-Ringuet, CNRS/IN2P3, Ecole Polytechnique, Institut Polytechnique de Paris, Palaiseau, France

S. Ahuja, F. Beaudette, M. Bonanomi, A. Buchot Perraguin, P. Busson, C. Charlot, O. Davignon, B. Diab, G. Falmagne, S. Ghosh, R. Granier de Cassagnac, A. Hakimi,

I. Kucher, A. Lobanov, M. Nguyen, C. Ochando, P. Paganini, J. Rembser, R. Salerno, J.B. Sauvan, Y. Sirois, A. Zabi, A. Zghiche

Université de Strasbourg, CNRS, IPHC UMR 7178, Strasbourg, France

J.-L. Agram¹⁷, J. Andrea, D. Apparú, D. Bloch, G. Bourgatte, J.-M. Brom, E.C. Chabert, C. Collard, D. Darej, J.-C. Fontaine¹⁷, U. Goerlach, C. Grimault, A.-C. Le Bihan, P. Van Hove

Institut de Physique des 2 Infinis de Lyon (IP2I), Villeurbanne, France

E. Asilar, S. Beauceron, C. Bernet, G. Boudoul, C. Camen, A. Carle, N. Chanon, D. Contardo, P. Depasse, H. El Mamouni, J. Fay, S. Gascon, M. Gouzevitch, B. Ille, Sa. Jain, I.B. Laktineh, H. Lattaud, A. Lesauvage, M. Lethuillier, L. Mirabito, K. Shchablo, L. Torterotot, G. Touquet, M. Vander Donckt, S. Viret

Georgian Technical University, Tbilisi, Georgia

I. Bagaturia¹⁸, Z. Tsamalaidze¹²

RWTH Aachen University, I. Physikalisches Institut, Aachen, Germany

L. Feld, K. Klein, M. Lipinski, D. Meuser, A. Pauls, M.P. Rauch, M. Teroerde

RWTH Aachen University, III. Physikalisches Institut A, Aachen, Germany

D. Eliseev, M. Erdmann, P. Fackeldey, B. Fischer, S. Ghosh, T. Hebbeker, K. Hoepfner, F. Ivone, H. Keller, L. Mastrolorenzo, M. Merschmeyer, A. Meyer, G. Mocellin, S. Mondal, S. Mukherjee, D. Noll, A. Novak, T. Pook, A. Pozdnyakov, Y. Rath, H. Reithler, J. Roemer, A. Schmidt, S.C. Schuler, A. Sharma, S. Wiedenbeck, S. Zaleski

RWTH Aachen University, III. Physikalisches Institut B, Aachen, Germany

C. Dziwok, G. Flüge, W. Haj Ahmad¹⁹, O. Hlushchenko, T. Kress, A. Nowack, C. Pistone, O. Pooth, D. Roy, H. Sert, A. Stahl²⁰, T. Ziemons

Deutsches Elektronen-Synchrotron, Hamburg, Germany

H. Aarup Petersen, M. Aldaya Martin, P. Asmuss, I. Babounikau, S. Baxter, O. Behnke, A. Bermúdez Martínez, A.A. Bin Anuar, K. Borras²¹, V. Botta, D. Brunner, A. Campbell, A. Cardini, P. Connor, S. Consuegra Rodríguez, V. Danilov, M.M. Defranchis, L. Didukh, G. Eckerlin, D. Eckstein, L.I. Estevez Banos, E. Gallo²², A. Geiser, A. Giraldi, A. Grohsjean, M. Guthoff, A. Harb, A. Jafari²³, N.Z. Jomhari, H. Jung, A. Kasem²¹, M. Kasemann, H. Kaveh, C. Kleinwort, J. Knolle, D. Krücker, W. Lange, T. Lenz, J. Lidrych, K. Lipka, W. Lohmann²⁴, T. Madlener, R. Mankel, I.-A. Melzer-Pellmann, J. Metwally, A.B. Meyer, M. Meyer, J. Mnich, A. Mussgiller, V. Myronenko, Y. Otari, D. Pérez Adán, D. Pitzl, A. Raspereza, J. Rübenach, A. Saggio, A. Saibel, M. Savitskyi, V. Scheurer, C. Schwanenberger²², A. Singh, R.E. Sosa Ricardo, N. Tonon, O. Turkot, A. Vagnerini, M. Van De Klundert, R. Walsh, D. Walter, Y. Wen, K. Wichmann, C. Wissing, S. Wuchterl, R. Zlebcik

University of Hamburg, Hamburg, Germany

R. Aggleton, S. Bein, L. Benato, A. Benecke, K. De Leo, T. Dreyer, M. Eich, F. Feindt, A. Fröhlich, C. Garbers, E. Garutti, P. Gunnellini, J. Haller, A. Hinzmann, A. Karavdina,

G. Kasieczka, R. Klanner, R. Kogler, V. Kutzner, J. Lange, T. Lange, A. Malara, A. Nigamova, K.J. Pena Rodriguez, O. Rieger, P. Schleper, M. Schröder, J. Schwandt, D. Schwarz, J. Sonneveld, H. Stadie, G. Steinbrück, A. Tews, B. Vormwald, I. Zoi

Karlsruher Institut fuer Technologie, Karlsruhe, Germany

J. Bechtel, T. Berger, E. Butz, R. Caspart, T. Chwalek, W. De Boer, A. Dierlamm, A. Droll, K. El Morabit, N. Faltermann, K. Flöh, M. Giffels, J.O. Gosewisch, A. Gottmann, F. Hartmann²⁰, C. Heidecker, U. Husemann, I. Katkov²⁵, P. Keicher, R. Koppenhöfer, S. Maier, M. Metzler, S. Mitra, Th. Müller, M. Musich, M. Neukum, G. Quast, K. Rabbertz, J. Rauser, D. Savoie, D. Schäfer, M. Schnepf, D. Seith, I. Shvetsov, H.J. Simonis, R. Ulrich, J. Van Der Linden, R.F. Von Cube, M. Wassmer, M. Weber, S. Wieland, R. Wolf, S. Wozniowski, S. Wunsch

Institute of Nuclear and Particle Physics (INPP), NCSR Demokritos, Aghia Paraskevi, Greece

G. Anagnostou, P. Asenov, G. Daskalakis, T. Gerasis, A. Kyriakis, D. Loukas, A. Stakia

National and Kapodistrian University of Athens, Athens, Greece

M. Diamantopoulou, D. Karasavvas, G. Karathanasis, P. Kontaxakis, C.K. Koraka, A. Manousakis-Katsikakis, A. Panagiotou, I. Papavergou, N. Saoulidou, K. Theofilatos, E. Tziaferi, K. Vellidis, E. Vourliotis

National Technical University of Athens, Athens, Greece

G. Bakas, K. Kousouris, I. Papakrivopoulos, G. Tsipolitis, A. Zacharopoulou

University of Ioánnina, Ioánnina, Greece

I. Evangelou, C. Foudas, P. Gianneios, P. Katsoulis, P. Kokkas, N. Manthos, I. Papadopoulos, J. Strogas

MTA-ELTE Lendület CMS Particle and Nuclear Physics Group, Eötvös Loránd University, Budapest, Hungary

M. Csanad, K. Farkas, M.M.A. Gadallah²⁶, S. Lökös²⁷, P. Major, K. Mandal, A. Mehta, G. Pasztor, A.J. Rádl, O. Surányi, G.I. Veres

Wigner Research Centre for Physics, Budapest, Hungary

M. Bartók²⁸, G. Bencze, C. Hajdu, D. Horvath²⁹, F. Sikler, V. Veszpremi, G. Vesztergombi[†]

Institute of Nuclear Research ATOMKI, Debrecen, Hungary

S. Czellar, J. Karancsi²⁸, J. Molnar, Z. Szillasi, D. Teyssier

Institute of Physics, University of Debrecen, Debrecen, Hungary

P. Raics, Z.L. Trocsanyi³⁰, B. Ujvari

Eszterhazy Karoly University, Karoly Robert Campus, Gyongyos, Hungary

T. Csorgo³¹, F. Nemes³¹, T. Novak

Indian Institute of Science (IISc), Bangalore, India

S. Choudhury, J.R. Komaragiri, D. Kumar, L. Panwar, P.C. Tiwari

National Institute of Science Education and Research, HBNI, Bhubaneswar, India

S. Bahinipati³², D. Dash, C. Kar, P. Mal, T. Mishra, V.K. Muraleedharan Nair Bindhu³³, A. Nayak³³, P. Saha, N. Sur, S.K. Swain

Panjab University, Chandigarh, India

S. Bansal, S.B. Beri, V. Bhatnagar, G. Chaudhary, S. Chauhan, N. Dhingra³⁴, R. Gupta, A. Kaur, S. Kaur, P. Kumari, M. Meena, K. Sandeep, J.B. Singh, A.K. Viridi

University of Delhi, Delhi, India

A. Ahmed, A. Bhardwaj, B.C. Choudhary, R.B. Garg, M. Gola, S. Keshri, A. Kumar, M. Naimuddin, P. Priyanka, K. Ranjan, A. Shah

Saha Institute of Nuclear Physics, HBNI, Kolkata, India

M. Bharti³⁵, R. Bhattacharya, S. Bhattacharya, D. Bhowmik, S. Dutta, B. Gomber³⁶, M. Maity³⁷, S. Nandan, P. Palit, P.K. Rout, G. Saha, B. Sahu, S. Sarkar, M. Sharan, B. Singh³⁵, S. Thakur³⁵

Indian Institute of Technology Madras, Madras, India

P.K. Behera, S.C. Behera, P. Kalbhor, A. Muhammad, R. Pradhan, P.R. Pujahari, A. Sharma, A.K. Sikdar

Bhabha Atomic Research Centre, Mumbai, India

D. Dutta, V. Jha, V. Kumar, D.K. Mishra, K. Naskar³⁸, P.K. Netrakanti, L.M. Pant, P. Shukla

Tata Institute of Fundamental Research-A, Mumbai, India

T. Aziz, S. Dugad, G.B. Mohanty, U. Sarkar

Tata Institute of Fundamental Research-B, Mumbai, India

S. Banerjee, S. Bhattacharya, R. Chudasama, M. Guchait, S. Karmakar, S. Kumar, G. Majumder, K. Mazumdar, S. Mukherjee, D. Roy

Indian Institute of Science Education and Research (IISER), Pune, India

S. Dube, B. Kansal, S. Pandey, A. Rane, A. Rastogi, S. Sharma

Department of Physics, Isfahan University of Technology, Isfahan, Iran

H. Bakhshiansohi³⁹, M. Zeinali⁴⁰

Institute for Research in Fundamental Sciences (IPM), Tehran, Iran

S. Chenarani⁴¹, S.M. Etesami, M. Khakzad, M. Mohammadi Najafabadi

University College Dublin, Dublin, Ireland

M. Felcini, M. Grunewald

INFN Sezione di Bari ^a, Università di Bari ^b, Politecnico di Bari ^c, Bari, Italy

M. Abbrescia^{a,b}, R. Aly^{a,b,42}, C. Aruta^{a,b}, A. Colaleo^a, D. Creanza^{a,c}, N. De Filippis^{a,c}, M. De Palma^{a,b}, A. Di Florio^{a,b}, A. Di Pilato^{a,b}, W. Elmetenawee^{a,b}, L. Fiore^a, A. Gelmi^{a,b}, M. Gul^a, G. Iaselli^{a,c}, M. Ince^{a,b}, S. Lezki^{a,b}, G. Maggi^{a,c}, M. Maggi^a, I. Margjeka^{a,b},

V. Mastrapasqua^{a,b}, J.A. Merlin^a, S. My^{a,b}, S. Nuzzo^{a,b}, A. Pellecchia^{a,b}, A. Pompili^{a,b}, G. Pugliese^{a,c}, A. Ranieri^a, G. Selvaggi^{a,b}, L. Silvestris^a, F.M. Simone^{a,b}, R. Venditti^a, P. Verwilligen^a

INFN Sezione di Bologna ^a, Università di Bologna ^b, Bologna, Italy

G. Abbiendi^a, C. Battilana^{a,b}, D. Bonacorsi^{a,b}, L. Borgonovi^a, S. Braibant-Giacomelli^{a,b}, L. Brigliadori^a, R. Campanini^{a,b}, P. Capiluppi^{a,b}, A. Castro^{a,b}, F.R. Cavallo^a, C. Ciocca^a, M. Cuffiani^{a,b}, G.M. Dallavalle^a, T. Diotallevi^{a,b}, F. Fabbri^a, A. Fanfani^{a,b}, E. Fontanesi^{a,b}, P. Giacomelli^a, L. Giommi^{a,b}, C. Grandi^a, L. Guiducci^{a,b}, F. Iemmi^{a,b}, S. Lo Meo^{a,43}, S. Marcellini^a, G. Masetti^a, F.L. Navarria^{a,b}, A. Perrotta^a, F. Primavera^{a,b}, A.M. Rossi^{a,b}, T. Rovelli^{a,b}, G.P. Siroli^{a,b}, N. Tosi^a

INFN Sezione di Catania ^a, Università di Catania ^b, Catania, Italy

S. Albergo^{a,b,44}, S. Costa^{a,b,44}, A. Di Mattia^a, R. Potenza^{a,b}, A. Tricomi^{a,b,44}, C. Tuve^{a,b}

INFN Sezione di Firenze ^a, Università di Firenze ^b, Firenze, Italy

G. Barbagli^a, A. Cassese^a, R. Ceccarelli^{a,b}, V. Ciulli^{a,b}, C. Civinini^a, R. D'Alessandro^{a,b}, F. Fiori^{a,b}, E. Focardi^{a,b}, G. Latino^{a,b}, P. Lenzi^{a,b}, M. Lizzo^{a,b}, M. Meschini^a, S. Paoletti^a, R. Seidita^{a,b}, G. Sguazzoni^a, L. Viliani^a

INFN Laboratori Nazionali di Frascati, Frascati, Italy

L. Benussi, S. Bianco, D. Piccolo

INFN Sezione di Genova ^a, Università di Genova ^b, Genova, Italy

M. Bozzo^{a,b}, F. Ferro^a, R. Mulargia^{a,b}, E. Robutti^a, S. Tosi^{a,b}

INFN Sezione di Milano-Bicocca ^a, Università di Milano-Bicocca ^b, Milano, Italy

A. Benaglia^a, F. Brivio^{a,b}, F. Cetorelli^{a,b}, V. Ciriolo^{a,b,20}, F. De Guio^{a,b}, M.E. Dinardo^{a,b}, P. Dini^a, S. Gennai^a, A. Ghezzi^{a,b}, P. Govoni^{a,b}, L. Guzzi^{a,b}, M. Malberti^a, S. Malvezzi^a, A. Massironi^a, D. Menasce^a, F. Monti^{a,b}, L. Moroni^a, M. Paganoni^{a,b}, D. Pedrini^a, S. Ragazzi^{a,b}, T. Tabarelli de Fatis^{a,b}, D. Valsecchi^{a,b,20}, D. Zuolo^{a,b}

INFN Sezione di Napoli ^a, Università di Napoli ‘Federico II’ ^b, Napoli, Italy, Università della Basilicata ^c, Potenza, Italy, Università G. Marconi ^d, Roma, Italy

S. Buontempo^a, F. Carnevali^{a,b}, N. Cavallo^{a,c}, A. De Iorio^{a,b}, F. Fabozzi^{a,c}, A.O.M. Iorio^{a,b}, L. Lista^{a,b}, S. Meola^{a,d,20}, P. Paolucci^{a,20}, B. Rossi^a, C. Sciacca^{a,b}

INFN Sezione di Padova ^a, Università di Padova ^b, Padova, Italy, Università di Trento ^c, Trento, Italy

P. Azzi^a, N. Bacchetta^a, D. Bisello^{a,b}, P. Bortignon^a, A. Bragagnolo^{a,b}, R. Carlin^{a,b}, P. Checchia^a, P. De Castro Manzano^a, T. Dorigo^a, F. Gasparini^{a,b}, U. Gasparini^{a,b}, S.Y. Hoh^{a,b}, L. Layer^{a,45}, M. Margoni^{a,b}, A.T. Meneguzzo^{a,b}, M. Presilla^{a,b}, P. Ronchese^{a,b}, R. Rossin^{a,b}, F. Simonetto^{a,b}, G. Strong^a, M. Tosi^{a,b}, H. YARAR^{a,b}, M. Zanetti^{a,b}, P. Zotto^{a,b}, A. Zucchetta^{a,b}, G. Zumerle^{a,b}

INFN Sezione di Pavia ^a, Università di Pavia ^b, Pavia, Italy

C. Aime^{a,b}, A. Braghieri^a, S. Calzaferri^{a,b}, D. Fiorina^{a,b}, P. Montagna^{a,b}, S.P. Ratti^{a,b}, V. Re^a, M. Ressegotti^{a,b}, C. Riccardi^{a,b}, P. Salvini^a, I. Vai^a, P. Vitulo^{a,b}

INFN Sezione di Perugia ^a, Università di Perugia ^b, Perugia, Italy

G.M. Bilei^a, D. Ciangottini^{a,b}, L. Fanò^{a,b}, P. Lariccia^{a,b}, G. Mantovani^{a,b}, V. Mariani^{a,b}, M. Menichelli^a, F. Moscatelli^a, A. Piccinelli^{a,b}, A. Rossi^{a,b}, A. Santocchia^{a,b}, D. Spiga^a, T. Tedeschi^{a,b}

INFN Sezione di Pisa ^a, Università di Pisa ^b, Scuola Normale Superiore di Pisa ^c, Pisa Italy, Università di Siena ^d, Siena, Italy

P. Azzurri^a, G. Bagliesi^a, V. Bertacchi^{a,c}, L. Bianchini^a, T. Boccali^a, E. Bossini, R. Castaldi^a, M.A. Ciocci^{a,b}, R. Dell’Orso^a, M.R. Di Domenico^{a,d}, S. Donato^a, A. Giassi^a, M.T. Grippo^a, F. Ligabue^{a,c}, E. Manca^{a,c}, G. Mandorli^{a,c}, A. Messineo^{a,b}, F. Palla^a, G. Ramirez-Sanchez^{a,c}, A. Rizzi^{a,b}, G. Rolandi^{a,c}, S. Roy Chowdhury^{a,c}, A. Scribano^a, N. Shafiei^{a,b}, P. Spagnolo^a, R. Tenchini^a, G. Tonelli^{a,b}, N. Turini^{a,d}, A. Venturi^a, P.G. Verдини^a

INFN Sezione di Roma ^a, Sapienza Università di Roma ^b, Rome, Italy

F. Cavallari^a, M. Cipriani^{a,b}, D. Del Re^{a,b}, E. Di Marco^a, M. Diemoz^a, E. Longo^{a,b}, P. Meridiani^a, G. Organtini^{a,b}, F. Pandolfi^a, R. Paramatti^{a,b}, C. Quaranta^{a,b}, S. Rahatlou^{a,b}, C. Rovelli^a, F. Santanastasio^{a,b}, L. Soffi^a, R. Tramontano^{a,b}

INFN Sezione di Torino ^a, Università di Torino ^b, Torino, Italy, Università del Piemonte Orientale ^c, Novara, Italy

N. Amapane^{a,b}, R. Arcidiacono^{a,c}, S. Argiro^{a,b}, M. Arneodo^{a,c}, N. Bartosik^a, R. Bellan^{a,b}, A. Bellora^{a,b}, J. Berenguer Antequera^{a,b}, C. Biino^a, A. Cappati^{a,b}, N. Cartiglia^a, S. Cometti^a, M. Costa^{a,b}, R. Covarelli^{a,b}, N. Demaria^a, B. Kiani^{a,b}, F. Legger^a, C. Mariotti^a, S. Maselli^a, E. Migliore^{a,b}, V. Monaco^{a,b}, E. Monteil^{a,b}, M. Monteno^a, M.M. Obertino^{a,b}, G. Ortona^a, L. Pacher^{a,b}, N. Pastrone^a, M. Pelliccioni^a, G.L. Pinna Angioni^{a,b}, M. Ruspa^{a,c}, R. Salvatico^{a,b}, K. Shchelina^{a,b}, F. Siviero^{a,b}, V. Sola^a, A. Solano^{a,b}, D. Soldi^{a,b}, A. Staiano^a, M. Tornago^{a,b}, D. Trocino^{a,b}

INFN Sezione di Trieste ^a, Università di Trieste ^b, Trieste, Italy

S. Belforte^a, V. Candelise^{a,b}, M. Casarsa^a, F. Cossutti^a, A. Da Rold^{a,b}, G. Della Ricca^{a,b}, G. Sorrentino^{a,b}, F. Vazzoler^{a,b}

Kyungpook National University, Daegu, Korea

S. Dogra, C. Huh, B. Kim, D.H. Kim, G.N. Kim, J. Lee, S.W. Lee, C.S. Moon, Y.D. Oh, S.I. Pak, B.C. Radburn-Smith, S. Sekmen, Y.C. Yang

Chonnam National University, Institute for Universe and Elementary Particles, Kwangju, Korea

H. Kim, D.H. Moon

Hanyang University, Seoul, Korea

T.J. Kim, J. Park

Korea University, Seoul, Korea

S. Cho, S. Choi, Y. Go, B. Hong, K. Lee, K.S. Lee, J. Lim, J. Park, S.K. Park, J. Yoo

Kyung Hee University, Department of Physics, Seoul, Republic of Korea

J. Goh, A. Gurtu

Sejong University, Seoul, Korea

H.S. Kim, Y. Kim

Seoul National University, Seoul, Korea

J. Almond, J.H. Bhyun, J. Choi, S. Jeon, J. Kim, J.S. Kim, S. Ko, H. Kwon, H. Lee, S. Lee, B.H. Oh, M. Oh, S.B. Oh, H. Seo, U.K. Yang, I. Yoon

University of Seoul, Seoul, Korea

D. Jeon, J.H. Kim, B. Ko, J.S.H. Lee, I.C. Park, Y. Roh, D. Song, I.J. Watson

Yonsei University, Department of Physics, Seoul, Korea

S. Ha, H.D. Yoo

Sungkyunkwan University, Suwon, Korea

Y. Choi, Y. Jeong, H. Lee, Y. Lee, I. Yu

College of Engineering and Technology, American University of the Middle East (AUM), Egaila, Kuwait

T. Beyrouthy, Y. Maghrbi

Riga Technical University, Riga, Latvia

V. Veckalns⁴⁶

Vilnius University, Vilnius, Lithuania

M. Ambrozas, A. Juodagalvis, A. Rinkevicius, G. Tamulaitis, A. Vaitkevicius

National Centre for Particle Physics, Universiti Malaya, Kuala Lumpur, Malaysia

N. Bin Norjoharuddeen, W.A.T. Wan Abdullah, M.N. Yusli, Z. Zolkapli

Universidad de Sonora (UNISON), Hermosillo, Mexico

J.F. Benitez, A. Castaneda Hernandez, J.A. Murillo Quijada, L. Valencia Palomo

Centro de Investigacion y de Estudios Avanzados del IPN, Mexico City, Mexico

G. Ayala, H. Castilla-Valdez, E. De La Cruz-Burelo, I. Heredia-De La Cruz⁴⁷, R. Lopez-Fernandez, C.A. Mondragon Herrera, D.A. Perez Navarro, A. Sanchez-Hernandez

Universidad Iberoamericana, Mexico City, Mexico

S. Carrillo Moreno, C. Oropeza Barrera, M. Ramirez-Garcia, F. Vazquez Valencia

Benemerita Universidad Autonoma de Puebla, Puebla, Mexico

I. Pedraza, H.A. Salazar Ibarguen, C. Uribe Estrada

University of Montenegro, Podgorica, Montenegro

J. Mijuskovic⁴⁸, N. Raicevic

University of Auckland, Auckland, New Zealand

D. Krofcheck

University of Canterbury, Christchurch, New Zealand

S. Bheesette, P.H. Butler

National Centre for Physics, Quaid-I-Azam University, Islamabad, Pakistan

A. Ahmad, M.I. Asghar, A. Awais, M.I.M. Awan, H.R. Hoorani, W.A. Khan, M.A. Shah, M. Shoaib, M. Waqas

AGH University of Science and Technology Faculty of Computer Science, Electronics and Telecommunications, Krakow, Poland

V. Avati, L. Grzanka, M. Malawski

National Centre for Nuclear Research, Swierk, Poland

H. Bialkowska, M. Bluj, B. Boimska, T. Frueboes, M. Górski, M. Kazana, M. Szleper, P. Traczyk, P. Zalewski

Institute of Experimental Physics, Faculty of Physics, University of Warsaw, Warsaw, Poland

K. Bunkowski, K. Doroba, A. Kalinowski, M. Konecki, J. Krolikowski, M. Walczak

Laboratório de Instrumentação e Física Experimental de Partículas, Lisboa, Portugal

M. Araujo, P. Bargassa, D. Bastos, A. Boletti, P. Faccioli, M. Gallinaro, J. Hollar, N. Leonardo, T. Niknejad, J. Seixas, O. Toldaiev, J. Varela

Joint Institute for Nuclear Research, Dubna, Russia

S. Afanasiev, D. Budkouski, P. Bunin, M. Gavrilenko, I. Golutvin, I. Gorbunov, A. Kamenev, V. Karjavine, A. Lanev, A. Malakhov, V. Matveev^{49,50}, V. Palichik, V. Pereygin, M. Savina, D. Seitova, V. Shalaev, S. Shmatov, S. Shulha, V. Smirnov, O. Teryaev, N. Voytishin, A. Zarubin, I. Zhizhin

Petersburg Nuclear Physics Institute, Gatchina (St. Petersburg), Russia

G. Gavrilo, V. Golovtcov, Y. Ivanov, V. Kim⁵¹, E. Kuznetsova⁵², V. Murzin, V. Oreshkin, I. Smirnov, D. Sosnov, V. Sulimov, L. Uvarov, S. Volkov, A. Vorobyev

Institute for Nuclear Research, Moscow, Russia

Yu. Andreev, A. Dermenev, S. Gninenko, N. Golubev, A. Karneyeu, M. Kirsanov, N. Krasnikov, A. Pashenkov, G. Pivovarov, D. Tlisov[†], A. Toropin

Institute for Theoretical and Experimental Physics named by A.I. Alikhanov of NRC ‘Kurchatov Institute’, Moscow, Russia

V. Epshteyn, V. Gavrilo, N. Lychkovskaya, A. Nikitenko⁵³, V. Popov, G. Safronov, A. Spiridonov, A. Stepenov, M. Toms, E. Vlasov, A. Zhokin

Moscow Institute of Physics and Technology, Moscow, Russia

T. Aushev

National Research Nuclear University ‘Moscow Engineering Physics Institute’ (MEPhI), Moscow, Russia

O. Bychkova, R. Chistov⁵⁴, M. Danilov⁵⁵, A. Oskin, S. Polikarpov⁵⁴

P.N. Lebedev Physical Institute, Moscow, Russia

V. Andreev, M. Azarkin, I. Dremin, M. Kirakosyan, A. Terkulov

Skobeltsyn Institute of Nuclear Physics, Lomonosov Moscow State University, Moscow, Russia

A. Belyaev, E. Boos, V. Bunichev, M. Dubinin⁵⁶, L. Dudko, A. Ershov, A. Gribushin, V. Klyukhin, O. Kodolova, I. Lokhtin, S. Obraztsov, S. Petrushanko, V. Savrin

Novosibirsk State University (NSU), Novosibirsk, Russia

V. Blinov⁵⁷, T. Dimova⁵⁷, L. Kardapoltsev⁵⁷, I. Ovtin⁵⁷, Y. Skovpen⁵⁷

Institute for High Energy Physics of National Research Centre ‘Kurchatov Institute’, Protvino, Russia

I. Azhgirey, I. Bayshev, V. Kachanov, A. Kalinin, D. Konstantinov, V. Petrov, R. Ryutin, A. Sobol, S. Troshin, N. Tyurin, A. Uzunian, A. Volkov

National Research Tomsk Polytechnic University, Tomsk, Russia

A. Babaev, V. Okhotnikov, L. Sukhikh

Tomsk State University, Tomsk, Russia

V. Borchsh, V. Ivanchenko, E. Tcherniaev

University of Belgrade: Faculty of Physics and VINCA Institute of Nuclear Sciences, Belgrade, Serbia

P. Adzic⁵⁸, M. Dordevic, P. Milenovic, J. Milosevic, V. Milosevic

Centro de Investigaciones Energéticas Medioambientales y Tecnológicas (CIEMAT), Madrid, Spain

M. Aguilar-Benitez, J. Alcaraz Maestre, A. Álvarez Fernández, I. Bachiller, M. Barrio Luna, Cristina F. Bedoya, C.A. Carrillo Montoya, M. Cepeda, M. Cerrada, N. Colino, B. De La Cruz, A. Delgado Peris, J.P. Fernández Ramos, J. Flix, M.C. Fouz, O. Gonzalez Lopez, S. Goy Lopez, J.M. Hernandez, M.I. Josa, J. León Holgado, D. Moran, Á. Navarro Tobar, A. Pérez-Calero Yzquierdo, J. Puerta Pelayo, I. Redondo, L. Romero, S. Sánchez Navas, M.S. Soares, L. Urda Gómez, C. Willmott

Universidad Autónoma de Madrid, Madrid, Spain

J.F. de Trocóniz, R. Reyes-Almanza

Universidad de Oviedo, Instituto Universitario de Ciencias y Tecnologías Espaciales de Asturias (ICTEA), Oviedo, Spain

B. Alvarez Gonzalez, J. Cuevas, C. Erice, J. Fernandez Menendez, S. Folgueras, I. Gonzalez Caballero, E. Palencia Cortezon, C. Ramón Álvarez, J. Ripoll Sau, V. Rodríguez Bouza, A. Trapote

Instituto de Física de Cantabria (IFCA), CSIC-Universidad de Cantabria, Santander, Spain

J.A. Brochero Cifuentes, I.J. Cabrillo, A. Calderon, B. Chazin Quero, J. Duarte Campderros, M. Fernandez, C. Fernandez Madrazo, P.J. Fernández Manteca, A. García Alonso, G. Gomez, C. Martinez Rivero, P. Martinez Ruiz del Arbol, F. Matorras, J. Piedra Gomez, C. Prieels, F. Ricci-Tam, T. Rodrigo, A. Ruiz-Jimeno, L. Scodellaro, N. Trevisani, I. Vila, J.M. Vizan Garcia

University of Colombo, Colombo, Sri Lanka

MK Jayananda, B. Kailasapathy⁵⁹, D.U.J. Sonnadara, DDC Wickramarathna

University of Ruhuna, Department of Physics, Matara, Sri Lanka

W.G.D. Dharmaratna, K. Liyanage, N. Perera, N. Wickramage

CERN, European Organization for Nuclear Research, Geneva, Switzerland

T.K. Aarrestad, D. Abbaneo, J. Alimena, E. Auffray, G. Auzinger, J. Baechler, P. Baillon[†], A.H. Ball, D. Barney, J. Bendavid, N. Beni, M. Bianco, A. Bocci, E. Brondolin, T. Camporesi, M. Capeans Garrido, G. Cerminara, S.S. Chhibra, L. Cristella, D. d’Enterria, A. Dabrowski, N. Daci, A. David, A. De Roeck, M. Deile, R. Di Maria, M. Dobson, M. Dünser, N. Dupont, A. Elliott-Peisert, N. Emriskova, F. Fallavollita⁶⁰, D. Fasanella, S. Fiorendi, A. Florent, G. Franzoni, J. Fulcher, W. Funk, S. Giani, D. Gigi, K. Gill, F. Glege, L. Gouskos, M. Haranko, J. Hegeman, Y. Iiyama, V. Innocente, T. James, P. Janot, J. Kaspar, J. Kieseler, M. Komm, N. Kratochwil, C. Lange, S. Laurila, P. Lecoq, K. Long, C. Lourenço, L. Malgeri, S. Mallios, M. Mannelli, F. Meijers, S. Mersi, E. Meschi, F. Moortgat, M. Mulders, S. Orfanelli, L. Orsini, F. Pantaleo, L. Pape, E. Perez, M. Peruzzi, A. Petrilli, G. Petrucciani, A. Pfeiffer, M. Pierini, M. Pitt, H. Qu, T. Quast, D. Rabad, A. Racz, M. Rieger, M. Rovere, H. Sakulin, J. Salfeld-Nebgen, S. Scarfi, C. Schäfer, C. Schwick, M. Selvaggi, A. Sharma, P. Silva, W. Snoeys, P. Sphicas⁶¹, S. Summers, V.R. Tavolaro, D. Treille, A. Tsiros, G.P. Van Onsem, M. Verzetti, J. Wanczyk⁶², K.A. Wozniak, W.D. Zeuner

Paul Scherrer Institut, Villigen, Switzerland

L. Caminada⁶³, A. Ebrahimi, W. Erdmann, R. Horisberger, Q. Ingram, H.C. Kaestli, D. Kotlinski, U. Langenegger, M. Missiroli, T. Rohe

ETH Zurich - Institute for Particle Physics and Astrophysics (IPA), Zurich, Switzerland

K. Androsov⁶², M. Backhaus, P. Berger, A. Calandri, N. Chernyavskaya, A. De Cosa, G. Dissertori, M. Dittmar, M. Donegà, C. Dorfer, F. Eble, T. Gadek, T.A. Gómez Espinosa, C. Grab, D. Hits, W. Lustermann, A.-M. Lyon, R.A. Manzoni, C. Martin Perez, M.T. Meinhard, F. Micheli, F. Nessi-Tedaldi, J. Niedziela, F. Pauss, V. Perovic, G. Perrin, S. Pigazzini, M.G. Ratti, M. Reichmann, C. Reissel, T. Reitenspiess, B. Ristic, D. Ruini, D.A. Sanz Becerra, M. Schönenberger, V. Stampf, J. Steggemann⁶², R. Wallny, D.H. Zhu

Universität Zürich, Zurich, Switzerland

C. Amsler⁶⁴, P. Bärtshi, C. Botta, D. Brzhechko, M.F. Canelli, A. De Wit, R. Del Burgo, J.K. Heikkilä, M. Huwiler, A. Jofrehei, B. Kilminster, S. Leontsinis, A. Macchiolo, P. Meiring, V.M. Mikuni, U. Molinatti, I. Neutelings, G. Rauco, A. Reimers, P. Robmann, S. Sanchez Cruz, K. Schweiger, Y. Takahashi

National Central University, Chung-Li, Taiwan

C. Adloff⁶⁵, C.M. Kuo, W. Lin, A. Roy, T. Sarkar³⁷, S.S. Yu

National Taiwan University (NTU), Taipei, Taiwan

L. Ceard, P. Chang, Y. Chao, K.F. Chen, P.H. Chen, W.-S. Hou, Y.y. Li, R.-S. Lu, E. Paganis, A. Psallidas, A. Steen, E. Yazgan, P.r. Yu

Chulalongkorn University, Faculty of Science, Department of Physics, Bangkok, Thailand

B. Asavapibhop, C. Asawatangtrakuldee, N. Srimanobhas

Çukurova University, Physics Department, Science and Art Faculty, Adana, Turkey

F. Boran, S. Damarsecin⁶⁶, Z.S. Demiroglu, F. Dolek, I. Dumanoglu⁶⁷, E. Eskut, G. Gokbulut, Y. Guler, E. Gurpinar Guler⁶⁸, I. Hos⁶⁹, C. Isik, E.E. Kangal⁷⁰, O. Kara, A. Kayis Topaksu, U. Kiminsu, G. Onengut, K. Ozdemir⁷¹, A. Polatoz, A.E. Simsek, B. Tali⁷², U.G. Tok, S. Turkcapar, I.S. Zorbakir, C. Zorbilmez

Middle East Technical University, Physics Department, Ankara, Turkey

B. Isildak⁷³, G. Karapinar⁷⁴, K. Ocalan⁷⁵, M. Yalvac⁷⁶

Bogazici University, Istanbul, Turkey

B. Akgun, I.O. Atakisi, E. Gülmez, M. Kaya⁷⁷, O. Kaya⁷⁸, Ö. Özçelik, S. Tekten⁷⁹, E.A. Yetkin⁸⁰

Istanbul Technical University, Istanbul, Turkey

A. Cakir, K. Cankocak⁶⁷, Y. Komurcu, S. Sen⁸¹

Istanbul University, Istanbul, Turkey

F. Aydogmus Sen, S. Cerci⁷², B. Kaynak, S. Ozkorucuklu, D. Sunar Cerci⁷²

Institute for Scintillation Materials of National Academy of Science of Ukraine, Kharkov, Ukraine

B. Grynyov

National Scientific Center, Kharkov Institute of Physics and Technology, Kharkov, Ukraine

L. Levchuk

University of Bristol, Bristol, United Kingdom

E. Bhal, S. Bologna, J.J. Brooke, A. Bundock, E. Clement, D. Cussans, H. Flacher, J. Goldstein, G.P. Heath, H.F. Heath, L. Kreczko, B. Krikler, S. Paramesvaran, T. Sakuma, S. Seif El Nasr-Storey, V.J. Smith, N. Stylianou⁸², J. Taylor, A. Titterton

Rutherford Appleton Laboratory, Didcot, United Kingdom

K.W. Bell, A. Belyaev⁸³, C. Brew, R.M. Brown, D.J.A. Cockerill, K.V. Ellis, K. Harder, S. Harper, J. Linacre, K. Manolopoulos, D.M. Newbold, E. Olaiya, D. Petyt, T. Reis, T. Schuh, C.H. Shepherd-Themistocleous, A. Thea, I.R. Tomalin, T. Williams

Imperial College, London, United Kingdom

R. Bainbridge, P. Bloch, S. Bonomally, J. Borg, S. Breeze, O. Buchmuller, V. Cepaitis, G.S. Chahal⁸⁴, D. Colling, P. Dauncey, G. Davies, M. Della Negra, S. Fayer, G. Fedi, G. Hall, M.H. Hassanshahi, G. Iles, J. Langford, L. Lyons, A.-M. Magnan, S. Malik, A. Martelli, J. Nash⁸⁵, V. Palladino, M. Pesaresi, D.M. Raymond, A. Richards, A. Rose, E. Scott, C. Seez, A. Shtipliyski, A. Tapper, K. Uchida, T. Virdee²⁰, N. Wardle, S.N. Webb, D. Winterbottom, A.G. Zecchinelli

Brunel University, Uxbridge, United Kingdom

J.E. Cole, A. Khan, P. Kyberd, C.K. Mackay, I.D. Reid, L. Teodorescu, S. Zahid

Baylor University, Waco, U.S.A.

S. Abdullin, A. Brinkerhoff, B. Caraway, J. Dittmann, K. Hatakeyama, A.R. Kanuganti, B. McMaster, N. Pastika, S. Sawant, C. Smith, C. Sutantawibul, J. Wilson

Catholic University of America, Washington, DC, U.S.A.

R. Bartek, A. Dominguez, R. Uniyal, A.M. Vargas Hernandez

The University of Alabama, Tuscaloosa, U.S.A.

A. Buccilli, O. Charaf, S.I. Cooper, D. Di Croce, S.V. Gleyzer, C. Henderson, C.U. Perez, P. Rumerio⁸⁶, C. West

Boston University, Boston, U.S.A.

A. Akpinar, A. Albert, D. Arcaro, C. Cosby, Z. Demiragli, D. Gastler, J. Rohlf, K. Salyer, D. Sperka, D. Spitzbart, I. Suarez, A. Tsatsos, S. Yuan, D. Zou

Brown University, Providence, U.S.A.

G. Benelli, B. Burkle, X. Coubez²¹, D. Cutts, Y.t. Duh, M. Hadley, U. Heintz, J.M. Hogan⁸⁷, E. Laird, G. Landsberg, K.T. Lau, J. Lee, J. Luo, M. Narain, S. Sagir⁸⁸, E. Usai, W.Y. Wong, X. Yan, D. Yu, W. Zhang

University of California, Davis, Davis, U.S.A.

C. Brainerd, R. Breedon, M. Calderon De La Barca Sanchez, M. Chertok, J. Conway, P.T. Cox, R. Erbacher, F. Jensen, O. Kukral, R. Lander, M. Mulhearn, D. Pellett, B. Regnery, D. Taylor, M. Tripathi, Y. Yao, F. Zhang

University of California, Los Angeles, U.S.A.

M. Bachtis, R. Cousins, A. Dasgupta, A. Datta, D. Hamilton, J. Hauser, M. Ignatenko, M.A. Iqbal, T. Lam, N. Mccoll, W.A. Nash, S. Regnard, D. Saltzberg, C. Schnaible, B. Stone, V. Valuev

University of California, Riverside, Riverside, U.S.A.

K. Burt, Y. Chen, R. Clare, J.W. Gary, G. Hanson, G. Karapostoli, O.R. Long, N. Manganeli, M. Olmedo Negrete, W. Si, S. Wimpenny, Y. Zhang

University of California, San Diego, La Jolla, U.S.A.

J.G. Branson, P. Chang, S. Cittolin, S. Cooperstein, N. Deelen, J. Duarte, R. Gerosa, L. Giannini, D. Gilbert, J. Guiang, R. Kansal, V. Krutelyov, R. Lee, J. Letts, M. Masciovecchio, S. May, S. Padhi, M. Pieri, B.V. Sathia Narayanan, V. Sharma, M. Tadel, A. Vartak, F. Würthwein, Y. Xiang, A. Yagil

University of California, Santa Barbara - Department of Physics, Santa Barbara, U.S.A.

N. Amin, C. Campagnari, M. Citron, A. Dorsett, V. Dutta, J. Incandela, M. Kilpatrick, J. Kim, B. Marsh, H. Mei, M. Oshiro, A. Ovcharova, M. Quinnan, J. Richman, U. Sarica, D. Stuart, S. Wang

California Institute of Technology, Pasadena, U.S.A.

A. Bornheim, O. Cerri, I. Dutta, J.M. Lawhorn, N. Lu, J. Mao, H.B. Newman, J. Ngadiuba, T.Q. Nguyen, M. Spiropulu, J.R. Vlimant, C. Wang, S. Xie, Z. Zhang, R.Y. Zhu

Carnegie Mellon University, Pittsburgh, U.S.A.

J. Alison, M.B. Andrews, T. Ferguson, T. Mudholkar, M. Paulini, I. Vorobiev

University of Colorado Boulder, Boulder, U.S.A.

J.P. Cumalat, W.T. Ford, E. MacDonald, R. Patel, A. Perloff, K. Stenson, K.A. Ulmer, S.R. Wagner

Cornell University, Ithaca, U.S.A.

J. Alexander, Y. Cheng, J. Chu, D.J. Cranshaw, K. McDermott, J. Monroy, J.R. Patterson, D. Quach, J. Reichert, A. Ryd, W. Sun, S.M. Tan, Z. Tao, J. Thom, P. Wittich, M. Zientek

Fermi National Accelerator Laboratory, Batavia, U.S.A.

M. Albrow, M. Alyari, G. Apollinari, A. Apresyan, A. Apyan, S. Banerjee, L.A.T. Bauerdick, A. Beretvas, D. Berry, J. Berryhill, P.C. Bhat, K. Burkett, J.N. Butler, A. Canepa, G.B. Cerati, H.W.K. Cheung, F. Chlebana, M. Cremonesi, K.F. Di Petrillo, P. Dong⁸⁹, V.D. Elvira, J. Freeman, Z. Gecse, L. Gray, D. Green, S. Grünendahl, K. Gumpula⁸⁹, O. Gutsche, R.M. Harris, R. Heller, T.C. Herwig, J. Hirschauer, B. Jayatilaka, S. Jindariani, M. Johnson, U. Joshi, P. Klabbers, T. Klijnsma, B. Klima, M.J. Kortelainen, K.H.M. Kwok, S. Lammel, D. Lincoln, R. Lipton, T. Liu, J. Lykken, C. Madrid, K. Maeshima, C. Mantilla, D. Mason, P. McBride, P. Merkel, S. Mrenna, S. Nahn, V. O'Dell, V. Papadimitriou, K. Pedro, C. Pena⁵⁶, O. Prokofyev, F. Ravera, A. Reinsvold Hall, L. Ristori, B. Schneider, E. Sexton-Kennedy, N. Smith, A. Soha, L. Spiegel, S. Stoynev, J. Strait, L. Taylor, S. Tkaczyk, N.V. Tran, L. Uplegger, E.W. Vaandering, A. Vanderploeg⁸⁹, H.A. Weber, A. Woodard

University of Florida, Gainesville, U.S.A.

D. Acosta, P. Avery, D. Bourilkov, L. Cadamuro, V. Cherepanov, F. Errico, R.D. Field, D. Guerrero, B.M. Joshi, M. Kim, J. Konigsberg, A. Korytov, K.H. Lo, K. Matchev, N. Menendez, G. Mitselmakher, D. Rosenzweig, K. Shi, J. Sturdy, J. Wang, E. Yigitbasi, X. Zuo

Florida State University, Tallahassee, U.S.A.

T. Adams, A. Askew, D. Diaz, R. Habibullah, S. Hagopian, V. Hagopian, K.F. Johnson, R. Khurana, T. Kolberg, G. Martinez, H. Prosper, C. Schiber, R. Yohay, J. Zhang

Florida Institute of Technology, Melbourne, U.S.A.

M.M. Baarmand, S. Butalla, T. Elkafrawy¹³, M. Hohlmann, R. Kumar Verma, D. Noonan, M. Rahmani, M. Saunders, F. Yumiceva

University of Illinois at Chicago (UIC), Chicago, U.S.A.

M.R. Adams, L. Apanasevich, H. Becerril Gonzalez, R. Cavanaugh, X. Chen, S. Dittmer, O. Evdokimov, C.E. Gerber, D.A. Hangal, D.J. Hofman, C. Mills, G. Oh, T. Roy, M.B. Tonjes, N. Varelas, J. Viinikainen, X. Wang, Z. Wu, Z. Ye

The University of Iowa, Iowa City, U.S.A.

M. Alhusseini, K. Dilsiz⁹⁰, S. Durgut, R.P. Gandrajula, M. Haytmyradov, V. Khristenko, O.K. Köseyan, J.-P. Merlo, A. Mestvirishvili⁹¹, A. Moeller, J. Nachtman, H. Ogul⁹², Y. Onel, F. Ozok⁹³, A. Penzo, C. Snyder, E. Tiras⁹⁴, J. Wetzel

Johns Hopkins University, Baltimore, U.S.A.

O. Amram, B. Blumenfeld, L. Corcodilos, J. Davis, M. Eminizer, A.V. Gritsan, S. Kyriacou, P. Maksimovic, J. Roskes, M. Swartz, T.Á. Vámi

The University of Kansas, Lawrence, U.S.A.

C. Baldenegro Barrera, P. Baringer, A. Bean, A. Bylinkin, T. Isidori, S. Khalil, J. King, G. Krintiras, A. Kropivnitskaya, C. Lindsey, N. Minafra, M. Murray, C. Rogan, C. Royon, S. Sanders, E. Schmitz, J.D. Tapia Takaki, Q. Wang, J. Williams, G. Wilson

Kansas State University, Manhattan, U.S.A.

S. Duric, A. Ivanov, K. Kaadze, D. Kim, Y. Maravin, T. Mitchell, A. Modak, K. Nam

Lawrence Livermore National Laboratory, Livermore, U.S.A.

F. Rebassoo, D. Wright

University of Maryland, College Park, U.S.A.

E. Adams, A. Baden, O. Baron, A. Belloni, S.C. Eno, Y. Feng, N.J. Hadley, S. Jabeen, R.G. Kellogg, T. Koeth, A.C. Mignerey, S. Nabili, M. Seidel, A. Skuja, S.C. Tonwar, L. Wang, K. Wong

Massachusetts Institute of Technology, Cambridge, U.S.A.

D. Abercrombie, G. Andreassi, R. Bi, S. Brandt, W. Busza, I.A. Cali, Y. Chen, M. D'Alfonso, G. Gomez Ceballos, M. Goncharov, P. Harris, M. Hu, M. Klute, D. Kovalskyi, J. Krupa, Y.-J. Lee, B. Maier, A.C. Marini, C. Mironov, C. Paus, D. Rankin, C. Roland, G. Roland, Z. Shi, G.S.F. Stephans, K. Tatar, J. Wang, Z. Wang, B. Wyslouch

University of Minnesota, Minneapolis, U.S.A.

R.M. Chatterjee, A. Evans, P. Hansen, J. Hiltbrand, Sh. Jain, M. Krohn, Y. Kubota, Z. Lesko, J. Mans, M. Revering, R. Rusack, R. Saradhy, N. Schroeder, N. Strobbe, M.A. Wadud

University of Mississippi, Oxford, U.S.A.

J.G. Acosta, S. Oliveros

University of Nebraska-Lincoln, Lincoln, U.S.A.

K. Bloom, M. Bryson, S. Chauhan, D.R. Claes, C. Fangmeier, L. Finco, F. Golf, J.R. González Fernández, C. Joo, I. Kravchenko, J.E. Siado, G.R. Snow[†], W. Tabb, F. Yan

State University of New York at Buffalo, Buffalo, U.S.A.

G. Agarwal, H. Bandyopadhyay, L. Hay, I. Iashvili, A. Kharchilava, C. McLean, D. Nguyen, J. Pekkanen, S. Rappoccio, A. Williams

Northeastern University, Boston, U.S.A.

G. Alverson, E. Barberis, C. Freer, Y. Haddad, A. Hortiangtham, J. Li, G. Madigan, B. Marzocchi, D.M. Morse, V. Nguyen, T. Orimoto, A. Parker, L. Skinnari, A. Tishelman-Charny, T. Wamorkar, B. Wang, A. Wisecarver, D. Wood

Northwestern University, Evanston, U.S.A.

S. Bhattacharya, J. Bueghly, Z. Chen, A. Gilbert, T. Gunter, K.A. Hahn, N. Odell, M.H. Schmitt, K. Sung, M. Velasco

University of Notre Dame, Notre Dame, U.S.A.

R. Band, R. Bucci, N. Dev, R. Goldouzian, M. Hildreth, K. Hurtado Anampa, C. Jessop, K. Lannon, N. Loukas, N. Marinelli, I. Mcalister, F. Meng, K. Mohrman, Y. Musienko⁴⁹, R. Ruchti, P. Siddireddy, M. Wayne, A. Wightman, M. Wolf, M. Zarucki, L. Zygala

The Ohio State University, Columbus, U.S.A.

B. Bylsma, B. Cardwell, L.S. Durkin, B. Francis, C. Hill, A. Lefeld, B.L. Winer, B.R. Yates

Princeton University, Princeton, U.S.A.

F.M. Addesa, B. Bonham, P. Das, G. Dezoort, P. Elmer, A. Frankenthal, B. Greenberg, N. Haubrich, S. Higginbotham, A. Kalogeropoulos, G. Kopp, S. Kwan, D. Lange, M.T. Lucchini, D. Marlow, K. Mei, I. Ojalvo, J. Olsen, C. Palmer, D. Stickland, C. Tully

University of Puerto Rico, Mayaguez, U.S.A.

S. Malik, S. Norberg

Purdue University, West Lafayette, U.S.A.

A.S. Bakshi, V.E. Barnes, R. Chawla, S. Das, L. Gutay, M. Jones, A.W. Jung, S. Karmarkar, M. Liu, G. Negro, N. Neumeister, G. Paspalaki, C.C. Peng, S. Piperov, A. Purohit, J.F. Schulte, M. Stojanovic¹⁶, J. Thieman, F. Wang, R. Xiao, W. Xie, M. Yang

Purdue University Northwest, Hammond, U.S.A.

J. Dolen, N. Parashar

Rice University, Houston, U.S.A.

A. Baty, S. Dildick, K.M. Ecklund, S. Freed, F.J.M. Geurts, A. Kumar, W. Li, B.P. Padley, R. Redjimi, J. Roberts[†], W. Shi, A.G. Stahl Leiton

University of Rochester, Rochester, U.S.A.

A. Bodek, P. de Barbaro, R. Demina, J.L. Dulemba, C. Fallon, T. Ferbel, M. Galanti, A. Garcia-Bellido, O. Hindrichs, A. Khukhunaishvili, E. Ranken, R. Taus

Rutgers, The State University of New Jersey, Piscataway, U.S.A.

B. Chiarito, J.P. Chou, A. Gandrakota, Y. Gershtein, E. Halkiadakis, A. Hart, M. Heindl, E. Hughes, S. Kaplan, O. Karacheban²⁴, I. Laflotte, A. Lath, R. Montalvo, K. Nash, M. Osherson, S. Salur, S. Schnetzer, S. Somalwar, R. Stone, S.A. Thayil, S. Thomas, H. Wang

University of Tennessee, Knoxville, U.S.A.

H. Acharya, A.G. Delannoy, S. Spanier

Texas A&M University, College Station, U.S.A.

O. Bouhali⁹⁵, M. Dalchenko, A. Delgado, R. Eusebi, J. Gilmore, T. Huang, T. Kamon⁹⁶, H. Kim, S. Luo, S. Malhotra, R. Mueller, D. Overton, D. Rathjens, A. Safonov

Texas Tech University, Lubbock, U.S.A.

N. Akchurin, J. Damgov, V. Hegde, S. Kunori, K. Lamichhane, S.W. Lee, T. Mengke, S. Muthumuni, T. Peltola, S. Undleeb, I. Volobouev, Z. Wang, A. Whitbeck

Vanderbilt University, Nashville, U.S.A.

E. Appelt, S. Greene, A. Gurrola, W. Johns, C. Maguire, A. Melo, H. Ni, K. Padeken, F. Romeo, P. Sheldon, S. Tuo, J. Velkovska

University of Virginia, Charlottesville, U.S.A.

M.W. Arenton, B. Cox, G. Cummings, J. Hakala, R. Hirosky, M. Joyce, A. Ledovskoy, A. Li, C. Neu, B. Tannenwald, E. Wolfe

Wayne State University, Detroit, U.S.A.

P.E. Karchin, N. Poudyal, P. Thapa

University of Wisconsin - Madison, Madison, WI, U.S.A.

K. Black, T. Bose, J. Buchanan, C. Caillol, S. Dasu, I. De Bruyn, P. Everaerts, F. Fienga, C. Galloni, H. He, M. Herndon, A. Hervé, U. Hussain, A. Lanaro, A. Loeliger, R. Loveless, J. Madhusudanan Sreekala, A. Mallampalli, A. Mohammadi, D. Pinna, A. Savin, V. Shang, V. Sharma, W.H. Smith, D. Teague, S. Trembath-reichert, W. Vetens

†: Deceased

1: Also at Vienna University of Technology, Vienna, Austria

2: Also at Institute of Basic and Applied Sciences, Faculty of Engineering, Arab Academy for Science, Technology and Maritime Transport, Alexandria, Egypt

3: Also at Université Libre de Bruxelles, Bruxelles, Belgium

4: Also at Universidade Estadual de Campinas, Campinas, Brazil

5: Also at Federal University of Rio Grande do Sul, Porto Alegre, Brazil

6: Also at University of Chinese Academy of Sciences, Beijing, China

7: Also at Department of Physics, Tsinghua University, Beijing, China

8: Also at UFMS, Nova Andradina, Brazil

- 9: Also at Nanjing Normal University Department of Physics, Nanjing, China
- 10: Now at The University of Iowa, Iowa City, U.S.A.
- 11: Also at Institute for Theoretical and Experimental Physics named by A.I. Alikhanov of NRC ‘Kurchatov Institute’, Moscow, Russia
- 12: Also at Joint Institute for Nuclear Research, Dubna, Russia
- 13: Also at Ain Shams University, Cairo, Egypt
- 14: Now at British University in Egypt, Cairo, Egypt
- 15: Also at Zewail City of Science and Technology, Zewail, Egypt
- 16: Also at Purdue University, West Lafayette, U.S.A.
- 17: Also at Université de Haute Alsace, Mulhouse, France
- 18: Also at Ilia State University, Tbilisi, Georgia
- 19: Also at Erzincan Binali Yildirim University, Erzincan, Turkey
- 20: Also at CERN, European Organization for Nuclear Research, Geneva, Switzerland
- 21: Also at RWTH Aachen University, III. Physikalisches Institut A, Aachen, Germany
- 22: Also at University of Hamburg, Hamburg, Germany
- 23: Also at Department of Physics, Isfahan University of Technology, Isfahan, Iran, Isfahan, Iran
- 24: Also at Brandenburg University of Technology, Cottbus, Germany
- 25: Also at Skobeltsyn Institute of Nuclear Physics, Lomonosov Moscow State University, Moscow, Russia
- 26: Also at Physics Department, Faculty of Science, Assiut University, Assiut, Egypt
- 27: Also at Eszterhazy Karoly University, Karoly Robert Campus, Gyongyos, Hungary
- 28: Also at Institute of Physics, University of Debrecen, Debrecen, Hungary, Debrecen, Hungary
- 29: Also at Institute of Nuclear Research ATOMKI, Debrecen, Hungary
- 30: Also at MTA-ELTE Lendület CMS Particle and Nuclear Physics Group, Eötvös Loránd University, Budapest, Hungary
- 31: Also at Wigner Research Centre for Physics, Budapest, Hungary
- 32: Also at IIT Bhubaneswar, Bhubaneswar, India
- 33: Also at Institute of Physics, Bhubaneswar, India
- 34: Also at G.H.G. Khalsa College, Punjab, India
- 35: Also at Shoolini University, Solan, India
- 36: Also at University of Hyderabad, Hyderabad, India
- 37: Also at University of Visva-Bharati, Santiniketan, India
- 38: Also at Indian Institute of Technology (IIT), Mumbai, India
- 39: Also at Deutsches Elektronen-Synchrotron, Hamburg, Germany
- 40: Also at Sharif University of Technology, Tehran, Iran
- 41: Also at Department of Physics, University of Science and Technology of Mazandaran, Behshahr, Iran
- 42: Now at INFN Sezione di Bari ^a, Università di Bari ^b, Politecnico di Bari ^c, Bari, Italy
- 43: Also at Italian National Agency for New Technologies, Energy and Sustainable Economic Development, Bologna, Italy
- 44: Also at Centro Siciliano di Fisica Nucleare e di Struttura Della Materia, Catania, Italy
- 45: Also at Università di Napoli ‘Federico II’, Napoli, Italy
- 46: Also at Riga Technical University, Riga, Latvia, Riga, Latvia
- 47: Also at Consejo Nacional de Ciencia y Tecnología, Mexico City, Mexico
- 48: Also at IRFU, CEA, Université Paris-Saclay, Gif-sur-Yvette, France
- 49: Also at Institute for Nuclear Research, Moscow, Russia
- 50: Now at National Research Nuclear University ‘Moscow Engineering Physics Institute’ (MEPhI), Moscow, Russia

- 51: Also at St. Petersburg State Polytechnical University, St. Petersburg, Russia
- 52: Also at University of Florida, Gainesville, U.S.A.
- 53: Also at Imperial College, London, United Kingdom
- 54: Also at P.N. Lebedev Physical Institute, Moscow, Russia
- 55: Also at Moscow Institute of Physics and Technology, Moscow, Russia
- 56: Also at California Institute of Technology, Pasadena, U.S.A.
- 57: Also at Budker Institute of Nuclear Physics, Novosibirsk, Russia
- 58: Also at Faculty of Physics, University of Belgrade, Belgrade, Serbia
- 59: Also at Trincomalee Campus, Eastern University, Sri Lanka, Nilaveli, Sri Lanka
- 60: Also at INFN Sezione di Pavia ^a, Università di Pavia ^b, Pavia, Italy
- 61: Also at National and Kapodistrian University of Athens, Athens, Greece
- 62: Also at Ecole Polytechnique Fédérale Lausanne, Lausanne, Switzerland
- 63: Also at Universität Zürich, Zurich, Switzerland
- 64: Also at Stefan Meyer Institute for Subatomic Physics, Vienna, Austria
- 65: Also at Laboratoire d'Annecy-le-Vieux de Physique des Particules, IN2P3-CNRS, Annecy-le-Vieux, France
- 66: Also at Şirnak University, Şirnak, Turkey
- 67: Also at Near East University, Research Center of Experimental Health Science, Nicosia, Turkey
- 68: Also at Konya Technical University, Konya, Turkey
- 69: Also at Istanbul University - Cerraphasa, Faculty of Engineering, Istanbul, Turkey
- 70: Also at Mersin University, Mersin, Turkey
- 71: Also at Piri Reis University, Istanbul, Turkey
- 72: Also at Adiyaman University, Adiyaman, Turkey
- 73: Also at Ozyegin University, Istanbul, Turkey
- 74: Also at Izmir Institute of Technology, Izmir, Turkey
- 75: Also at Necmettin Erbakan University, Konya, Turkey
- 76: Also at Bozok Universiteleri Rektörlüğü, Yozgat, Turkey
- 77: Also at Marmara University, Istanbul, Turkey
- 78: Also at Milli Savunma University, Istanbul, Turkey
- 79: Also at Kafkas University, Kars, Turkey
- 80: Also at Istanbul Bilgi University, Istanbul, Turkey
- 81: Also at Hacettepe University, Ankara, Turkey
- 82: Also at Vrije Universiteit Brussel, Brussel, Belgium
- 83: Also at School of Physics and Astronomy, University of Southampton, Southampton, United Kingdom
- 84: Also at IPPP Durham University, Durham, United Kingdom
- 85: Also at Monash University, Faculty of Science, Clayton, Australia
- 86: Also at Università di Torino, Torino, Italy
- 87: Also at Bethel University, St. Paul, Minneapolis, U.S.A., St. Paul, U.S.A.
- 88: Also at Karamanoğlu Mehmetbey University, Karaman, Turkey
- 89: Also at Illinois Mathematics and Science Academy, Aurora, U.S.A.
- 90: Also at Bingol University, Bingol, Turkey
- 91: Also at Georgian Technical University, Tbilisi, Georgia
- 92: Also at Sinop University, Sinop, Turkey
- 93: Also at Mimar Sinan University, Istanbul, Istanbul, Turkey
- 94: Also at Erciyes University, Kayseri, Turkey
- 95: Also at Texas A&M University at Qatar, Doha, Qatar
- 96: Also at Kyungpook National University, Daegu, Korea, Daegu, Korea